

การสร้างและพัฒนาวัสดุป้องกันรังสีนิวตรอนจากวัสดุคอมโพสิต
ของยางธรรมชาติและโบรอนคาร์ไบด์



วิทยานิพนธ์นี้เป็นส่วนหนึ่งของการศึกษาตามหลักสูตรปริญญาวิทยาศาสตรมหาบัณฑิต
สาขาวิชาฟิสิกส์ประยุกต์
มหาวิทยาลัยเทคโนโลยีสุรนารี
ปีการศึกษา 2565

FABRICATION AND DEVELOPMENT OF NEUTRON SHIELDING
MATERIALS BASED ON NATURAL RUBBER AND
BORON CARBIDE COMPOSITE



A Thesis Submitted in Partial Fulfillment of the Requirements for the
Degree of Master of Science in Applied Physics
Suranaree University of Technology
Academic Year 2022

FABRICATION AND DEVELOPMENT OF NEUTRON SHIELDING MATERIALS BASED ON NATURAL RUBBER AND BORON CARBIDE COMPOSITE

Suranaree University of Technology has approved this thesis submitted in partial fulfillment of the requirements for a Master's Degree.

Thesis Examining Committee

Wanchaloem

(Dr. Wanchaloem Poonsawat)

Chairperson

C. Kobdaj

(Asst. Prof. Dr. Chinorat Kobdaj)

Member (Thesis Advisor)

Chaivat

(Assoc. Prof. Dr. Chaivat Ruksakulpiwat)

Member (Thesis Co-Advisor)

Christoph Herold

(Asst. Prof. Dr. Christoph Herold)

Member

Panom Sak Meemon

(Assoc. Prof. Dr. Panomsak Meemon)

Member

Yupaporn Ruksakulpiwat

(Assoc. Prof. Dr. Yupaporn Ruksakulpiwat)

Vice Rector for Academic Affairs
and Quality Assurance

Santi Maensiri

(Prof. Dr. Santi Maensiri)

Dean of Institute of Science

จิตตินันท์ แสนภูวา : การสร้างและพัฒนาวัสดุป้องกันรังสีนิวตรอนจากวัสดุคอมโพสิตของยางธรรมชาติและโบรอนคาร์ไบด์ (FABRICATION AND DEVELOPMENT OF NEUTRON SHIELDING MATERIALS BASED ON NATURAL RUBBER AND BORON CARBIDE COMPOSITE) อาจารย์ที่ปรึกษา : ผู้ช่วยศาสตราจารย์ ดร.ชินรัตน์ กอบเดช, 91 หน้า.

คำสำคัญ: นิวตรอน/ ยางธรรมชาติ/ วัสดุป้องกันรังสี/ มอนติคาร์โล

วัสดุป้องกันรังสีนิวตรอนจากยางธรรมชาติและโบรอนคาร์ไบด์ถูกสร้างขึ้นด้วยส่วนผสมของวัสดุต่าง ๆ ที่ต่างกันทั้งหมดสิบสูตร โดยสามารถแบ่งการศึกษาผลกระทบที่ส่งผลต่อวัสดุออกเป็นห้าการศึกษา ประกอบด้วยการศึกษาผลกระทบของความแตกต่างของปริมาณโบรอนคาร์ไบด์ (B_4C) ที่ 0, 20, 40, 60 และ 139.6 ส่วนต่ออย่างร้อยละ (phr) การศึกษาผลกระทบของชนิดของยางธรรมชาติคือยางธรรมชาติ (NR) ยางธรรมชาติอีพอกไซด์ (ENR) และยางผสมระหว่าง NR และ ENR การศึกษาผลกระทบของความแตกต่างของปริมาณคาร์บอนแบล็คหรือเขม่าดำที่ 30 และ 60 phr นอกจากนี้ยังมีอีกสองการศึกษาที่ได้ทำการศึกษาผลของความแตกต่างของสารเร่งปฏิกิริยาหลัก N-cyclohexylbenzothiazole-2-sulfenamide (CBS) ที่ 0.5 และ 1 phr และการศึกษาสุดท้ายคือการศึกษาสารคงรูปโดยใช้ไดคูมิลเปอร์ออกไซด์ (DCP) เทียบกับการใช้กำมะถัน ซึ่งวัสดุตัวอย่างจากทั้งสิบสูตรจะถูกนำไปทดสอบถึงคุณสมบัติเชิงกล คุณสมบัติการป้องกันเทอร์มอลนิวตรอน (Thermal neutron) และคุณสมบัติการป้องกันนิวตรอนเร็ว (Fast neutron) รวมไปถึงการหาค่าภาคตัดขวางมหภาค (Macroscopic Cross Section) ของนิวตรอน ทั้งนี้แบบจำลองทางคอมพิวเตอร์มอนติคาร์โล (Monte Carlo N-Particles, MCNP) จะถูกนำมาหาค่าภาคตัดขวางมหภาคของนิวตรอนเร็วสำหรับเปรียบเทียบที่ได้จากการทดลอง เครื่องปฏิกรณ์ปรมาณูวิจัยประเภท TRIGA Mark II และ ^{241}Am - ^{90}Sr ถูกใช้เป็นแหล่งเทอร์มอลนิวตรอนและแหล่งกำเนิดนิวตรอนเร็วตามลำดับ การเพิ่มขึ้นของคาร์บอนแบล็คที่ 60 phr ส่งผลให้ระดับความแข็ง Shore A สูงที่สุดซึ่งมีค่าเท่ากับ 76.53 โดยมีค่าความถ่วงจำเพาะเท่ากับ 1.30 และพลังงานกระตุ้นคือ 120.56 กิโลจูลต่อโมล การเพิ่มขึ้นของ CBS ที่ 1 phr ทำให้มีเวลาคงรูปต่ำสุดที่ 2.07 นาที ในขณะที่การใช้ DCP เป็นสารคงรูปทำให้ใช้เวลาในการคงรูปนานที่สุดคือ 5.17 นาที การถ่ายภาพนิวตรอนถูกนำมาใช้เพื่อกำหนดและเปรียบเทียบคุณสมบัติการป้องกันเทอร์มอลนิวตรอนของวัสดุสูตรต่าง ๆ โดยการวัดการป้องกันเทอร์มอลนิวตรอนของตัวอย่างที่มีความหนา 6 มิลลิเมตรพบว่า B_4C ที่ 139.6 phr สามารถป้องกันเทอร์มอลนิวตรอนได้ดีที่สุดในบรรดาตัวอย่างทั้งหมด โดยมีค่าเศษส่วนความสว่างต่ำสุดคือ 0.045 และภาคตัดขวางมหภาคที่ 19.97 cm^{-1} และสามารถป้องกันนิวตรอนได้ใกล้เคียงกับตัวอย่างของผลิตภัณฑ์เชิงพาณิชย์ที่ได้รับมาจากบริษัทประเทศญี่ปุ่นโดยทั้งคู่ทดสอบที่ความหนา 5 mm.

นอกจากนี้ยังพบว่า B_4C ที่ 20 phr มีความสามารถในการกำบังนิวตรอนเร็วที่ดีที่สุด โดยมี
ภาคตัดขวางมหภาคเท่ากับ 0.264 cm^{-1} .



สาขาวิชาฟิสิกส์
ปีการศึกษา 2565

ลายมือชื่อนักศึกษา พิชญ์นิภา
ลายมือชื่ออาจารย์ที่ปรึกษา ไพโรจน์ กอมาตย์

JITTINUN SAENPOOWA : FABRICATION AND DEVELOPMENT OF NEUTRON SHIELDING MATERIALS BASED ON NATURAL RUBBER AND BORON CARBIDE COMPOSITE. THESIS ADVISOR : ASST. PROF. CHINORAT KOBDAJ, Ph.D. 91 PP.

Keyword: Neutron Shielding/ Natural Rubber/ MCNP simulation

The neutron shielding materials based on natural rubber were fabricated in ten different formulas for five studies, including the study of the effect on differences in boron carbide (B_4C) contents of 0, 20, 40, 60, and 139.6 parts per hundred rubbers (phr). Furthermore, the study focuses on the effect of rubber-based types, including natural rubber (NR), epoxidized natural rubber (ENR), and a blend of NR and ENR. Additionally, the study of the effect of the difference in carbon black contents of 30 and 60 phr in natural rubber-based materials is compared. Two other studies that study the effect of differences in the contents of a primary accelerator, N-cyclohexylbenzothiazole-2-sulfenamide (CBS), at 0.5 and 1 phr in a natural rubber base, are also analyzed. Dicumyl peroxide (DCP) served as both a vulcanization and activation agent in the final formula. This work examined the effects of all shielding formulas on mechanical, thermal, and fast neutron shielding properties. The macroscopic cross sections of thermal and fast neutrons for each sample were determined by taking into account the variation in sample thickness. The Monte Carlo N-Particles (MCNP) were used to simulate and compare the fast neutron macroscopic cross section value with the experiment. The TRIGA Mark III type atomic research reactor and ^{241}Am -Beryllium were used as a thermal neutron source and a fast neutron source, respectively. The increase in carbon black at 60 phr resulted in a Shore hardness degree of 76.53, a specific gravity of 1.30, and an activation energy of 120.56 kJ/mol. An increase in CBS at 1 phr gave rise to a minimum cure time of 2.07 minutes, whereas using DCP had the longest curing time of 5.17 minutes. Neutron imaging was used to determine and compare the thermal neutron properties of different formulas. We found that B_4C at 139.6 phr has the best thermal neutron shielding among all our samples, with the lowest level of a 0.045 brightness fraction and the thermal macroscopic cross-section of 19.97 cm^{-1} . According to the results of

fast neutron attenuation tests performed on a sample of the commercial product obtained from a Japanese company, the sample of 50 weight percent boron carbide had similar neutron shielding properties, with both being 5 mm thick. B_4C at 20 phr has the best fast neutron shielding, with a macroscopic cross-section of 0.264 cm^{-1} .



School of Physics
Academic Year 2022

Student's Signature *จิรพัฒน์*
Advisor's Signature C. Kobdaj

ACKNOWLEDGEMENTS

Firstly, I would like to express my sincere gratitude to my thesis advisor, Assistant Professor Dr. Chinorat Kobdaj, who is a lecturer in the School of Physics at the Suranaree University of Technology, for every great encouragement, assistance, and support that has enabled me to complete my thesis.

I would like to thank my thesis Co-advisor, Assoc. Prof. Dr. Chaiwat Rukakulpiwat, who is a lecturer in the School of Polymer Engineering, Institute of Engineering, Suranaree University of Technology, for his support and teaching in polymer processing and the fabrication of natural rubber products.

Additionally, I would like to thank Asst. Prof. Dr. Siriyaporn Sangaroon, who is a lecturer in the department of physics at the Faculty of Science, Mahasarakham University, for her support and teaching in the basics of Monte Carlo N-Particles (MCNP) simulation.

Furthermore, I would like to thank Asst. Prof. Chadet Yenchai, who is a lecturer in the department of Nuclear Engineering, Faculty of Engineering, Chulalongkorn University, for his support, teaching, and courtesy in the neutron shielding experiment.

In addition, the authors would like to thank Mr. Weerawat Pornroongruengchok and the Thailand Institute of Nuclear Technology (Public Organization) or TINT for their courtesy in the thermal neutron shielding experiment. The authors would like to thank colleagues in the nuclear and particle physics group and the polymer lab group at SUT for providing fruitful discussions and advice to improve this work.

Moreover, This work was financially supported by the Thailand Center of Excellence in Physics (Contract No.ThEP-61-PHM-SUT4), Suranaree University of Technology (SUT), Thailand Science Research and Innovation (Contract No. IRN62W0006), National Science, Research and Innovation Fund (Grant No.FF1-105-65-36-28), and the Boron Neutron Capture Therapy Research Center (BNCT).

I also would like to thank all lecturers in the School of Physics, who have taught me and made it possible for the expansion of my knowledge and my professional development in the past three academic years.

Lastly, I would like to express my sincere appreciation to my parents and friends, especially Mr. Wacharin Khamtanat, for their constant encouragement and

life advice until the completion of my master's degree program. Without them, this achievement is unthinkable.

Jittinun Saenpoowa



CONTENTS

	Page
ABSTRACT IN THAI	I
ABSTRACT IN ENGLISH	III
ACKNOWLEDGEMENTS	V
CONTENTS	VII
LIST OF TABLES	X
LIST OF FIGURES	XI
LIST OF ABBREVIATIONS	XV
CHAPTER	
I INTRODUCTION	1
II RESEARCH BACKGROUND	3
2.1 Radiation	3
2.1.1 Radiation classification according to the nature of radiation	3
2.1.2 Radiation classification according to interaction with medium	3
2.1.3 Radiation dose limit	5
2.2 Neutron	5
2.2.1 Introduction to neutron	5
2.2.2 Classification and utilization of neutrons	6
2.2.3 Beta decay of a free neutron	7
2.2.4 Diffusion and slowing down of neutrons	7
2.3 Natural Rubber	8
2.3.1 Chemical formula of natural rubber	9
2.3.2 Block rubber	9
2.3.3 Epoxidized natural rubber	9
2.4 The Main Processes of Rubber	10
2.4.1 Compounding formulation	10
2.4.2 Softening and mixing	11

CONTENTS (Continued)

		Page
	2.4.3 Shaping	11
	2.4.4 Vulcanization	12
2.5	Rubber Analysis and Testing	12
	2.5.1 Viscosity and curing characteristics	12
	2.5.2 Mechanical and technological testing	13
2.6	Neutron Shielding	13
2.7	Monte Carlo Transport Code	14
	2.7.1 Introduction	14
	2.7.2 MCNP input file	14
	Cell card	16
	Surface cards	16
	Material data card	18
	Source specification	19
	2.7.3 Tally specification	22
III	PROCESSING OF NEUTRON SHIELDING MATERIAL BASED ON NATURAL RUBBER AND BORON CARBIDE COMPOSITE	34
	3.1 Introduction	34
	3.2 Material and Method	35
	3.2.1 Material selection and compounding formulation	35
	3.2.2 Neutron shielding material fabrication	36
	Mixing	37
	Vulcanization characteristics of rubber compounds	38
	Forming and vulcanization	39
	3.3 Results and Discussion	40
	3.3.1 Mooney viscosity	40
	3.3.2 MDR test	41
	3.4 Summary	42
IV	MECHANICAL TEST	46
	4.1 Introduction	46
	4.2 Material and Method	47
	4.2.1 Hardness test	47

CONTENTS (Continued)

	Page
4.2.2 Tensile test	47
4.3 Results and Discussion	48
4.3.1 Hardness test	48
4.3.2 Tensile test	49
V NEUTRON SHIELDING TEST	51
5.1 Material and Method	51
5.1.1 Thermal neutron shielding tests	51
5.1.2 Fast neutron shielding tests	52
5.2 Results and Discussion	53
5.2.1 Thermal neutron shielding tests	53
5.2.2 Fast neutron shielding tests	55
VI MCNP SIMULATION FOR NEUTRON SHIELDING MATERIAL	58
6.1 Introduction	58
6.2 Problem Description and Geometry	59
6.3 Surface and Cell Cards	59
6.3.1 Surface cards	59
6.3.2 Cell cards	60
6.4 Material Specification	61
6.5 Source Definition	64
6.6 Tallies and Miscellaneous Data Cards	64
6.7 MCNP Execution	66
6.8 Results and Discussion	67
VII CONCLUSION	72
REFERENCES	75
APPENDICES	
APPENDIX A SAMPLE OF INPUT FILE FOR MCNP SIMULATION	81
APPENDIX B FMESH TALLY PLOT FOR SAMPLE	85
CURRICULUM VITAE	91

LIST OF TABLES

Table		Page
2.1	Radiation dose limit (ICRP, 2007).	6
2.2	Classification of neutrons according to their energy (Alhussain and Abuhoza, 2009).	7
2.3	MCNP tally type.	25
2.4	The description of the surface and cell tally types 1, 2, 4, 6, and 7 form.	26
3.1	Compounding of formula.	36
3.2	The formula for each sample in gram unit.	37
3.3	MDR data of the sample at 150 °C	45
4.1	Tensile test of the sample.	50
5.1	The thermal neutron macroscopic cross-section (Σ) for each sample using neutron imaging techniques, The TRIGA Mark III type atomic research reactor, Thailand Institute of Nuclear Technology (public organization).	55
5.2	The fast neutron macroscopic cross-section (Σ) for each sample, test with ²⁴¹ Americium-Beryllium source at department of Nuclear Engineering, Faculty of Engineering, Chulalongkorn University, Bangkok, Thailand.	57
6.1	Element fraction of each formula.	63
6.2	The number of neutron particles crossing a detector surface.	68
6.3	Neutron transmission of the sample with different thickness.	68
6.4	The microscopic crosssection of each sample from MCNP simulation.	69

LIST OF FIGURES

Figure		Page
2.1	Radioactive decay of an atom (Tiwari, 2022).	4
2.2	Electromagnetic radiation (Wikiversity, 2021).	5
2.3	Types of Ionizing Radiation (Ministry of the Environment, 2016).	6
2.4	Moderator for slowing down neutrons (Encyclopædia Britannica, 2012).	8
2.5	Cis (1,4) - Polyisoprene (chimicaemateriali, 2019).	9
2.6	Molecular structure of epoxidised natural rubber (Surya et al., 2018).	10
2.7	Network formation (Coran, 2013).	12
2.8	The initiate-run file of MCNP (Sweezy et al., 2003).	15
2.9	Symbol of original MCNP Particles (Sweezy et al., 2003).	15
2.10	An example of a cell card form for cell card definition in MCNP (Sweezy et al., 2003).	16
2.11	The description of each parameter in the cell card form (Sweezy et al., 2003).	27
2.12	Surface defined by equation form (Sweezy et al., 2003).	27
2.13	The description of each parameter in the surfaces defined by equation form (Sweezy et al., 2003).	28
2.14	The equation mnemonic to describe a parameter that specifies the type of surface (Sweezy et al., 2003).	28
2.15	The equation mnemonic to describe a parameter that specifies the type of surface (Sweezy et al., 2003), continue.	29
2.16	Axisymmetric surfaces defined by points form (Sweezy et al., 2003).	29
2.17	The description of each parameter in axisymmetric surfaces defined by points form (Sweezy et al., 2003).	29
2.18	Macrobody box form (Sweezy et al., 2003).	30
2.19	Macrobody box form parameter description (Sweezy et al., 2003).	30
2.20	The rectangular parallelepiped form (Sweezy et al., 2003).	30

LIST OF FIGURES (Continued)

Figure		Page
2.21	The description of each parameter in the rectangular parallelepiped form (Sweezy et al., 2003).	30
2.22	The material specification of M form (Sweezy et al., 2003).	30
2.23	The description of each parameter in the material specification of M form.	31
2.24	The description of each keyword parameter in the material specification of M form (Sweezy et al., 2003).	32
2.25	The general source (SDEF) specification form (Sweezy et al., 2003).	32
2.26	The general source (SDEF) keyword (Sweezy et al., 2003).	33
2.27	The surface and cell tallies form of tally types 1, 2, 4, 6, and 7 (Sweezy et al., 2003).	33
3.1	Research procedure.	35
3.2	Internal mixer is the equipment for mixing natural rubber and fillers.	38
3.3	Two roll mill is the equipment for mix sulfur into composite materials and shape samples into sheets.	39
3.4	MDR 3000 moving die rheometer is used to determine curing time of composite material.	40
3.5	Mooney viscometer is the equipment for determine the Mooney viscosity of composite material.	41
3.6	A compression molding machine model LP20-B from Labtech Engineering Company Ltd. was used for vulcanizing the sample.	42
3.7	Neutron shielding materials samples with dimensions of 15 × 15 × 0.2 cm ³ (width x length x thickness).	43
3.8	Mooney viscosity of the sample.	44
3.9	Characteristics of dimensional stability of the sample at 150 °C.	44
3.10	The activation energy of the sample.	45
4.1	Shore A hardness tester is used in this work. We follow the ASTM D2240 standard. All samples of 6 mm thickness were put through a hardness test.	48

LIST OF FIGURES (Continued)

Figure		Page
4.2	The 5569A INSTRON tensile machine is used in this work. Tensile testing were done on C-shaped samples. The 500 mm/min displacement was employed with a 10 kN load cell.	48
4.3	Hardness of the sample.	49
5.1	Experiment setup for thermal neutron shielding test.	52
5.2	Experiment setup for our fast neutron shielding test.	53
5.3	Sample image from neutron imaging.	54
5.4	Brightness fraction of the sample.	54
5.5	Fast neutron attenuation of samples.	56
5.6	Fast neutron attenuation of F5 and a commercial sample from Japan (Silicone).	56
6.1	Geometry.	59
6.2	Surface cards of our simulation setup.	60
6.3	Cell cards of our simulation setup.	61
6.4	Cell position of our simulation setup.	61
6.5	Materials card of sample F1.	62
6.6	Source definition of our model.	64
6.7	Tallies cards of our model.	65
6.8	Fmesh tally card to plot energy in the geometry of our model.	65
6.9	Miscellaneous cards of our model.	65
6.10	command line.	66
6.11	Options for MCNP execution.	67
6.12	Exponential attenuation of neutrons in matter: Beer-Lambert law.	69
6.13	Fmesh tally plot results of F0 (no sample), F1, F2, and F5 with 2 cm. thick, neutron, nps = 5000000 particks, XY plane.	71
6.14	Fmesh tally plot results of F2 sample with different of thickness, nps = 5000000 particks, XY plane.	71
B.1	Fmesh tally plot results of F1 sample with different of thickness, nps = 5000000 particks, XY plane.	85
B.2	Fmesh tally plot results of F2 sample with different of thickness, nps = 5000000 particks, XY plane.	86

LIST OF FIGURES (Continued)

Figure		Page
B.3	Fmesh tally plot results of F3 sample with different of thickness, nps = 5000000 particks, XY plane.	86
B.4	Fmesh tally plot results of F4 sample with different of thickness, nps = 5000000 particks, XY plane.	87
B.5	Fmesh tally plot results of F5 sample with different of thickness, nps = 5000000 particks, XY plane.	87
B.6	Fmesh tally plot results of F6 sample with different of thickness, nps = 5000000 particks, XY plane.	88
B.7	Fmesh tally plot results of F7 sample with different of thickness, nps = 5000000 particks, XY plane.	88
B.8	Fmesh tally plot results of F8 sample with different of thickness, nps = 5000000 particks, XY plane.	89
B.9	Fmesh tally plot results of F9 sample with different of thickness, nps = 5000000 particks, XY plane.	89
B.10	Fmesh tally plot results of F10 sample with different of thickness, nps = 5000000 particks, XY plane.	90

LIST OF ABBREVIATIONS

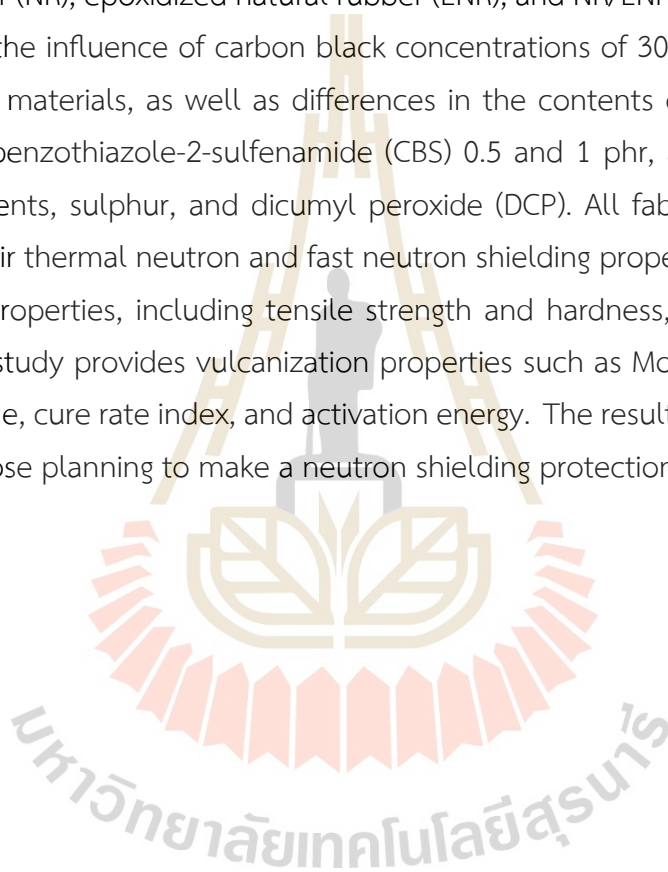
phr	Parts per hundred rubbers
NR	Natural rubber
ENR	Epoxidized natural rubber
CBS	N-cyclohexylbenzothiazole-2-sulfenamide
DCP	Dicumyl peroxide
MCNP	Monte Carlo N-Particles
SUT	Suranaree University of Technology
BNCT	The Boron Neutron Capture Therapy Research Cente
ICRP	The International Commission on Radiological Protection
LEU	Low Enrichment Uranium
EPDM	Ethylene Propylene Diene monomer
hBN	hexagonal Boron Nitride
PMMA	Poly methyl methacrylate
B ₄ C	Boron carbide
TMTM	Tetramethylthiuram monosulfide
MDR	Moving Die Rheometer
M _H	Maximum torque
M _L	Minimum torque
CRI	Cure rate index
MU	Mooney viscosity unit
ZnS	Zinc sulfide
PE	Polyethylene

CHAPTER I

INTRODUCTION

Nuclear technology is applied in industry (Szczepankowski et al., 2022), agriculture (Zaman et al., 2018), and, in particular, the expanding field of worldwide medicine (Altieri and Protti, 2018). Applications for these technologies often require high-energy radiation and particle sources, such as radioactive materials, particle accelerators, nuclear reactors, etc. These sources produce neutron radiation. Neutron radiation has high penetrating power and can cause significant damage to biological tissues and electronic equipment (Kuhne et al., 2009). Therefore, neutron shielding materials perform an essential function in protecting both the environment and operators from the dangers of neutron radiation. One of the characteristics of neutron shielding materials is their high hydrogen atom content, which is present in natural rubber. Natural rubber (NR) is a widely used polymer with excellent mechanical properties, a low cost, and adequate availability. The polymer is composed of lengthy chains of isoprene units that recur. NR can be cross-linked through vulcanization to increase its tensile strength, tensile durability, and heat resistance. Numerous applications, such as tire manufacturing, biomedical devices, and industrial products, have utilized NR due to its unique properties. The potential of NR in radiation shielding applications has recently been studied. Rubber was used as a neutron-shielding material and was mixed with styrene butadiene rubber and boron oxide to form a neutron-shielding material (Jumpee and Wongsawaeng, 2015). Additionally, research has been conducted on rubber compounds that contain iron and boron oxide (El-Khatib et al., 2020). Also, study was conducted on the utilization of slabs made from natural rubber as thermal neutron shielding (Onjuna et al., 2014). However, its effectiveness as a radiation shield can be limited due to its low atomic number and low density. Natural rubber is mainly used because of its high hydrogen content, which can reduce neutron energy. Therefore, combining NR with other materials with high atomic numbers and densities can lead to the development of effective and efficient radiation shielding materials. Due to its large cross-section for neutrons, boron carbide (B_4C) is a well-known neutron absorber (Kharita et al., 2011). In order to develop a low-cost, high-performance neutron shielding material, the combination of natural rubber and boron carbide has been

investigated. Hydrogen has an average thermal neutron cross-section of 82 barn (b), while boron, a typical neutron shielding material, has an average neutron cross-section of 767 b (Sears, 1992). Earlier research used natural rubber and boron carbide to shield fast neutrons (Saenpoowa et al., 2023). The objective of this study is to design and fabricate neutron shielding materials based on natural rubber and boron carbide. In this investigation, the effects of boron carbide concentrations of 0, 20, 40, 60, and 139.6 phr are examined. We investigate the impacts of various rubber base types, such as natural rubber (NR), epoxidized natural rubber (ENR), and NR/ENR blends. Furthermore, we evaluate the influence of carbon black concentrations of 30 and 60 phr in natural rubber-based materials, as well as differences in the contents of a main accelerator, N-cyclohexylbenzothiazole-2-sulfenamide (CBS) 0.5 and 1 phr, and the effect of vulcanization agents, sulphur, and dicumyl peroxide (DCP). All fabricated samples were tested for their thermal neutron and fast neutron shielding properties. In this work, the mechanical properties, including tensile strength and hardness, are described. Additionally, this study provides vulcanization properties such as Mooney viscosity, scorch time, cure time, cure rate index, and activation energy. The results of this study may be helpful to those planning to make a neutron shielding protection product from natural rubber.



CHAPTER II

RESEARCH BACKGROUND

2.1 Radiation

Radiation can be described as energy in the form of electromagnetic waves or streams of particles that travel through space or mediums. There are different types of radiation, which can be classified as follows.

2.1.1 Radiation classification according to the nature of radiation

1. Particle radiation

Particle radiation or particle beams, such as alpha, beta, neutron radiation, and cosmic rays, are radiation caused by particles traveling at high speeds. Another type of particle radiation occurs due to unstable nuclei that try to eliminate excess atomic energy by emitting a certain amount of energy. This emission is called radiation, as illustrated in Figure 2.1.

2. Electromagnetic radiation

Electromagnetic radiation is a transverse wave comprising a magnetic field and an electric field perpendicular to each other. Electromagnetic waves can travel without any moving medium, such as radio waves, light, ultraviolet rays, thermal radiation, X-rays, and gamma rays. The electromagnetic radiation is shown in Figure 2.2.

2.1.2 Radiation classification according to interaction with medium

1. Ionizing radiation

Ionizing radiation is the radiation that makes the atoms of the medium ionized, either directly or indirectly. It can be caused by alpha radiation, beta radiation, X-rays, gamma rays, and neutron rays. Ionization occurs when radiation passes through an atom, causing electrons around the nucleus to fall out of their orbits to become free electrons. Pairs of ions have formed as a result. Negative ions are formed when electrons are thrown out of orbit. The original atom was neutral because the number

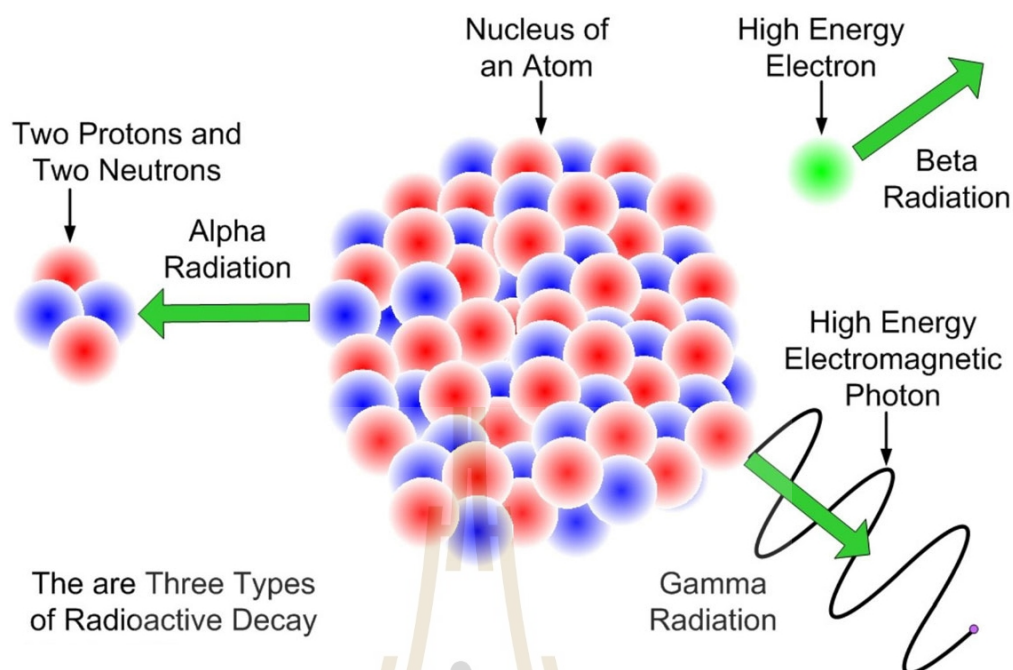


Figure 2.1 Radioactive decay of an atom (Tiwari, 2022).

of protons in the nucleus was equal to the number of electrons in the surrounding orbits. When an electron has been released from the orbit, the leftover part of an atom becomes positively charged and is classified as a positive ion.

This ionizing radiation produces a harmful effect on the cells of living things. It can be potentially dangerous if it is not properly protected. The ionizing radiation type can be shown in Figure 2.3

2. Non-ionizing radiation

Non-ionizing radiation is the radiation that cannot cause ionization in atoms of the medium where the ray passes. It just makes electrons excited and move to a higher orbit. For a short period of time, electrons then fall back into their original orbits or ground states. This phenomenon is called atoms in excited states. These type of radiation are low-energy radiation such as thermal radiation, microwaves, lasers, ultraviolet, and radio waves. Non-ionizing radiation does not cause much harm to the cells of living organisms. But, it can cause abnormal symptoms, such as a red rash on the skin.

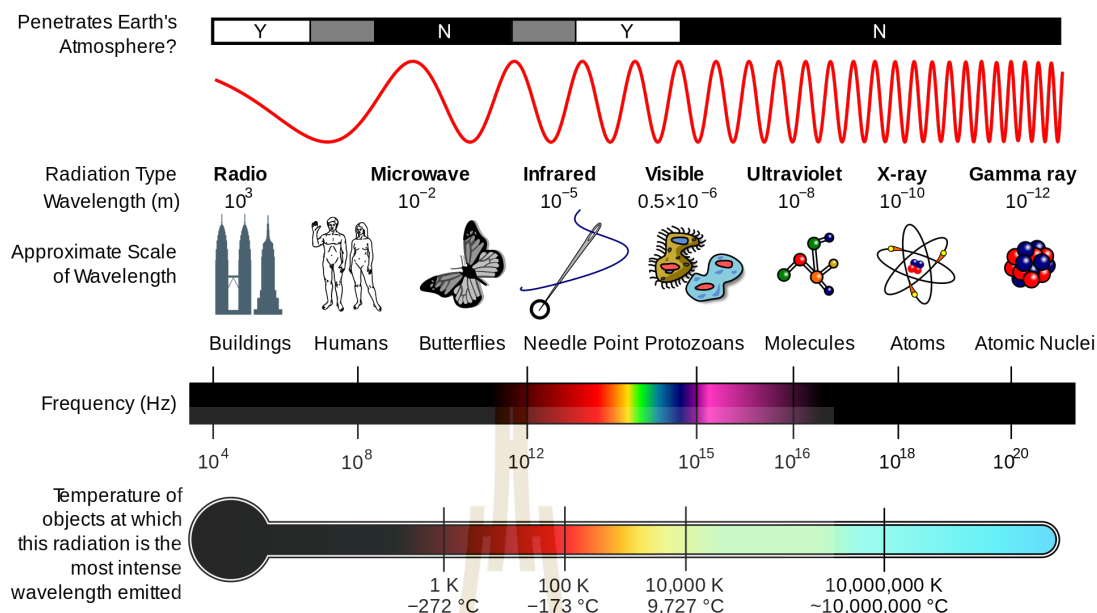


Figure 2.2 Electromagnetic radiation (Wikiversity, 2021).

2.1.3 Radiation dose limit

Radiation dose limits are established to safeguard workers and the general public from the harmful effects of ionizing radiation. They are set at a level that strikes a balance between the risks of radiation exposure and the advantages of utilizing it. We must decrease all ionizing radiation exposure to a level as low as practicable, which must be within the dosage limitations. The International Commission on Radiological Protection (ICRP) is a non-profit organization that was founded to develop the science of radiological protection for the public good, in particular by giving recommendations and advice on all areas of ionizing radiation protection. The recommendations of the ICRP are shown in the Table 2.1.

2.2 Neutron

2.2.1 Introduction to neutron

The neutron is one of the subatomic particles in the atomic nucleus. It is a neutral particle with no electric charge. The mass of neutron is 1.67493×10^{-27} kg or 939.56542 MeV/c with a mean square radius of 0.8×10^{-15} m. Normal coexistence of neutrons with protons are called nucleons. Neutrons and protons are also called

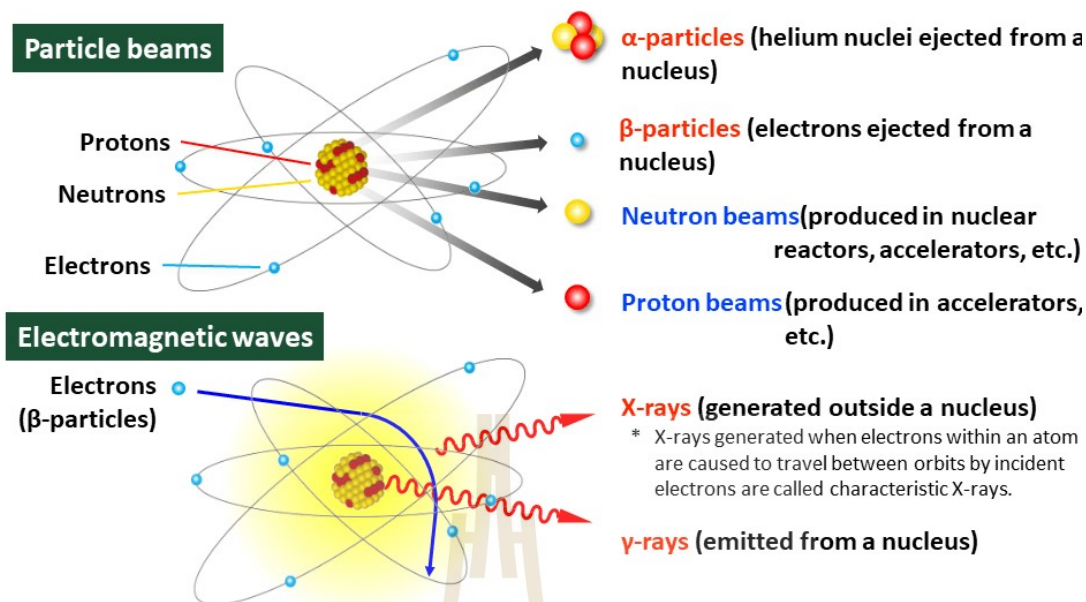


Figure 2.3 Types of Ionizing Radiation (Ministry of the Environment, 2016).

Table 2.1 Radiation dose limit (ICRP, 2007).

Type of Dose Limit	Limit on Dose from Occupational Exposure	Limit on Dose from Public Exposure
Effective Dose	20 mSv per year, averaged over defined periods of 5 years, with no single year exceeding 50 mSv	1 mSv in a year
Equivalent Dose to the Lens of the Eye	20 mSv per year, averaged over defined periods of 5 years, with no single year exceeding 50 mSv	15 mSv in a year
Equivalent Dose to the Skin Averaged over 1 cm ² of skin regardless of the area exposed	500 mSv in a year	50 mSv in a year
Equivalent Dose to the Hands and Feet	500 mSv in a year	-

nuclei.

2.2.2 Classification and utilization of neutrons

We can classify neutrons according to their energy. The details are shown in Table 2.2. At each neutron energy level, there is a wide range of usages, for example, slow neutrons can be used in civilian nuclear reactors to operate with nuclear fuel containing natural uranium or low enrichment uranium (LEU). It is also used to measure the moisture content of materials using neutron transmittance (Zhang et al., 2011). With the back scattering technique, we can measure the porosity of basements, oil,

Table 2.2 Classification of neutrons according to their energy (Alhussain and Abuhoza, 2009).

Energy regimes	Energy range
Cold Energies	below 0.01eV
Thermal	0.01eV to 0.3 eV
Epithermal	0.3 eV to 10 keV
Fast	10 keV to 20 MeV
Relativistic	>20 MeV

and natural gas (Sang et al., 2018). For carbon and hydrogen measurement in coal, it is possible to use neutron inelastic scattering (Martin et al., 1964). Neutron activation analysis is also a vital tool for metal elements (Abdel-Haleem et al., 2001). Currently, it has gained more popularity in the use of neutrons for cancer treatment (Suzuki, 2020).

2.2.3 Beta decay of a free neutron

A free neutron is an unstable particle. Its disintegration with a characteristic half-life value can be expressed by the following Eq (2.1).



where $\bar{\nu}$ is the antineutrino according to quantum mechanics theory. Particles exhibit wave particle duality as they are too small to be observed visually and moving at high speed. However, they can be studied mathematically since the electron, proton, and neutron have their own characteristic wavelengths.

2.2.4 Diffusion and slowing down of neutrons

Diffusion of neutrons occurs when neutrons travel through a medium, which can be gas, liquid, or solid. They interact with the nuclei of the atoms. A neutron can be absorbed by the nucleus or scattered, elastically or inelastically, in a collision. Absorption can cause the loss of a neutron through radiative capture or an increase in the amount of neutrons by fission. Fission neutrons have a variety of energies and travel in various directions. The position, energy, and direction of motion of the neutron will also be altered as a result of scattering. Neutrons are moved (or transported) from one

location to another, from one energy to another, and from one direction to another as a result of their interactions with nuclei in a medium. The slowing of neutrons is caused by elastic and inelastic collisions with atomic nuclei in the moderator, which normally consists of light elements such as hydrogen. The example can be seen in Figure 2.4. Slow neutrons collide with Uranium-235 (^{235}U) nuclei, splitting them apart and releasing fast neutrons. The nuclei of a graphite moderator absorb or delay the fast neutrons, allowing just enough slow neutrons to keep the fission chain reaction going at a consistent pace.

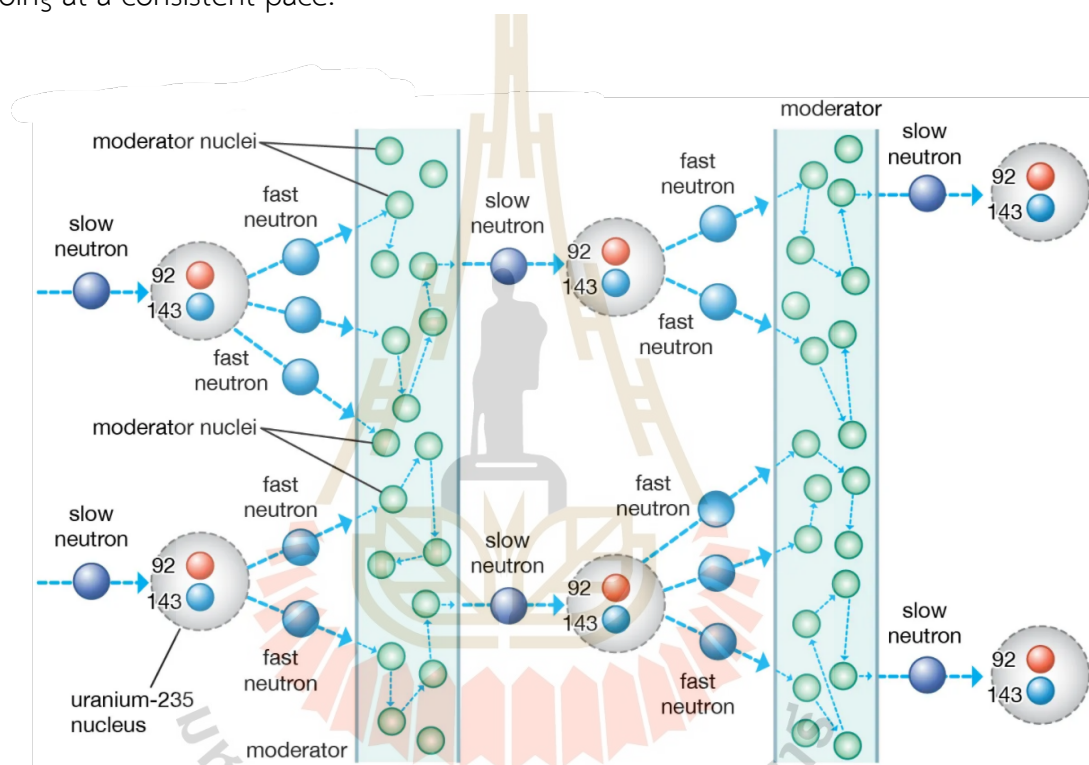


Figure 2.4 Moderator for slowing down neutrons (Encyclopædia Britannica, 2012).

2.3 Natural Rubber

Natural rubber (NR) is a rubber derived from a rubber tree. Most are *Hevea Braziliensis* species that originate from the Amazon river basin in Central America (Vaysse et al., 2012). Since 1876, NR has been a significant component of the global economy due to its great elasticity, adaptability, and durability. NR can end up in several products, such as soothers, shoes, mattresses, seals, etc.

2.3.1 Chemical formula of natural rubber

The empirical formula of natural rubber is $(C_5H_8)_n$ or isoprene in its chemical name. It mainly consists of cis-1, 4-polyisoprene (Brüning, 2015) as shown in Figure 2.5.

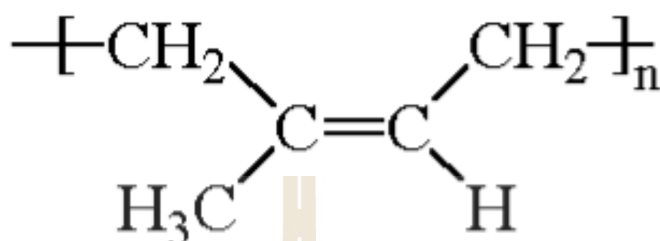


Figure 2.5 Cis (1,4) - Polyisoprene (chimicaemateriali, 2019).

2.3.2 Block rubber

Block rubber is one of the raw rubber industry's most popular products. Block rubber can be stored and transported easily since it has a long service life. The principle of producing block rubber is to harden the rubber latex into lumps and then cut them into smaller pieces. Then they are dried and extruded into a standard size of $330.0 \times 670.0 \times 170.0 \text{ mm}^3$ bars, weighing approximately 33.33 kg. The raw materials for block rubber production are latex or sheet rubber, depending on the grade of block rubber to be produced. For example, the production of block rubber grades Standard Thai Rubber (STR) XL or STR SL is very pale (L stands for light and XL stands for extra light). Latex is used as a raw material, and formic acid is used to bind rubber particles under well-controlled conditions. STR10 or STR20 block rubber grades are highly contaminated and have darker colors. They may be used as rubber sheets or rubber scraps as raw materials.

2.3.3 Epoxidized natural rubber

Epoxidized natural rubber (ENR) is one of rubber derivatives that have been improved the properties of natural rubber to make it more suitable for use in a specific field. ENR is produced by adding oxygen to the double bond of the natural rubber molecule through epoxidation, shown in Figure 2.6. Epoxidation is formed as an epoxide ring with a degree of reaction ranging from 10% to 50% (ENR10-ENR50). ENR can be prepared in both latex and dry rubber form. Due to the lesser amount of double

bonds in the structure and greater polarity than NR, ENR has better ozone resistance and air permeability (Tanrattanakul et al., 2003). ENR is therefore better resistant to heat, oil and non-polar solvents. ENR50 has a high polarity equivalent to that of nitrile butadiene rubber (NBR) with a medium acrylonitrile content. However, ENR has some disadvantages such as, ENR has lower flexibility and ENR is not resistant to heat when vulcanized with sulfur (Larpkasemsek et al., 2019).

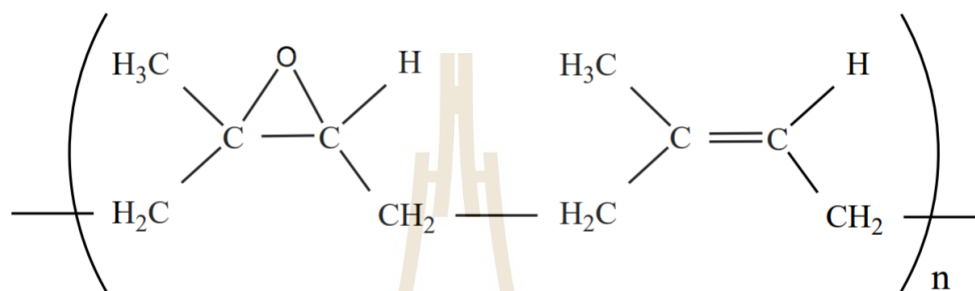


Figure 2.6 Molecular structure of epoxidised natural rubber (Surya et al., 2018).

2.4 The Main Processes of Rubber

2.4.1 Compounding formulation

The purpose of rubber formulation is to provide the rubber with the desired properties, such as flexibility, strength, and heat, by applying different rubber additives. The formula for rubber comprises:

1. Rubber, which is the main component.
2. Fillers: fillers increase the strength of the rubber. It can be divided into basic, carbon black, and non-black fillers such as silica.
3. Vulcanizing agents, such as sulfur, sulfur donors, metal oxides, peroxides, and resins, form intermolecular lattice structures.
4. Accelerators: accelerators reduce the cure time (vulcanization time) of rubber and increase the vulcanization rate. In addition, the accelerators can affect the properties of the vulcanization.
5. Activators: activators serve to stimulate the accelerator's work by forming complex compounds with the accelerator.
6. Plasticizers and/or softeners to soften rubber.
7. Age resisters such as antioxidants, antiozonant.

8. Processing aids.
9. Other additives depend on the purpose of use, such as pigments and fire retardants.

2.4.2 Softening and mixing

Softening and mixing are the most important steps in the rubber forming process. NR requires a soft grinding process before chemical mixing because NR has a large molecular weight (Miller, 2018). The viscosity of NR is reduced by the shear force of the mixer. The mixing process can ensure that the various additives are evenly distributed and dispersed throughout the rubber compounds. The crucial steps in the mixing process are

1. Incorporation, which is the first step in mixing. It consists of two mechanisms, the shear forces in the combination cause the rubber to alter format first. This permits the rubber to make greater contact with the filler on the surface. As for the second mechanism, the rubber will tear, making it smaller due to shear force.
2. Dispersion is causing a filler to break apart.
3. Distribution process is to make the components in the rubber formulation distributed randomly.
4. Plasticization is a step to decrease in viscosity of the rubber.

These four steps cannot be separated from each other. Especially, the distribution will occur throughout all the mixing period. The most commonly used mixers are two-roller mixer and internal mixer.

2.4.3 Shaping

There are numerous ways to shape the rubber. Extrusion, transfer or compression molding, and injection are often used. Molding is the most commonly utilized method since it involves pressing and curing the rubber compound. Injection molding is used to create intricate rubber product pieces. It consists of the use of pistons to transfer the heated compound into the cavity of the mold.

2.4.4 Vulcanization

Rubber vulcanization is the process that transforms rubber molecules to a network by forming a cross-linked structure. It can improve the properties of rubber, such as flexibility, strength, thermal properties, and solvent resistance. Figure 2.7 illustrates the non-forming rubber and the forming reticular structure, which could potentially consist of a group of sulfur atoms in a short chain. The cross-link occurs at the position where a sulfur atom binds between a carbon and a carbon or polyvalent metal ion.

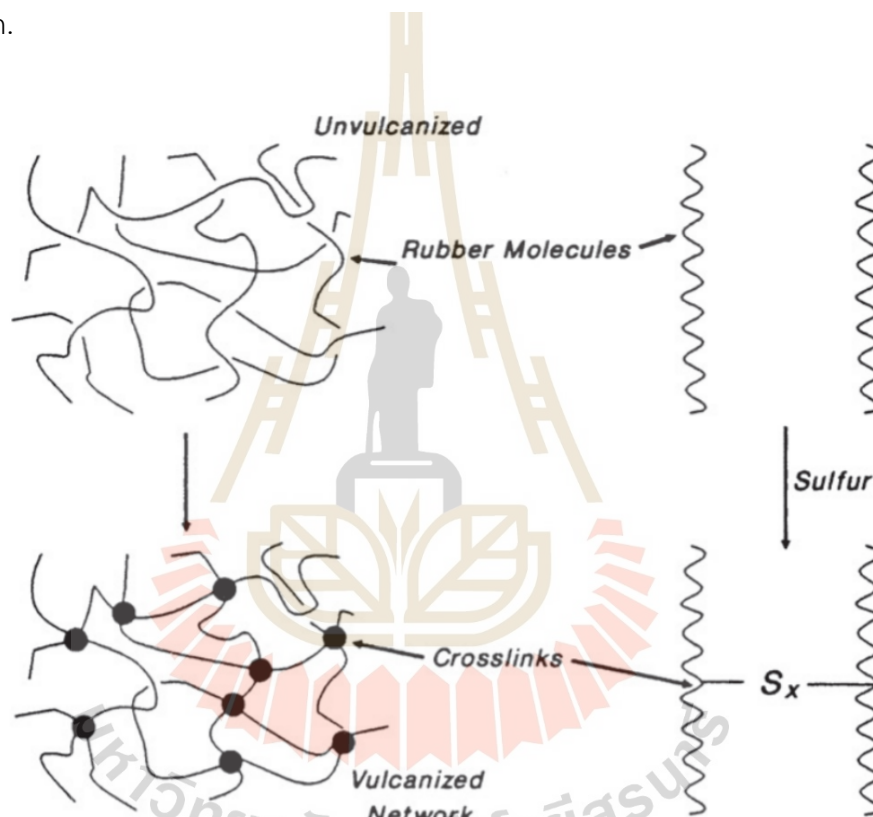


Figure 2.7 Network formation (Coran, 2013).

2.5 Rubber Analysis and Testing

2.5.1 Viscosity and curing characteristics

The viscosity and curing time of a rubber compound are critical in determining the compound's characteristics and formability. The viscosity of the rubber indicates the difficulty of mixing the additive into the rubber. Low viscosity rubber mixes with additives faster than high viscosity rubber, but rubber with too low a viscosity will cause

poor filler dispersion. Also, low viscosity rubber consumes less energy to process than high viscosity rubber.

A Mooney viscometer is used to determine the viscosity of rubber. Temperature and time for rubber viscosity testing follow the standard test methods of ASTM D1646-2004. The temperature used is 100 °C. The time required for the test is 4 minutes after 1 minute of preheating. The reading from the machine will be in the form of ML(100) 1 + 4, which is the reading parameter in the Mooney viscometer. The 100 represents measurement temperature at 100 °C, number 1 represents preheating without spindle turning for 1 minute, and number 4 shows spindle rotation for 4 minutes at approximately 2 rpm. The Mooney viscometer can measure scorch time and cure index. The scorch time is the condition at which the rubber stabilizes to determine how long it can be compounded with the chemical in the process at the temperature without vulcanization.

The Cure Rate Index (CRI) is an essential parameter in the rubber industry, particularly for natural rubber composites, due to its significant impact on the manufacturing process and the final product's properties. The curing characteristics are mostly measured by the moving die rheometer (MDR). It can perform rubber testing to determine torque, scorch time, and vulcanization time.

2.5.2 Mechanical and technological testing

Mechanical and technological tests are critical components of material fabrication. The majority of rubber's mechanical and technological tests include hardness, tear resistance, compression set, stress relaxation and creep, abrasion resistance, ozone cracking, liquid resistance, and accelerated aging or heat resistance.

2.6 Neutron Shielding

There have been many studies on materials for shielding neutron radiation. Essentially, it has to be a material with a high hydrogen content because hydrogen is similar in size to that of a neutron. There was a study of mixing Ethylene Propylene Diene Monomer (EPDM) rubber with hexagonal Boron Nitride (hBN) to be used for thermal neutron shielding composites (Güngör et al., 2019). A multilayer for shielding both neutrons and gamma in one material composite contains lead, polymethyl methacrylate (PMMA) and Boric Oxide (Mahmoud, 2018). Silicone mixed with nano materials,

Iron Oxide and Boron Carbide was also reported (Afkham et al., 2020). And also, the study of NR as a thermoplastic natural rubber with boron carbide content for thermal neutron shielding was done by Mat Zali (Mat Zali et al., 2017). For the NR mixed with Boron Carbide was investigated by Jumpee (Jumpee et al., 2020). However, there are still some issues found in various studies from the past. For example, hBN is very expensive. In the case of mixing with PMMA, the compound materials are found to be hard and unable to bend. And using natural rubber mixed with lead can be toxic and harmful to the people who are exposed to it.

2.7 Monte Carlo Transport Code

2.7.1 Introduction

MCNP5 is a general-purpose Monte Carlo N-Particle code version 5 that may be used to compute eigenvalues for critical systems and can be used for neutron, photon, electron, or coupled neutron/photon/electron transport. Researchers have conducted numerous studies using MCNP5 in neutron simulations to design neutron shielding materials, aiming to identify the most suitable materials and ingredients before using actual materials. For example, one can use MCNP5 to determine the efficiency of the designed shielding materials composed of high-density concrete, waste rubber, lead, and boron carbide (Aim-O et al., 2017). Moreover, using the MCNP5 code can also be applied to simulate the materials composite for a multi-layer sheet of materials (Jumpee et al., 2020) or a multi-layer cylinder (Mahmoud, 2018).

2.7.2 MCNP input file

Defining the correct problem is important for the simulation. To run the MCNP, we must first create the problem we want in the input file with the structure of the input file to initiate-run, as shown in Figure 2.8. For the geometry to be accurate, all the information must be defined in the input file so that the characteristics and properties of the geometry are consistent with the problem.

MCNP interprets a blank line as the end of the preceding information block. MCNP will stop reading the input file after encountering the blank line terminator. In order to discriminate between input data for tracking particles, many input cards call for a particle determinant. Figure 2.9 shows the symbols for these particles.

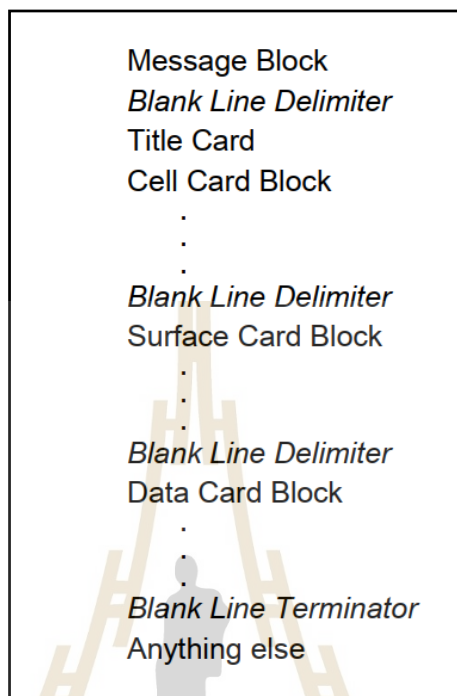


Figure 2.8 The initiate-run file of MCNP (Sweezy et al., 2003).

IPT*	Name of Particle	Symbol
Original MCNP Particles		
1	neutron (n)	n
-1	anti-neutron (n)	-n
2	photon (γ)	p
3	electron (e^-)	e
-3	positron (e^+)	-e

Figure 2.9 Symbol of original MCNP Particles (Sweezy et al., 2003).

Cell card

In defining cell cards, two forms can be defined as shown in Figure 2.10. Figure 2.11 provides a description of each parameter in cell card forms.

Form 1:	<i>j</i>	<i>m</i>	<i>d</i>	<i>geom</i>	<i>params</i>
Form 2:	<i>j</i>	LIKE	<i>n</i>	BUT	<i>list</i>

Figure 2.10 An example of a cell card form for cell card definition in MCNP (Sweezy et al., 2003).

Surface cards

Surfaces can be defined by equations, points, or macrobodies. Each of the methods is discussed below.

-Surface defined by equation

Figure 2.12, 2.13, 2.14, and 2.15 show forms and parameter descriptions for surface defined by equation.

-Axisymmetric surfaces defined by points

Axisymmetric surfaces defined by points is given in Figure 2.16, and each parameter can be described in Figure 2.17.

-Surfaces defined by macrobodies

A macrobody is a simplified, efficient way to define complex shapes in geometric modeling by using predefined forms and configuring them with specific parameters. Essentially, a macrobody acts as a template or shortcut that helps us create the shape of a given geometry tree without having to describe every surface in detail. These macrobodies are categorized into different types based on their geometric shapes.

1. BOX—Arbitrarily oriented orthogonal box

This shape represents a box where the sides (faces) are perpendicular to each other, but the box itself can be oriented in any direction in 3D space. This means we can rotate the box freely around any axis, and it remains a box, just oriented differently.

2. RPP—Rectangular parallelepiped

A rectangular parallelepiped is a 3D shape with six rectangular faces, and all its edges are aligned with the coordinate axes. It is like a stretched or squashed box where the opposite faces are parallel, and all angles between adjacent faces are 90 degrees.

3. SPH—Sphere

This is a perfectly symmetrical 3D shape where every point on the surface is equidistant from the center. In geometric terms, it is defined by its center point and radius.

4. RCC—Right circular cylinder

A right circular cylinder is a cylinder with circular bases that are aligned directly above each other, making the axis of the cylinder perpendicular to these bases. The "right" in its name refers to the fact that the sides are perpendicular to the base.

5. RHP or HEX—Right hexagonal prism

This shape is a prism with two identical hexagonal (six-sided) bases that are parallel and aligned directly above each other. The "right" means the prism's height (distance between the bases) is perpendicular to the hexagonal faces.

6. REC—Right elliptical cylinder

Similar to the RCC, this is a cylinder with elliptical bases instead of circular ones. The height of the cylinder is perpendicular to the bases, making it a "right" elliptical cylinder.

7. TRC—Truncated right angle cone

This is a cone that has been "truncated" or cut off at a certain height. It still has a circular base, but the top is flat, forming a smaller circle parallel to the base.

8. ELL—Ellipsoid

An ellipsoid is a 3D shape that resembles a stretched or compressed sphere, where all cross-sections are ellipses. It can be described by its three axes of different lengths, with each axis corresponding to the width, height, and depth.

9. ED—Wedge

A wedge is a shape that looks like a triangular prism with a slanted top. It can be thought of as a rectangular block with one end sliced off at an angle, forming a tapered edge.

10. ARB—Arbitrary polyhedron

This shape is the most flexible and complex, as it can have any number of faces with any shape. It is used to create irregular or custom 3D objects that do not fit the standard geometric shapes.

Figures like 2.18, and Figure 2.19 (for BOX) and Figure 2.20, and Figure 2.21 (for RPP) typically illustrate these shapes and their corresponding parameters, providing a visual guide to understanding how each macrobody is configured and used in geometric modeling.

Material data card

The material data card is used to define the materials present in a simulation. There are several forms that can be specified within this card, each serving a different purpose or providing different options for material specification.

-M Form

The "M" form is the most basic and commonly used method for specifying materials in MCNP. It defines a material by listing the elemental or isotopic compositions along with their corresponding atomic fractions. This form is typically used when we need to define a material that consists of specific elements or isotopes.

-MT Form

The "MT" form is an extension of the M form, which includes additional information like temperature. It allows for specifying the temperature of the material, which can affect the cross-sections used in the simulation.

-T Form

The "T" form is used to specify the thermal treatment of the material. This form is important when we need to define materials that have undergone certain thermal processes, which can alter their physical properties.

-AB Form

The "AB" form specifies absorption materials, particularly for use in criticality safety calculations. It helps to define materials that have significant neutron absorption properties.

-XS Form

The "XS" form is used to override default cross-sections or to provide user-defined

cross-sections for certain isotopes or elements. This form is essential when we need to use specific cross-section data that differs from the standard library.

-VOID Form

The "VOID" form is used to specify regions that are voids or have no material. This is particularly useful in simulations where we need to define empty spaces or vacuum regions.

-PIKMT Form

The "PIKMT" form is an advanced option that allows for the specification of special treatment of certain materials or interactions within the simulation. It is used when more complex material behavior needs to be modeled.

-MGOPT Form

The "MGOPT" form provides options for multigroup treatment of materials. This is used when the simulation involves energy-dependent neutron interactions that require multigroup cross-section data.

-DRXS Form

The "DRXS" form allows for direct specification of cross-sections in a detailed manner. It gives the user control over the exact cross-section data used in the simulation, which is useful for highly specialized cases.

In the upcoming section, we will provide an example of material specification using the M form, as illustrated in Figure 2.22, 2.23, and 2.24. These figures will show how materials are defined using this form, with details on how to list the elements or isotopes and their atomic fractions.

Source specification

The source specification is used to define the characteristics of the radiation source to be simulated. It provides information about the type, energy, location, direction, and intensity of the particles emitted by the source. In MCNP, the source specification consists of several parameters that define the source's properties by providing the type of particle emitted by the source, such as neutrons, photons, electrons, or positrons. Energy distribution is a parameter that describes the energy spectrum of the emitted particles. It can be defined using various distributions, such as monoenergetic, continuous, or discrete energy values. Moreover, the spatial distribution determines

the spatial distribution of source particles. It can be defined as a point source at a specific location or distributed over a volume using various geometries, such as spheres or cylinders. Additionally, directional distribution specifies the direction in which the particles are emitted from the source. This can be isotropic (equally likely in all directions) or anisotropic (preferential emission in specific directions). Furthermore, intensity is defined as the number of particles emitted per unit time. It can be specified as a constant value, a function of time, or other parameters. The key abbreviations used for source specification include below.

-SDEF (Source definition)

The SDEF card is the most commonly used form for defining a source in MCNP. It allows users to specify the essential characteristics of the source, such as its type (point, surface, or volumetric), energy distribution, spatial distribution, angular distribution, and time distribution. The SDEF card is highly flexible, enabling the modeling of a wide variety of source configurations.

-SI (Source input)

The SI card is used to define the set of values that a source parameter can take. For example, if we are defining a spatial distribution for a source, the SI card might specify the possible coordinates or positions where particles can originate.

-SP (Source probability)

The SP card is used in conjunction with the SI card to assign probabilities to the values defined by SI. This allows for the creation of probabilistic distributions for various source parameters, such as energy or position.

-SB (Source biasing)

The SB card is used for source biasing, which is a technique to improve the efficiency of simulations by modifying the source distribution to focus on areas of interest. It adjusts the probability distributions to enhance the sampling of particles in specific regions or with specific characteristics.

-DS (Discrete source) The DS card is used for defining a discrete source, where particles are emitted from a fixed set of positions or with specific energies. This card is useful when the source is not continuous but rather has distinct, well-defined emission points or energies.

-SC (Source correlation)

The SC card allows for the correlation of different source parameters, ensuring that certain parameters vary together in a controlled way. For example, it can link energy and angular distributions so that they change in a coordinated manner.

-KCODE (K-effective calculation)

The KCODE card is used for criticality calculations, where the objective is to find the effective multiplication factor (K-effective) of a system. This card defines the source settings necessary for these calculations, such as the number of particles per cycle and the number of cycles.

-KSRC (K-effective source definition)

The KSRC card specifies the initial source distribution for criticality calculations using the KCODE card. It allows the user to define where the initial neutrons are emitted in the system.

-BURN (Burnup calculation)

The BURN card is used in simulations that involve fuel burnup, where the material composition changes over time due to nuclear reactions. This card helps to define the source terms associated with the changing material as it burns up during the simulation.

-SSW (Surface source write)

The SSW card allows for the creation of a surface source file, where particles crossing a specified surface are recorded. This file can then be used as an input source for another simulation, enabling complex, multi-step simulations.

-SSR (Surface source read)

The SSR card is used to read a surface source file created by the SSW card. It imports the particle data from the file to define the source in the new simulation, allowing for the continuation of a simulation or the use of a source defined by another simulation.

-SOURCE

The SOURCE card is a general-purpose card that allows users to define a custom source that does not fit neatly into the predefined forms like SDEF. It provides the flexibility to describe more complex source behaviors and characteristics.

-SRCDX (Source expansion)

The SRCDX card is used to expand the source definition, often in conjunction with SDEF or SOURCE cards. It provides additional options for fine-tuning the source characteristics beyond the standard parameters.

The Figure 2.25 show the example of source specification of general source (SDEF) form and keyword used in form.

2.7.3 Tally specification

In MCNP, tally specifications are essential for measuring various physical quantities of interest, such as particle flux, energy deposition, or dose, during a simulation. MCNP offers several types of tallies, each tailored to measure different aspects of the simulation.

-Surface and cell tallies (Tally types 1, 2, 4, 6, and 7)

These tally types measure quantities like particle flux or current across surfaces (Surface Tallies) or within cells (Cell Tallies). For example, Tally type 1 measures the surface current, and Tally type 4 measures the flux within a cell.

-Detector tallies (Tally type 5)

Tally type 5 is used to simulate a detector response, measuring the interaction of particles with a point detector in the system. It is often used for simulating radiation detectors.

-Pulse-height tally (Tally type 8)

Tally type 8 measures the energy deposited in a detector or material, providing information akin to what we see in a pulse-height spectrum from a radiation detector. Each tally is defined using a set of tally cards, which provide additional details and modifiers:

-FC (Tally comment)

This card is used to add comments or labels to tallies for clarity, helping to identify the purpose or configuration of each tally in the input file.

-E (Tally energy)

The E card specifies the energy bins or ranges for the tally, allowing the user to divide the results by energy intervals, which is useful for energy-dependent studies.

-T (Tally time)

The T card allows the user to specify time intervals for the tally, enabling the measurement of time-dependent quantities in a dynamic simulation.

-C (Cosine card)

The C card is used to define angular bins based on the cosine of the angle between the particle's direction and a specified axis. This is crucial for studying angular distributions.

-FQ (Print hierarchy)

The FQ card controls the format and hierarchy of the tally output, determining how detailed and structured the printed tally results will be.

-FM (Tally multiplier)

The FM card allows the application of multipliers to tally results, which can be used to scale the results or combine different tally contributions.

-DE and DF (Dose Energy and Dose Function)

The DE and DF cards are used to calculate dose-related quantities by applying energy-dependent conversion factors to the tally results.

-EM (Energy multiplier)

The EM card applies an energy-dependent multiplier to the tally results, which can be used to account for factors like energy deposition efficiency.

-TM (Time multiplier)

The TM card applies a time-dependent multiplier, allowing for the scaling of results based on the duration of the simulation or specific time intervals.

-CM (Cosine multiplier)

The CM card applies a multiplier based on the cosine of the angle, used for angularly dependent scaling of the tally results.

-CF (Cell-Flagging)

The CF card is used to flag or identify specific cells in the tally, which can help isolate or highlight results from particular regions of the geometry.

-SF (Surface-flagging)

Similar to the CF card, the SF card flags specific surfaces, allowing the user to focus on tally results associated with particular boundaries or interfaces.

-FS (Tally segment)

The FS card divides a tally into segments, enabling detailed analysis of different parts of a simulation, such as breaking down a detector response by energy or position.

-SD (Segment divisor)

The SD card specifies how the tally segments are divided, controlling the granularity of the segmentation and ensuring that the results are properly normalized.

-FU (Special tally or TALLYX input)

The FU card is used for special tally operations or to input data for a user-defined tally function (TALLYX), which allows for custom tally calculations.

-FT (Special treatments for tallies)

The FT card provides options for applying special treatments or corrections to the tally results, such as variance reduction techniques or special scoring methods.

-TALLYX (User-supplied subroutine)

The TALLYX card allows users to implement custom tallying routines by writing their own subroutines, providing maximum flexibility for advanced users.

-TF (Tally fluctuation)

The TF card is used to calculate the statistical fluctuations or uncertainties associated with tally results, providing an estimate of the precision of the simulation.

-The radiography tally

This tally type is specialized for simulating radiographic imaging, allowing the user to measure the transmitted or scattered radiation through an object, mimicking an X-ray or neutron imaging process.

-TALNP (Control printing of tallies)

The TALNP card controls how tally results are printed or output, allowing users to manage the level of detail and formatting of the tally results in the output file.

Table 2.3 MCNP tally type.

Mnemonic	Tally Description	Fn units	*Fn units
F1:<pl>	Current integrated over a surface	particles	MeV
F2:<pl>	Flux averaged over a surface	particles/cm ²	MeV/cm ²
F4:<pl>	Flux averaged over a cell	particles/cm ²	MeV/cm ²
F5a:N or F5a:P	Flux at a point or ring detector	particles/cm ²	MeV/cm ²
F6:<pl>	Energy deposition averaged over a cell	MeV/g	jerks/g
+F6	Collision heating	MeV/g	N/A
F7:N	Fission energy deposition averaged over a cell	MeV/g	jerks/g
F8:<pl>	Energy distribution of pulses created in a detector by radiation	pulses	MeV
+F8:<pl>	Deposition	charge	N/A

-PERT (Perturbation)

The PERT card is used for perturbation analysis, which allows the user to study how small changes in the system (such as material composition or geometry) affect the tally results.

-TMESH (The mesh tally)

The TMESH card allows for tallying results on a spatial mesh, enabling the user to obtain detailed spatial distributions of quantities like flux, energy deposition, or dose across the simulation domain.

Users can choose any kind of information they wish to obtain from the Monte Carlo calculation using tally cards. Options include measures such as surface current, flux at a place, region heating, etc. By combining the cards mentioned in this section, user can obtain information needed. Only the F card is necessary to acquire tally results. The other tally cards offer a variety of other capabilities. The other tally types can be seen in Table 2.3.

The following are the tally types and particle types used to identify the tallies. In addition to provide a particle designator (pl), which is selected from 2.9 , tallies are given the numbers 1, 2, 4, 5, 6, 7, 8, or increments of 10 thereof. Therefore, we are free to create as many variations of any basic tally as we need, each with a different set of energy bins, flagging bins, or other bins. For examples, the neutron cell flux tallies F4:N, F14:N, F104:N, and F234:N are all valid. They could all be for the same cell(s), but with various energy or multiplier bins. Similar to F5:P, F15:P, and *F305:P, these measurements come from photon point detectors. It is not allowed to store both an F1:N card and an F1:P card in the same INP file. The surface and cell tallies form of

Input Parameter	Description
<i>j</i>	Cell number assigned by the user. Restriction: $1 \leq j \leq 99999$ Restriction: If the cell is affected by a transformation, $1 \leq j \leq 999$ (See Sections 5.2.3.5 and 5.2.3.7.)
<i>m</i>	Material number if the cell is not a void. If $m > 0$, the cell contains material <i>m</i> , which is specified on the M card located in the data-card section of the INP file. If $m = 0$, the cell is a void. Restriction: $1 \leq m \leq 99999$
<i>d</i>	Cell material density. If $d > 0$, interpret the value as the atomic density in units of 10^{24} atoms/cm ³ (i.e., atoms/b-cm). If $d < 0$, interpret the value as the mass density in units of g/cm ³ . This parameter is absent if the cell is a void.
<i>geom</i>	Specification of the geometry of the cell. This specification consists of signed surface numbers and Boolean operators that specify how the regions bounded by the surfaces are to be combined. Boolean operators include the following: “<space>” indicates intersection, “:” indicates union; and “#” indicates complement.
<i>params</i>	Optional specification of cell parameters by entries in the KEYWORD=value form. Allowed keywords include IMP, VOL, PWT, EXT, FCL, WWN, DXC, NONU, PD, TMP, U, TRCL, LAT, and FILL.
<i>n</i>	Name of another cell. Restriction: Cell card for cell <i>n</i> must appear in the INP file before the cell card for cell <i>j</i> .
<i>list</i>	Set of KEYWORD=value specifications that define the attributes that differ between cells <i>n</i> and <i>j</i> . Allowed keywords include MAT (material number) and RHO (density) as well as the cell parameter keywords IMP, VOL, PWT, EXT, FCL, WWN, DXC, NONU, PD, TMP, U, TRCL, LAT, and FILL.

Figure 2.11 The description of each parameter in the cell card form (Sweezy et al., 2003).

Form: $j \ k \ a \ list$

Figure 2.12 Surface defined by equation form (Sweezy et al., 2003).

Input Parameter	Description
j	Surface number assigned by the user. Restriction: $1 \leq j \leq 99999$ Restriction: If surface defines a cell that is transformed with TRCL or TR, $1 \leq j \leq 999$. See Sections 5.2.3.5 and 5.2.3.7.
$*j$	Reflecting surface number. A particle track that hits a reflecting surface is reflected specularly.
$+j$	White boundary surface number. A particle hitting a white boundary is reflected with a cosine distribution relative to the surface normal.
k	If $k > 0$, the value specifies a transformation number k of a TR card. If $k < 0$, the value specifies that surface j is periodic with surface k . If k is absent or $k = 0$, then no coordinate transformation is specified.
a	Equation mnemonic from Table 5-4 that specifies the type of surface.
$list$	One to ten numerical entries required to define a surface.

Figure 2.13 The description of each parameter in the surfaces defined by equation form (Sweezy et al., 2003).

Mnemonic	Type	Description	Equation	Card Entries
P	Plane	General	$Ax + By + Cz - D = 0$	A B C D
PX		Normal to x-axis	$x - D = 0$	D
PY		Normal to y-axis	$y - D = 0$	D
PZ		Normal to z-axis	$z - D = 0$	D
SO	Sphere	Centered at Origin	$x^2 + y^2 + z^2 - R^2 = 0$	R
S		General	$(x - \bar{x})^2 + (y - \bar{y})^2 + (z - \bar{z})^2 - R^2 = 0$	$\bar{x} \ \bar{y} \ \bar{z} \ R$
SX		Centered on x-axis	$(x - \bar{x})^2 + y^2 + z^2 - R^2 = 0$	$\bar{x} \ R$
SY		Centered on y-axis	$x^2 + (y - \bar{y})^2 + z^2 - R^2 = 0$	$\bar{y} \ R$
SZ		Centered on z-axis	$x^2 + y^2 + (z - \bar{z})^2 - R^2 = 0$	$\bar{z} \ R$
C/X	Cylinder	Parallel to x-axis	$(y - \bar{y})^2 + (z - \bar{z})^2 - R^2 = 0$	$\bar{y} \ \bar{z} \ R$
C/Y		Parallel to y-axis	$(x - \bar{x})^2 + (z - \bar{z})^2 - R^2 = 0$	$\bar{x} \ \bar{z} \ R$
C/Z		Parallel to z-axis	$(x - \bar{x})^2 + (y - \bar{y})^2 - R^2 = 0$	$\bar{x} \ \bar{y} \ R$
CX		On x-axis	$y^2 + z^2 - R^2 = 0$	R
CY		On y-axis	$x^2 + z^2 - R^2 = 0$	R
CZ		On z-axis	$x^2 + y^2 - R^2 = 0$	R
K/X	Cone	Parallel to x-axis	$\sqrt{(y - \bar{y})^2 + (z - \bar{z})^2} - t(x - \bar{x}) = 0$	$\bar{x} \ \bar{y} \ \bar{z} \ t^2 \pm 1$
K/Y		Parallel to y-axis	$\sqrt{(x - \bar{x})^2 + (z - \bar{z})^2} - t(y - \bar{y}) = 0$	$\bar{x} \ \bar{y} \ \bar{z} \ t^2 \pm 1$
K/Z		Parallel to z-axis	$\sqrt{(x - \bar{x})^2 + (y - \bar{y})^2} - t(z - \bar{z}) = 0$	$\bar{x} \ \bar{y} \ \bar{z} \ t^2 \pm 1$
KX		On x-axis	$\sqrt{y^2 + z^2} - t(x - \bar{x}) = 0$	$\bar{x} \ t^2 \pm 1$
KY		On y-axis	$\sqrt{x^2 + z^2} - t(y - \bar{y}) = 0$	$\bar{y} \ t^2 \pm 1$
KZ		On z-axis	$\sqrt{x^2 + y^2} - t(z - \bar{z}) = 0$	$\bar{z} \ t^2 \pm 1$

± 1 used only for 1 sheet cone

Figure 2.14 The equation mnemonic to describe a parameter that specifies the type of surface (Sweezy et al., 2003).

Mnemonic	Type	Description	Equation	Card Entries
SQ	Ellipsoid Hyperboloid Paraboloid	Axis not parallel to x-, y-, or z-axis	$A(x-\bar{x})^2 + B(y-\bar{y})^2 + C(z-\bar{z})^2 + 2D(x-\bar{x}) + 2E(y-\bar{y}) + 2F(z-\bar{z}) + G = 0$	A B C D E F G \bar{x} \bar{y} \bar{z}
GQ	Cylinder Cone Ellipsoid Hyperboloid Paraboloid	Axes not parallel to x-, y-, or z-axis	$Ax^2 + By^2 + Cz^2 + Dxy + Eyz + Fzx + Gx + Hy + Jz + K = 0$	A B C D E F G H J K
TX TY TZ	Elliptical or Circular Torus.	Axis is parallel to x-, y-, or z-axis	$(x-\bar{x})^2/B^2 + (\sqrt{(y-\bar{y})^2 + (z-\bar{z})^2} - A)^2/C^2 - 1 = 0$ $(y-\bar{y})^2/B^2 + (\sqrt{(x-\bar{x})^2 + (z-\bar{z})^2} - A)^2/C^2 - 1 = 0$ $(z-\bar{z})^2/B^2 + (\sqrt{(x-\bar{x})^2 + (y-\bar{y})^2} - A)^2/C^2 - 1 = 0$	\bar{x} \bar{y} \bar{z} A B C \bar{x} \bar{y} \bar{z} A B C \bar{x} \bar{y} \bar{z} A B C
X Y Z P	Surfaces defined by points (See Sections 5.2.2.2 and 5.2.2.3)			
BOX RPP SPH RCC RHP or HEX REC TRC ELL WED ARB	Surfaces defined by macrobodies (See Section 5.2.2.4)			

Figure 2.15 The equation mnemonic to describe a parameter that specifies the type of surface (Sweezy et al., 2003), continue.

Form: *j n a list*

Figure 2.16 Axisymmetric surfaces defined by points form (Sweezy et al., 2003).

Input Parameter	Description
<i>j</i>	Surface number assigned by user. Restriction: $1 \leq j \leq 99999$ Restriction: $1 \leq j \leq 999$ if <i>j</i> is the surface number of a repeated structure or if surface <i>j</i> defines a cell that is transformed with TRCL. See Section 5.2.3.5.
<i>n</i>	Transformation number on TR card. If <i>n</i> is absent, then no coordinate transformation is specified.
<i>a</i>	The letter X, Y, or Z.
<i>list</i>	One to three coordinate pairs.

Figure 2.17 The description of each parameter in axisymmetric surfaces defined by points form (Sweezy et al., 2003).

BOX $v_x v_y v_z a1_x a1_y a1_z a2_x a2_y a2_z a3_x a3_y a3_z$

Figure 2.18 Macrobody box form (Sweezy et al., 2003).

Input Parameter	Description
$v_x v_y v_z$	The x, y, z coordinates of corner.
$a1_x a1_y a1_z$	Vector of 1 st side.
$a2_x a2_y a2_z$	Vector of 2 nd side.
$a3_x a3_y a3_z$	Vector of 3 rd side.

Note: All corners are 90°.

Figure 2.19 Macrobody box form parameter description (Sweezy et al., 2003).

RPP $x_{min} x_{max} y_{min} y_{max} z_{min} z_{max}$

Figure 2.20 The rectangular parallelepiped form (Sweezy et al., 2003).

Input Parameter	Description
$x_{min} x_{max}$	Termini of box sides normal to the x-axis.
$y_{min} y_{max}$	Termini of box sides normal to the y-axis.
$z_{min} z_{max}$	Termini of box sides normal to the z-axis.

Figure 2.21 The description of each parameter in the rectangular parallelepiped form (Sweezy et al., 2003).

Form: $Mm\ zaid_1\ fraction_1\ zaid_2\ fraction_2\ \dots\ [KEYWORD=value(s)\ \dots]$

Figure 2.22 The material specification of M form (Sweezy et al., 2003).

Input Parameter	Description
m	Arbitrary material number; same as material number, m , on cell card (Section 5.2.1). When $m=0$, keyword entries on that card are applied to all other M cards (see note below). Restriction: $0 \leq m \leq 99999$.
$zaid_i$	Either a full ZZZAAA.abX or partial ZZZAAA element or nuclide identifier for each constituent, where a) ZZZ represents the atomic number; b) AAA, if $AAA > 0$, represents the atomic mass number, and if $AAA=000$ indicates a naturally occurring element (valid for $1 \leq ZZZ \leq 92$); c) ab is the alphanumeric library identifier; and d) X is the class of data. To represent a metastable isotope, adjust the AAA value using the following convention: $AAA' = (AAA+300) + (m \times 100)$, where m is the metastable level and $m=1, 2, 3, \text{ or } 4$.
$fraction_i$	Fraction of the i^{th} constituent in the material, where if $fraction > 0$, then the value is interpreted as an atomic fraction and if $fraction < 0$, then the value is interpreted as the weight fraction. Atomic and weight fractions may not both appear on a single M card.

Figure 2.23 The description of each parameter in the material specification of M form.

Input Parameter	Description
Keyword	Value
GAS	Flag for density-effect correction to electron stopping power. If GAS=0, calculation appropriate for material in the condensed (solid or liquid) state is used (DEFAULT), or If GAS=1, calculation appropriate for material in the gaseous state used.
ESTEP= <i>n1</i>	Causes the number of electron sub-steps per energy step to be increased to <i>n1</i> for the material. Both the default value and the ESTEP value actually used are printed in Table 85 in the output file. (DEFAULT: internally set)
HSTEP= <i>n2</i>	Causes the number of proton or other charged-particle sub-steps (exclusive of electrons, but including heavy ions) per energy step to be increased to <i>n2</i> for the material. If ESTEP is specified and HSTEP is not, then the ESTEP value is used for HSTEP. Both the default value and the HSTEP value actually used are printed in Table 85 in the output file. (DEFAULT: internally set)
NLIB= <i>id</i>	Changes the default neutron table identifier to the string <i>id</i> . (DEFAULT: blank string, which selects the first matching entry in XSDIR)
PLIB= <i>id</i>	Changes the default photon table identifier to <i>id</i> . (DEFAULT: first match in XSDIR)
PNLIB= <i>id</i>	Changes the default photonuclear table identifier to <i>id</i> . (DEFAULT: first match in XSDIR)
ELIB= <i>id</i>	Changes the default electron table identifier to <i>id</i> . (DEFAULT: first match in XSDIR)
HLIB= <i>id</i>	Changes the default proton table identifier to <i>id</i> . (DEFAULT: first match in XSDIR)
COND	Sets conduction state of a material only for the EL03 electron-transport evaluation. If COND<0, material is a nonconductor. If COND=0, material is a nonconductor if there is at least one nonconducting component; otherwise it is a conductor (DEFAULT) If COND>0, material is a conductor if there is at least one conducting component.

Figure 2.24 The description of each keyword parameter in the material specification of M form (Sweezy et al., 2003).

Form: SDEF KEYWORD= <i>value(s)</i> ...

Figure 2.25 The general source (SDEF) specification form (Sweezy et al., 2003).

Keyword	Value
CEL	Cell number. [DEFAULT: Determined from XXX, YYY, ZZZ (the position of the particle), and possibly UUU, VVV, WWW (the direction of the flight of the particle)].
SUR	Surface number. [DEFAULT: SUR=0, which indicates a cell (volume) source] Always required when source points lie on the boundary (surface) of a cell.
ERG [†]	Kinetic energy (MeV). (DEFAULT: ERG=14)
TME	Time (shakes). (DEFAULT: TME=0)
DIR	μ , the cosine of the angle between \vec{VEC} and UUU, VVV, WWW. (Azimuthal angle is always sampled uniformly in 0° to 360°.) (DEFAULT for volume source: μ is sampled uniformly in -1 to 1, i.e., the source is isotropic.) (DEFAULT for surface source: $p(\mu)=2\mu$ in 0 to 1, i.e., cosine distribution.)
VEC	Reference vector for DIR in vector notation. (DEFAULT for volume source: Required unless source is isotropic.) (DEFAULT for surface source: Vector normal to the surface with sign determined by NRM.)
NRM	Sign of the surface normal. (DEFAULT: NRM=+1)
POS	Reference point for position sampling in vector notation. (DEFAULT POS=0, 0, 0)
RAD	Radial distance of the position from POS or AXS. (DEFAULT: RAD=0)
EXT	For a volume source is the distance from POS along AXS. For a surface source is the cosine of angle from AXS. (DEFAULT: EXT=0)
AXS	Reference vector for EXT and RAD in vector notation. (DEFAULT: No direction)
X	X-coordinate of position. (DEFAULT: X=0)
Y	Y-coordinate of position. (DEFAULT: Y=0)
Z	Z-coordinate of position. (DEFAULT: Z=0)
CCC	Cookie-cutter cell. (DEFAULT: no cookie-cutter cell)
ARA	Area of surface. (Required only for direct contributions to point detectors from plane surface source.) (DEFAULT: none)
WGT	Particle weight (input as explicit value only). (DEFAULT: WGT=1)
TR	Source transformation number. A corresponding TR card is required. (Section 5.2.3.7)
EFF	Rejection efficiency criterion for position sampling (input as explicit value only). (DEFAULT: EFF=0.01)

Figure 2.26 The general source (SDEF) keyword (Sweezy et al., 2003).

Simple Form:	$F_n: \langle pl \rangle \quad s_1 \dots s_k$
General Form:	$F_n: \langle pl \rangle \quad s_1 (s_2 \dots s_3) (s_4 \dots s_5) s_6 s_7 \dots T$

Figure 2.27 The surface and cell tallies form of tally types 1, 2, 4, 6, and 7 (Sweezy et al., 2003).

CHAPTER III

PROCESSING OF NEUTRON SHIELDING MATERIAL BASED ON NATURAL RUBBER AND BORON CARBIDE COMPOSITE

This chapter describes the fabrication of a neutron shielding material based on natural rubber and boron carbide composite. We provide consideration given to the selection of various materials. Mixture design is used to study the effects of compound materials that occur in various quantities, including the use of various tools and conditions in the production process to get the sample materials. Sample materials were tested for both mechanical properties and neutron shielding properties.

3.1 Introduction

In the field of radiation protection, the development of efficient neutron shielding materials is important to ensure the safety of personnel and the environment. Among the various materials explored, the combination of natural rubber and boron carbide has emerged as a promising option for neutron shielding. Natural rubber, renowned for its flexibility, durability, and ease of processing, serves as an ideal matrix for the incorporation of neutron-absorbing boron carbide particles. This composite material offers a unique synergy, harnessing the advantageous properties of both constituents to achieve enhanced shielding performance. The process involved in the fabrication of neutron shielding material based on natural rubber and boron carbide requires careful consideration of vulcanized characterization and mechanical properties. By effectively controlling these parameters, it is possible to produce a composite material that not only exhibits outstanding neutron shielding properties but also possesses properties suitable for use in practical applications. This work highlights the significance of the processing techniques and the potential of the natural rubber-boron carbide composite in neutron shielding, paving the way for advancements in radiation protection technologies.

The aim this work is to develop a neutron shielding material with appropriate characteristics for its intended usage. This includes both the material's intrinsic qualities and its capability to successfully block neutron radiation. The process of making neutron shielding material based on natural rubber and boron carbide is shown in Figure 3.1. The final product can satisfy the criteria and standards required for its use in various radiation shielding scenarios by carefully balancing both variables.

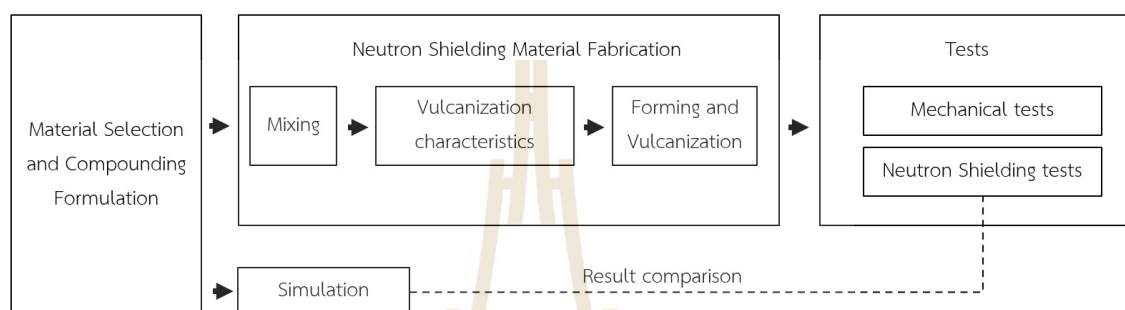


Figure 3.1 Research procedure.

3.2 Material and Method

Natural rubber and boron carbide were the primary aims of this study, so both the material selection process and the manufacturing process were largely conducted using the natural rubber.

3.2.1 Material selection and compounding formulation

In the fabrication of neutron shielding materials from a natural rubber (NR) and boron carbide (B_4C), compound selection is the most crucial. It impacts neutron absorption, homogeneous dispersion, mechanical properties, thermal stability, the manufacturing procedure, and compliance with regulations. By judiciously selecting the appropriate additives, the shielding material can effectively attenuate neutron radiation.

For the reason of its capacity to act as a neutron capturer, B_4C was utilized in this investigation. The composition included carbon black to provide reinforcement. To make the molecules of rubber stick together, sulfur and dicumyl peroxide (DCP) were used. The primary accelerator, the N-cyclohexylbenzothiazole-2-sulfenamide (CBS) compound, served as the accelerating agent for the vulcanization reaction. Because

Table 3.1 Compounding of formula.

Materials	Function	Formula (Per hundred rubber (phr))									
		F1	F2	F3	F4	F5	F6	F7	F8	F9	F10
NR	Polymeric Material	100.0	100.0	100.0	100.0	100.0	0.0	50.0	100.0	100.0	100.0
ENR	Polymeric Material	0.0	0.0	0.0	0.0	0.0	100.0	50.0	0.0	0.0	0.0
B ₄ C	Neutron absorber	0.0	20.0	40.0	60.0	139.0	40.0	40.0	40.0	40.0	40.0
Carbon black	Filler	30.0	30.0	30.0	30.0	30.0	30.0	30.0	60.0	30.0	30.0
Stearic acid	Activator	2.0	2.0	2.0	2.0	2.0	2.0	2.0	2.0	2.0	0.0
Zinc oxide	Activator	4.0	4.0	4.0	4.0	4.0	4.0	4.0	4.0	4.0	0.0
CBS	Primary accelerator	0.5	0.5	0.5	0.5	0.5	0.5	0.5	0.5	1.0	0.0
TMTM	Secondary accelerator	0.6	0.6	0.6	0.6	0.6	0.6	0.6	0.6	0.6	0.0
Sulphur	Crosslinking agent	2.0	2.0	2.0	2.0	2.0	2.0	2.0	2.0	2.0	0.0
DCP	Crosslinking agent	0.0	0.0	0.0	0.0	0.0	0.0	0.0	0.0	0.0	5.0

of its excellent forming safety, CBS was utilized as the major accelerator in this process. Since the stabilizing reaction of tetramethylthiuram monosulfide (TMTM) is significantly slower than that of the dithiocarbonate group, it is typically used as a secondary accelerator in conjunction with a faster accelerator. Zinc oxide and stearic acid were selected to serve as activators for the reaction's accelerator since they are not only readily available but also very affordable. Table 3.1 presents ten different formulations, each of which contains a different B₄C content of 0, 20, 40, 60, and 139.6 (50 weight percent of B₄C) parts per hundred rubber (phr). These formulas are designated by the letters F1, F2, F3, F4, and F5, respectively, where F is an abbreviation for formula. The process of replacing NR with ENR is referred to as F6. F7 is the abbreviation for a mixer that has an equal proportion of NR and ENR. F8 is a formula that raises the amount of carbon black contained in NR-based materials to 60 phr. F9 is an additional formula that varies from the others in terms of the principal accelerator that it contains, CBS at 1 phr in an NR base. The F10 formulation, which contained DCP as both the activation and vulcanization component, was the last formulation to be examined as part of this research.

3.2.2 Neutron shielding material fabrication

In order to fabricate the rubber-based polymer material used in neutron radiation shielding, several materials must first be mixed together in the rubber, and then the material's curing properties must be examined. The best values for the preservation of composite materials can be obtained by using compounded rubber.

Table 3.2 The formula for each sample in gram unit.

Materials	Formula (gram)									
	F1	F2	F3	F4	F5	F6	F7	F8	F9	F10
NR	179.73	157.13	139.59	125.57	89.54	0.00	69.79	119.56	139.20	142.86
ENR	0.00	0.00	0.00	0.00	0.00	139.59	69.79	0.00	0.00	0.00
BC	0.00	31.43	55.83	75.34	125.00	55.83	55.83	47.82	55.68	57.14
CB	53.92	47.14	41.88	37.67	26.86	41.88	41.88	71.74	41.76	42.86
Stearic acid	3.59	3.14	2.79	2.51	1.79	2.79	2.79	2.39	2.78	0.00
ZnO	7.19	6.29	5.58	5.02	3.58	5.58	5.58	4.78	5.57	0.00
CBS	0.90	0.79	0.70	0.63	0.90	0.70	0.70	0.60	1.39	0.00
TMTD	1.08	0.94	0.84	0.75	0.54	0.84	0.84	0.72	0.84	0.00
Sulfur	3.59	3.14	2.79	2.51	1.79	2.79	2.79	2.39	2.78	0.00
DCP	0.00	0.00	0.00	0.00	0.00	0.00	0.00	0.00	0.00	7.14
total	250.00	250.00	250.00	250.00	250.00	250.00	250.00	250.00	250.00	250.00

Mixing

The materials were mixed using an internal mixer and a two-roller mixer. The compounded formulation of 10 formulas of neutron shielding material in parts per hundred rubber (phr) units will be transferred to grams. As shown in Table 3.2, the total weight of mixing one batch is equal to 250 grams in order to fit the capacity of the internal mixer that can be accepted.

Initially, the rubber was placed inside the internal mixer to begin the process. After this step, the various fillers that are required for the molding of rubber products are added to the mixture, including any and all additional chemicals that contribute to the protective qualities against neutron radiation. The procedure for the mixing was carried out for a total of 25 minutes at a temperature of 60 degrees Celsius with a speed of 60 revolutions per second. The last stage was the addition of a stabilizer. We mixed it in a two-roller mixer to avoid the risk of premature curing of the rubber. A two-roller mixer consists of a roller with a diameter of 6 inches, a length of 15 inches, and a friction ratio between the surface speeds of the front roller and the rear roller equal to 1:1.05. After mixing, the rubber was rolled into a sheet and taken out to rest for 24 hours.



Figure 3.2 Internal mixer is the equipment for mixing natural rubber and fillers.

Vulcanization characteristics of rubber compounds

We perform the vulcanizing characterization in order to ascertain the optimum conditions for the vulcanization process. This step involves testing the rubber compound to ascertain its curing characteristics, such as the required time and temperature for comprehensive vulcanization. The objective is to ensure that the rubber is completely vulcanized without being over-vulcanized, which can result in brittleness and diminished performance. For vulcanizing characterization in this investigation, the Mooney Viscometer and Moving Die Rheometer (MDR) were utilized.

The Mooney viscosity was determined by using a Mon-Tech model MV 3000 Basic Mooney Viscometer. The rotor measured 3.81 cm in diameter and 0.508 cm in thickness. At a rate of 2 revolutions per minute, the rotor rotated. The temperature used is 100 °C, the chamber is prepared for one minute prior to testing, and the duration



Figure 3.3 Two roll mill is the equipment for mix sulfur into composite materials and shape samples into sheets.

of the test is four minutes. Moreover, vulcanization characteristics such as maximum torque (M_H), minimum torque (M_L), scorch time (t_{s1}), cure time (t_{90}), cure rate index (CRI), and activation energy were calculated by the Mon-Tech model MDR3000. In order to calculate the activation energy, each sample was tested at temperatures of 140, 150, and 160 °C. For the purpose of determining the optimal cure time, the temperature was set to 150 °C.

Forming and vulcanization

To form and vulcanize the rubber compound, we would like to use a rubber mold, since it can be formed and stabilized by heat and compression at the same time. Based on Moving Die Rheometer (MDR) test results, each sample was compression-molded using an electrically heated hydraulic press at 150 °C and 20 MPa for the required duration. Finally, we obtain rubber compound samples with the following dimensions: 15 × 15 × 0.2 cm³ (width × length × thickness).



Figure 3.4 MDR 3000 moving die rheometer is used to determine curing time of composite material.

3.3 Results and Discussion

The fabricated neutron shielding material were examined for various properties in order to improve the formulation and develop better samples to be more suitable for future applications.

3.3.1 Mooney viscosity

The Mooney viscosity indicates how difficult it is to mix the material with rubber. The more viscous it is, the more difficult it is to mix the material. The added amount of B_4C increased the sample's Mooney viscosity, as shown in Figure 3.8. The Mooney viscosity was reduced when the sample concentration reached 60 phr of B_4C . Samples F4 and F5 were found to have an excess of B_4C , which operates as peptizing agents. Sample F6 had the lowest Mooney viscosity, with a value of 0.38 MU (Mooney viscosity unit). Adding more carbon black increases the Mooney viscosity, while adding more accelerator causes it to decrease. Carbon black filler particles may prevent rubber chains from moving freely under shear stresses, making it more difficult to slide past one another.



Figure 3.5 Mooney viscometer is the equipment for determine the Mooney viscosity of composite material.

3.3.2 MDR test

The relationship between torque and curing time is shown in Fig.3.9. The results showed that the induction period of sample F5 was the narrowest. It has been demonstrated that increasing the amount of B_4C results in a minimum vulcanization safety period. Thereafter, the rate increased rapidly due to intermolecular cross-linking by natural rubber. The maximum torque (M_H), minimum torque (M_L), scorch time, cure time, and cure rate index (CRI) of each compound rubber formulation are given in Table 3.3. B_4C was found to increase the minimum torque, which measures the hardness or softness of the uncured rubber. The minimum torque value of sample F5 confirms that an excess of B_4C has a peptizing effect. The lowest minimum torque value was 0.69 dNm for Sample F6. Moreover, sample F10 exhibited the highest minimum torque value, at 3.97 dNm. The maximum torque value is the torque value following vulcanization when the bond content is at its peak. Sample F8 showed the highest maximum torque at 38.54 dNm. The maximum torque value of sample F3 was greater than that of sample F10, indicating that using sulphur as a vulcanizing agent produced more bonding than using DCP. It is possible to reduce scorch time by making use of



Figure 3.6 A compression molding machine model LP20-B from Labtech Engineering Company Ltd. was used for vulcanizing the sample.

ENR (F6 and F7), carbon black (F8), accelerator (F9), or DCP (F10). However, using DCP as a rubber vulcanizer doubled the cure time to 5.17 minutes. The increase in B_4C resulted in a higher cure rate index, with sample F5 having the highest CRI of 156.83, while sample F10 had the lowest CRI of 22.34.

The activation energy was decreased when B_4C was present in concentrations of 20 and 40 phr, as shown in Figure 3.10. Conversely, using B_4C at concentrations of 60 and 139.6 phr resulted in an increase in the activation energy. B_4C at a concentration of 40 phr can aid in the vulcanization of rubber. However, adding an excessive amount of B_4C will prevent vulcanization. The formation of sulphur cross-links was encouraged by an increase in carbon black, which enhanced the efficiency of the process.

3.4 Summary

In order to create the neutron shielding material based on rubber and boron carbide, a procedure that is commonly utilized in the rubber industry involves the addition of a boron carbide mixture. The equipment used consists of an internal mixer and a two-roll mixer. Then, the specific curing characteristics of the compound rubber



Figure 3.7 Neutron shielding materials samples with dimensions of $15 \times 15 \times 0.2 \text{ cm}^3$ (width x length x thickness).

were determined by MDR machine at $150 \text{ }^\circ\text{C}$. The result shows that B_4C increases NR compound Mooney viscosity, while 60 phr B_4C lowers Mooney viscosity. Samples F4 and F5 had too much peptizing B_4C . Sample F6 had the lowest Mooney viscosity, 0.38 MU. The accelerator reduces Mooney viscosity, while carbon black increases it. Carbon black's filler particles can hinder rubber chains' shear forces.

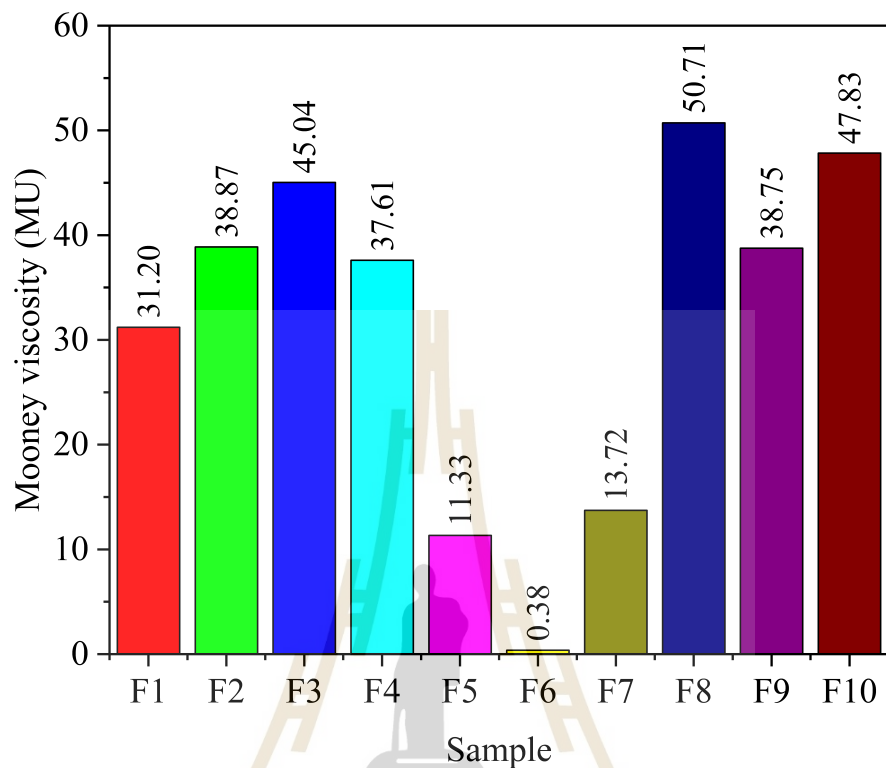


Figure 3.8 Mooney viscosity of the sample.

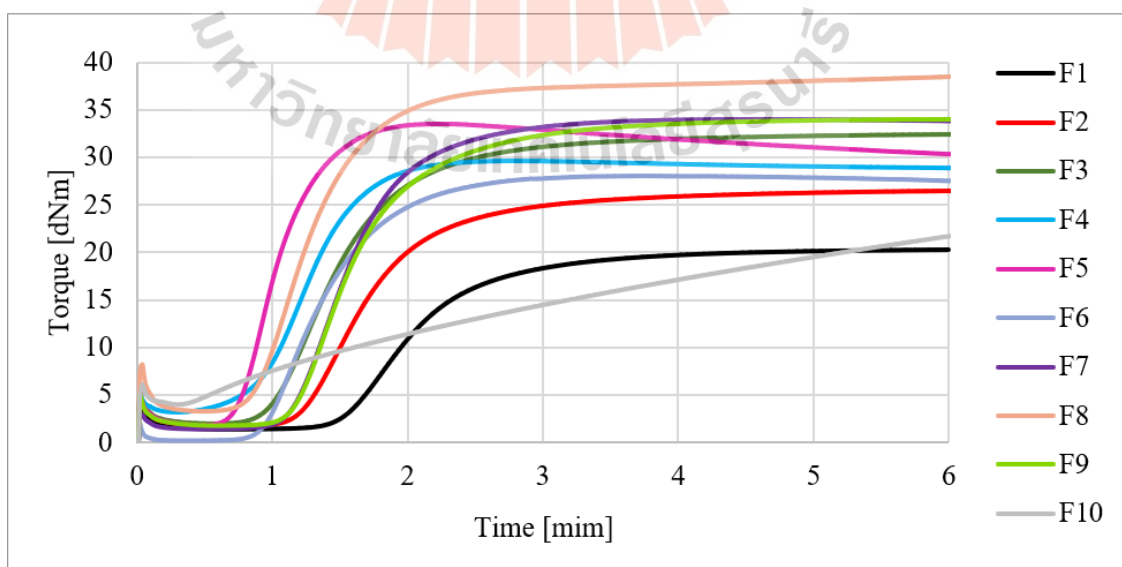


Figure 3.9 Characteristics of dimensional stability of the sample at 150 °C.

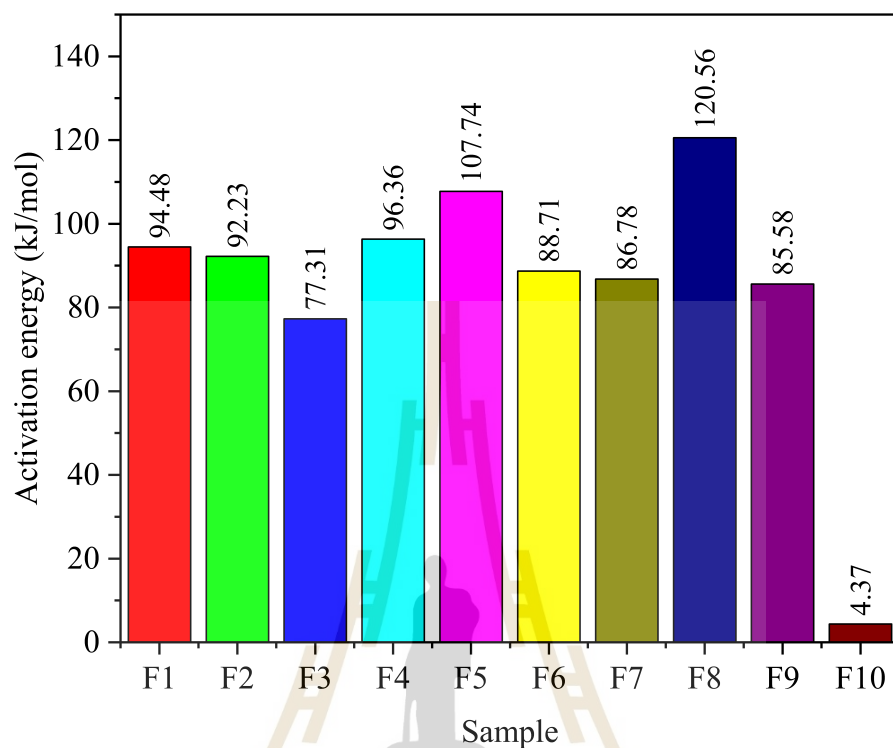


Figure 3.10 The activation energy of the sample.

Table 3.3 MDR data of the sample at 150 °C

Sample	M_H (dNm)	M_L (dNm)	$M_H - M_L$ (dNm)	Scorch Time (min.)	Cure time (min.)	CRI (min. ⁻¹)
F1	20.33	1.36	18.96	1.58	3.05	68.51
F2	26.52	1.71	24.80	1.24	2.61	72.82
F3	32.40	1.95	30.45	1.00	2.34	74.46
F4	29.73	2.76	26.97	0.82	1.70	114.68
F5	33.67	1.80	31.87	0.74	1.40	156.83
F6	28.27	0.17	28.10	0.96	2.50	91.50
F7	33.97	1.39	32.59	1.14	2.25	89.56
F8	38.54	3.26	35.28	0.85	2.00	87.29
F9	33.96	1.75	32.22	1.16	2.07	74.44
F10	21.73	3.97	17.76	0.69	5.17	22.34

CHAPTER IV

MECHANICAL TEST

Neutron shielding materials often serve as structural components in various applications, such as nuclear power plants or research facilities. Mechanical testing helps assess the material's ability to withstand mechanical stresses, such as tensile or hardness. It ensures that the material has the necessary strength, stiffness, and durability to maintain its structural integrity during installation, operation, and potential accidents or incidents.

4.1 Introduction

Neutron shielding materials are used in various applications where protection against neutron radiation is required. Some common areas where neutron shielding materials are used, for example, nuclear power plants, research reactors, and particle accelerators to ensure the safety of personnel and prevent radiation leakage. Shielding materials are employed in reactor cores, beam lines, and other areas to minimize the impact of neutron radiation on workers, equipment, and the surrounding environment.

The mechanical properties of radioactive materials are one of the properties to be considered and tested, for actual usage conditions. During installation, neutron shielding materials could be heavy or require particular handling techniques due to their characteristics. Mechanical testing provides insights into the behavior of the material under various loading conditions, allowing engineers and workers to learn how to safely and efficiently handle and install the shielding material. It assists in determining acceptable techniques of lifting, transporting, and securing in order to prevent any damage or failure that may occur during handling. Some neutron shielding materials need to support other equipment or structures. Mechanical testing helps determine the load-bearing capacity of the material, including its ability to withstand static or dynamic loads. By evaluating the material's deformation, stress distribution, and failure modes under load, engineers can ensure that the shielding material can adequately support the intended loads without experiencing excessive deflection, deformation, or collapse. Neutron shielding materials may be exposed to potential impact events, such

as accidental drops, collisions, or equipment malfunctions. Mechanical testing, such as impact or drop tests, assesses the material's ability to absorb and distribute impact energy, mitigating the risk of damage or penetration. Understanding the material's impact resistance helps in selecting suitable shielding materials for specific applications and minimizing the potential for critical failures. Materials used for neutron shielding can become exposed to a variety of environmental factors, such as temperature changes, moisture, radiation, or chemical exposure. To determine whether the material maintains its mechanical qualities, dimensional stability, and resistance to degradation under such circumstances, mechanical testing can assess the material's performance. This knowledge is essential for choosing shielding materials that are strong enough to resist the unique environmental difficulties they might face.

In this study, ten samples were tested for the main mechanical properties, including stiffness and tensile strength, of radiation shielding materials, to use as a guideline for improving the design of neutron shielding materials.

4.2 Material and Method

4.2.1 Hardness test

A hardness test is a technique employed to measure the hardness of a material, which is a quantification of its ability to resist deformation or scratching. Hardness tests are frequently employed in the field of materials science and engineering to evaluate the mechanical characteristics of various materials, including metals, polymers, ceramics, and composites. Various hardness tests exist, each employing specific methods and scales. The most common hardness test for rubber and elastomeric materials is the Shore Hardness test, which measures the depth of penetration of a specified indenter under a specified force. Shore A hardness test was performed on samples that were 6 mm thick in accordance with ASTM D2240 standard.

4.2.2 Tensile test

A tensile test was carried out on the prepared NR compound samples in order to assess their tensile modulus, tensile strength, and break elongation. This procedure was carried out using a model 5569A INSTRON tensile machine. Tensile tests were conducted on type C-shaped samples. A 10 kN load cell was used with a 500 mm/min displacement rate.



Figure 4.1 Shore A hardness tester is used in this work. We follow the ASTM D2240 standard. All samples of 6 mm thickness were put through a hardness test.



Figure 4.2 The 5569A INSTRON tensile machine is used in this work. Tensile testing were done on C-shaped samples. The 500 mm/min displacement was employed with a 10 kN load cell.

4.3 Results and Discussion

4.3.1 Hardness test

The results of the hardness test are displayed in Figure 4.3. It was found that mixing B_4C and carbon black increased the hardness values. ENR (F6) produced a

softer rubber composition compared to compound NR material (F3). F9 had a higher hardness than F10 because CBS contains a sulfenamide functional group, allowing it to react more readily with the rubber polymer chains. This leads to more effective cross-linking and a greater increase in strength.

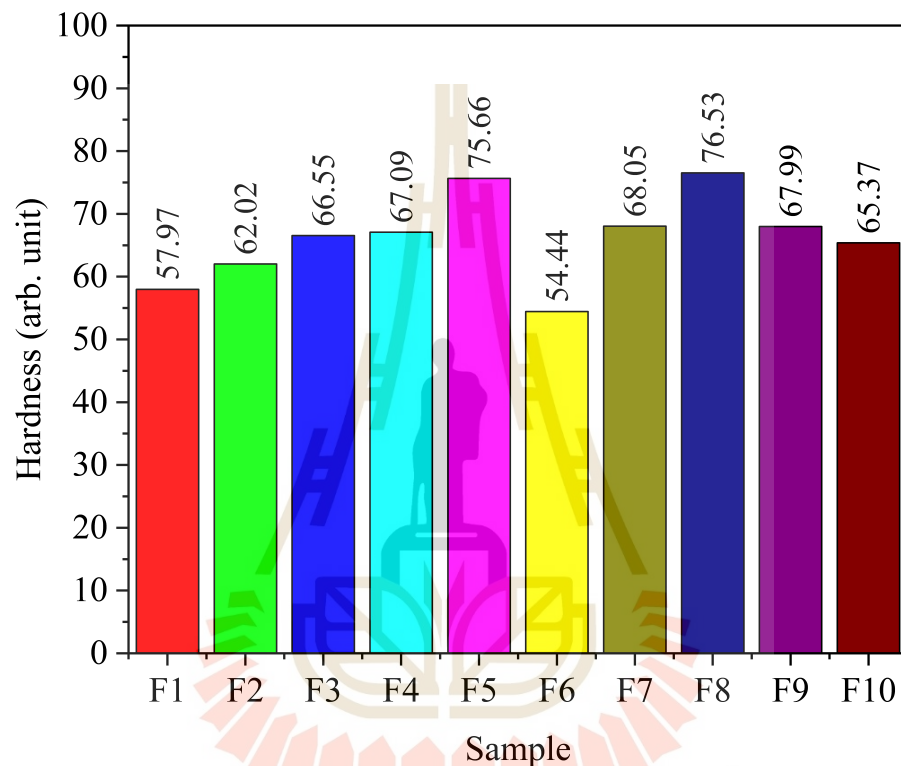


Figure 4.3 Hardness of the sample.

4.3.2 Tensile test

The tensile modulus, tensile strength, and break elongation of the NR compound samples are provided in Table 4.1. The results showed that when B_4C was added, the tensile modulus and tensile strength broke down. It indicates that the sample lost some of its hardness and resistance to deformation. The tensile modulus of F5 was the lowest of all the samples tested, at 2.35 GPa, making it less elastic and less capable of fully recovering from deformation. As a result of F1-F5, the material can become more rigid and less flexible, leading to a reduction in the break elongation

Table 4.1 Tensile test of the sample.

Sample	Property		
	Tensile modulus (GPa)	Tensile strength (MPa)	Break Elongation (%)
F1	5.87	22.26	451.40
F2	5.54	14.19	328.41
F3	4.70	9.84	265.36
F4	3.81	8.10	253.03
F5	2.35	5.32	234.99
F6	5.26	11.11	333.18
F7	5.90	10.94	282.62
F8	7.20	11.20	158.85
F9	4.16	9.21	243.07
F10	4.73	12.14	342.86

of the rubber. Since it enhanced cross-linking during epoxidation and produced more elastic material, NR (F3) has a lower tensile modulus and strength than ENR (F6). Moreover, the fact that F6 has a higher break elongation could indicate that the rubber is more flexible and less likely to crack. As seen in sample F8, the tensile strength and modulus increased with the addition of carbon black. Because of their strong polarity and substantial surface area, carbon black particles are able to form a direct physical connection with the matrix of the rubber. As a consequence of these physical linkages, the rubber has gained additional rigidity and lost some of its flexibility. Conversely, carbon black reduces the duration of the break elongation.

The tensile modulus, tensile strength, and break elongation decreased as CBS increased. Using DCP in sample F10 resulted in higher tensile strength compared to using sulphur sample because DCP increased cross-link density and greater intermolecular forces between the rubber chains.

CHAPTER V

NEUTRON SHIELDING TEST

Neutron shielding tests are conducted to evaluate the effectiveness of different materials or configurations for attenuating or stopping neutrons. There are various methods and techniques used for neutron shielding tests. Monte Carlo simulations are computational techniques that use random sampling to model the transport of particles, such as neutrons, through different materials. These simulations can provide valuable insights into the behavior of neutrons and the effectiveness of different shielding materials. Experimental tests involve exposing shielding materials to a known source of neutrons and measuring the resulting neutron flux and energy spectrum. This can be done using specialized neutron detectors or activation techniques that analyze the induced radioactivity in the materials. Additionally, neutron imaging techniques, such as neutron radiography or tomography, can be employed to visualize the distribution of neutrons and assess the effectiveness of shielding materials. These techniques allow for non-destructive testing and provide valuable insights into the interaction of neutrons with shielding. Moreover, benchmarking involves comparing the results of shielding tests against well-established reference data or standards. This helps validate the accuracy and reliability of the shielding measurements and provides a basis for evaluating the performance of different shielding materials.

In this chapter, both fast neutrons and thermal neutrons were used to test the ability to shield neutron radiation from its source. including a comparison to a commercial product sample obtained from a Japanese company.

5.1 Material and Method

5.1.1 Thermal neutron shielding tests

A neutron shielding characterization of NR compound samples was carried out at the Thailand Institute of Nuclear Technology (public organization). As a neutron source, a TRIGA Mark III type atomic research reactor was utilized. Using the neutron imaging technique, the thermal neutron shielding properties of all 6-millimeter-thick

NR compound samples were evaluated. The samples were positioned at the thermal neutron beam port for three minutes. Materials containing lithium fluoride (LiF) and zinc sulfide (ZnS) were used as neutron scintillators to emit photons. The light was absorbed and transformed into an electrical signal by a phosphor-coated/charge-coupled device (PC/CCD) chip, which was then digitally processed to create an image. Finally, the images were processed for brightness fraction using Image J version 1.53t. Figure 5.1 shows the experimental setup for neutron imaging.

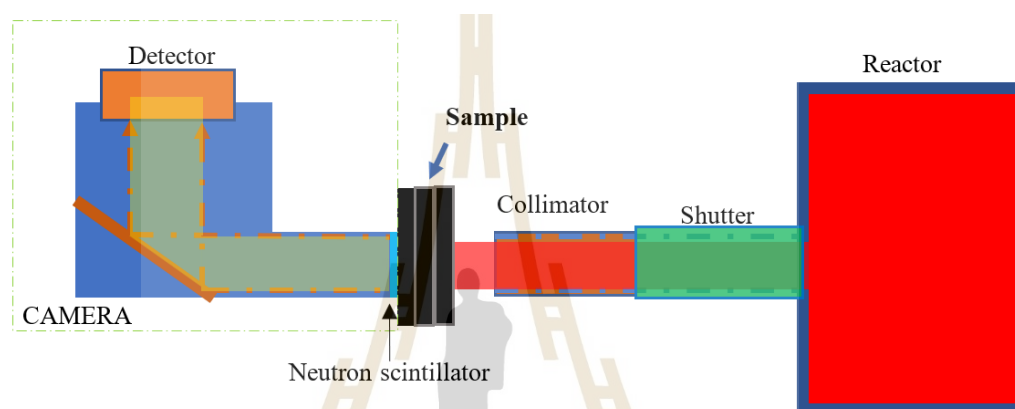


Figure 5.1 Experiment setup for thermal neutron shielding test.

5.1.2 Fast neutron shielding tests

For fast neutron attenuation testing, radiation sources of ^{241}Am -beryllium with a combined activity of 90 mCi were used. Thermal neutrons were removed using two cadmium sheets. While the second layer filtered the thermal neutrons that had already passed through the sample, the first sheet filtered the thermal neutrons from the radiation sources. Each sample was examined at various thicknesses of 5, 10, 15, 20, and 24 mm and dimensions of $150 \times 150 \text{ mm}^2$ to determine the macroscopic cross-section. The source was positioned at the base of the polyethylene (PE) source holder, 35 mm away from the sample. The Ludlum Model 42-41L PRESCILA neutron detector, which has a neutron efficiency of 29 cpm/Sv/hr, was used to measure the neutron dose rate. The neutron detector was 90 mm away from the source. There had been six minutes of counting. The experiment setup is shown graphically in Figure 5.2. The measurements for all samples were taken in the same way, using the same geometry and experimental setup.

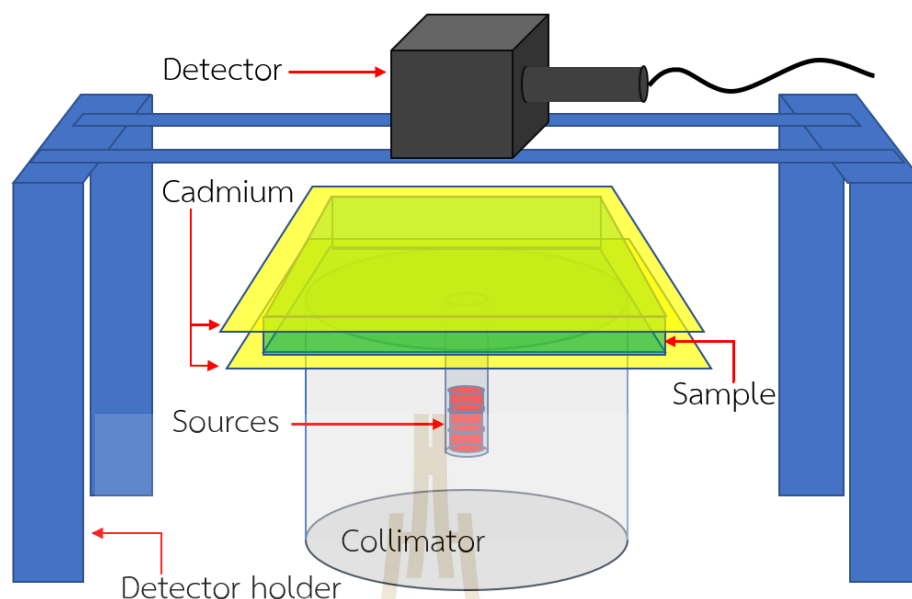


Figure 5.2 Experiment setup for our fast neutron shielding test.

5.2 Results and Discussion

5.2.1 Thermal neutron shielding tests

The analysis was performed by examining the brightness fraction of neutron images to determine the radiation shielding properties of the NR compound samples. Examples of neutron images of a 5 mm-thick sample are shown in Figure 5.3. The maximum brightness value was found by taking an image with no sample. The minimum brightness value was taken when there was no thermal neutron beam. The maximum and minimum brightness values were then normalized to 1 and 0, respectively. A brightness value close to 1 indicates that a large number of thermal neutrons are able to pass through the NR compound samples, whereas a value close to 0 indicates the ability to shield thermal neutrons.

Figure 5.4 shows comparison between different samples with the same thickness of 5 mm. It can be seen that the addition of B_4C to the NR compound samples enhanced their thermal neutron shielding properties. The best NR compound sample for thermal neutron shielding being observed is sample F5, since it exhibited the lowest photographic brightness fraction of 0.043. When B_4C was added in amounts larger than 40 phr, the thermal neutron shielding ability dose not increase significantly. The

thermal neutron shielding ability is unaffected by the impacts of ENR, DCP, carbon, or CBS, additions. The thermal neutron macroscopic cross-sections (Σ) for each sample obtained from neutron imaging techniques are given in Table 5.1.

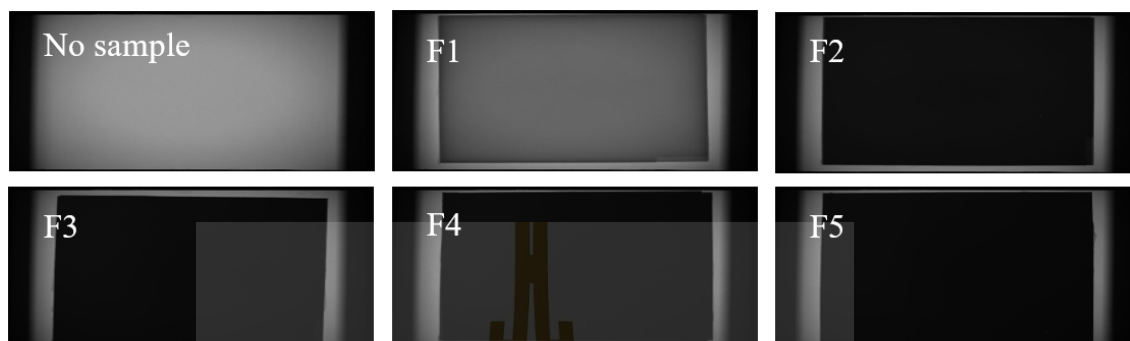


Figure 5.3 Sample image from neutron imaging.

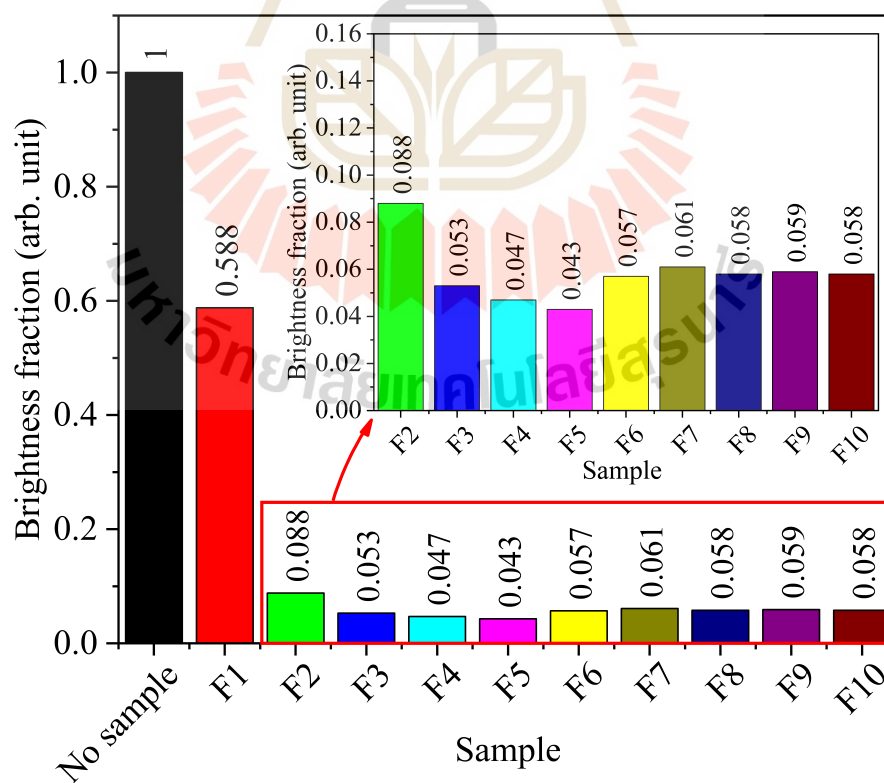


Figure 5.4 Brightness fraction of the sample.

Table 5.1 The thermal neutron macroscopic cross-section (Σ) for each sample using neutron imaging techniques, The TRIGA Mark III type atomic research reactor, Thailand Institute of Nuclear Technology (public organization).

Sample	Macroscopic cross-section (Σ)
F1	1.34
F2	5.72
F3	9.90
F4	13.56
F5	19.97
F6	9.97
F7	9.19
F8	9.96
F9	10.09
F10	9.61

5.2.2 Fast neutron shielding tests

Figure 5.5 shows the sample's fast neutron attenuation at various boron carbide concentrations. As boron carbide concentrations increase, the number of fast neutrons decreases. Additionally, sample F2's trendline was different from the trendlines of the other samples, maybe as a result of the uneven distribution of boron carbide inside the sample. Therefore, additional research into the material's spread will be needed. F1 and F2 both performed similarly in terms of neutron shielding, while F4 and F5 both performed similarly. Results are shown in Table 5.2 by looking at the macroscopic cross-section value. In other words, altering the concentration of boron carbide will result in the required attenuation. Neutron attenuation values for F5 and a commercial product from a Japanese company, both of which contain the same quantity of boron carbide (50 wt%), were identical at 14.1 and 14.6 percent, respectively, as seen in Figure 5.6.

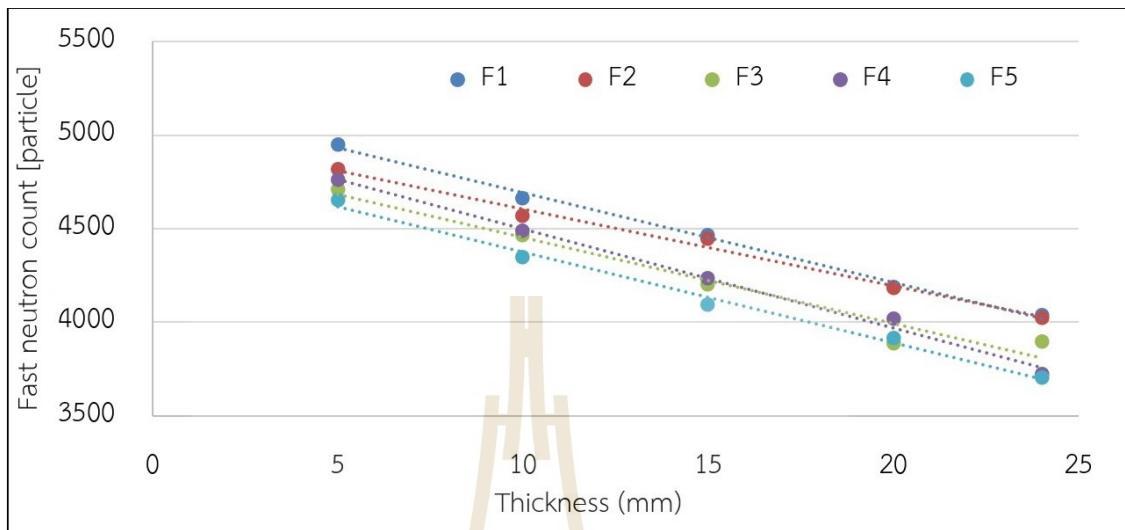


Figure 5.5 Fast neutron attenuation of samples.

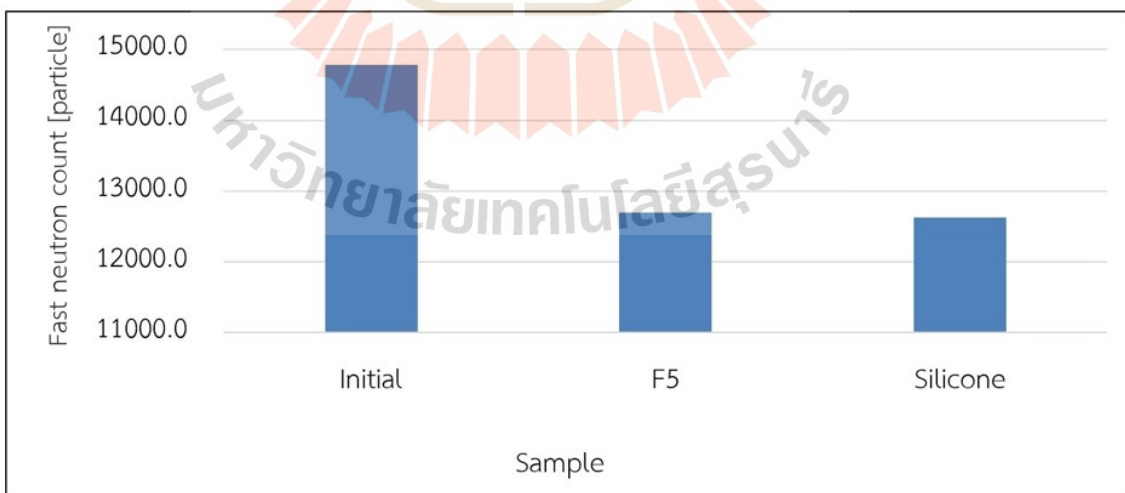


Figure 5.6 Fast neutron attenuation of F5 and a commercial sample from Japan (Silicone).

Table 5.2 The fast neutron macroscopic cross-section (Σ) for each sample, test with ^{241}Am -Beryllium source at department of Nuclear Engineering, Faculty of Engineering, Chulalongkorn University, Bangkok, Thailand.

Sample	Macroscopic cross-section (Σ)
F1	0.100
F2	0.104
F3	0.096
F4	0.113
F5	0.123

CHAPTER VI

MCNP SIMULATION FOR NEUTRON SHIELDING MATERIAL

6.1 Introduction

The MCNP (Monte Carlo N-Particle) program is a widely used software tool in the field of nuclear engineering and radiation physics. It is specifically designed for simulating and analyzing the behavior of neutrons in various materials and systems. Subatomic particles, particularly neutrons, are frequently observed in nuclear reactions and radioactive decay processes. In numerous applications, including nuclear power generation, radiation or particle therapy, and nuclear waste management, it is essential to comprehend how neutrons interact with other materials.

The MCNP program utilizes the Monte Carlo method, a statistical technique that simulates the behavior of particles through repeated random sampling. It models the movement and interactions of individual neutrons as they traverse through a given material or system. One important application of the MCNP program is predicting the neutron shielding ability of materials. In this work neutron shielding refers to the ability of a material to attenuate or absorb neutron radiation. It is essential to ensure the safety of personnel and equipment in environments with elevated neutron flux, such as nuclear power plants or radiation research facilities. By using the MCNP program, engineers and scientists can simulate the passage of neutrons through different shielding materials and assess their effectiveness in reducing neutron radiation levels. This allows for the optimization of shielding designs and the selection of suitable materials to meet specific requirements.

To simulate the material's neutron shielding properties for this research, the simulation was performed under MCNP version 5. We simulated the installation of real equipment with the corresponding simulation geometry. The models were selected from the actual experiments conducted at the Department of Nuclear Engineering, Faculty of Engineering, Chulalongkorn University. Americium-241/Beryllium was used as the neutron radiation source.

6.2 Problem Description and Geometry

We simulate the neutron shielding capability of materials in the MCNP program according to the actual equipment setup. The radiation strength of the sampled material is calculated by calculating the constituent elements of the material in each formula. The neutron source, Americium-241/Beryllium, was placed in the neutron container, which was positioned at 4.00 centimeters below the radiation shielding sample. The neutron detector is located at the top of the sample at the distance of 9.50 centimeters from the neutron source. Paraffin and heavy concrete were used as shielding materials to ensure the safety of the researchers. The geometry of the simulation is illustrated in Figure 6.1. The radiation shielding materials for all samples of different formula will use the same geometry.

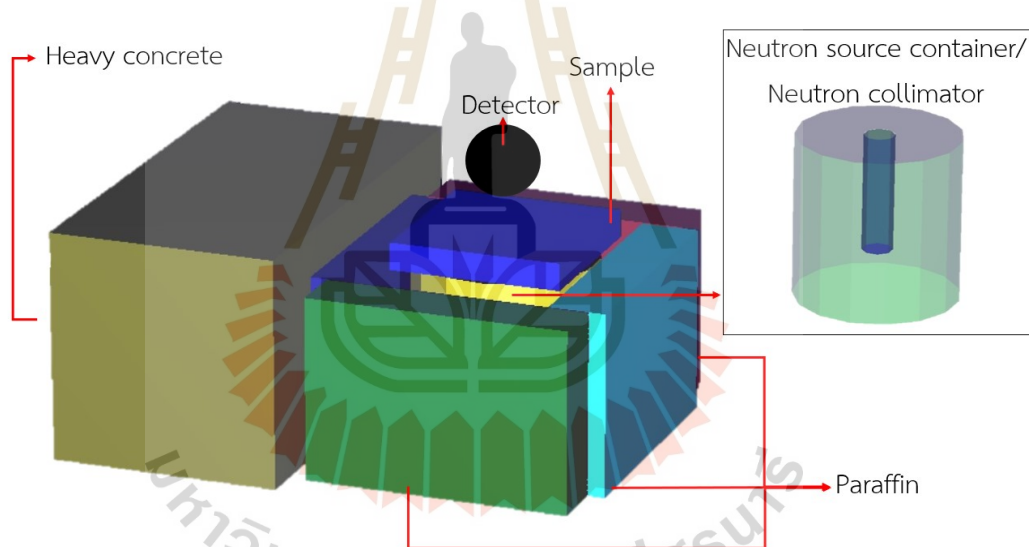


Figure 6.1 Geometry.

6.3 Surface and Cell Cards

6.3.1 Surface cards

Surface cards in MCNP are crucial for defining the geometry, determining particle interactions and tracking, and scoring particle interactions within the simulation model. They enable accurate representation of physical boundaries, materials, and interfaces, which ultimately affect the reliability and usefulness of the simulation results.

In our work, surfaces are defined by macrobodies as shown in Figure 6.2. Surface 1 was made spherical in order to define the universe's boundary for simulation. Surface 2 was used as the region of the sample material. Surface 3 was used as the boundary of the neutron detector. Surfaces 4 and 5 were used as the boundaries of the neutron collimator and the hole containing the neutron source, respectively. The boundaries of the paraffin were surfaces 6, 7, 8, and 9. Lastly, surface 10 was used as a heavy concrete boundary.

	Mnemonic	Input Parameter
1	so	100
2	box	0 -7.5 -7.5 0.2 0 0 0 15 0 0 0 15
3	s	10.5 0 0 5
4	RCC	-16 0 0 16 0 0 8
5	RCC	-11.5 0 0 11.5 0 0 1.5
6	box	-16 -11.5 8 16 0 0 0 23 0 0 0 5
7	box	-16 -16.5 -11.5 16 0 0 0 5 0 0 0 23
8	box	-16 11.5 -11.5 16 0 0 0 5 0 0 0 23
9	box	-16 -11.5 -13 16 0 0 0 23 0 0 0 5
10	box	-16 -18.5 -33 20 0 0 0 38 0 0 0 20

Figure 6.2 Surface cards of our simulation setup.

6.3.2 Cell cards

The geometric cells can now be defined since the surface cards have been established. Individual surfaces are identified, and these surfaces are then combined using the Boolean intersection, union, and complement operators to define cells. The gram density follows the material number. The cell cards are shown in Figure 6.3. A negative entry in the front of density indicates a mass density in grams per centimeter. Cell 1 is outside the universe, while cells 2 and 6 are the air inside the universe. The sample material is designated in cell 3. Cell 4 acts as a neutron detector that only considers neutrons crossing the surface and thus is defined as a vacuum. Cell 5 is defined as a neutron collimator. Cells 7, 8, 9, and 10 are paraffin. Concrete is designated in cell 11. In addition, in the option parts, every cell must be considered both neutrons and photons except cell 1. The position of all cells can be seen in Figure 6.4.

Cell number	Material number	Material density part	Geometry specification part	Option part
1	0		1	imp:n=0 imp:p=0
2	204	-0.001225	-1 2 3 4 5 6 7 8 9 10	imp:n=1 imp:p=1
3	444	-1.50938458	-2	imp:n=1 imp:p=1
4	0			imp:n=1 imp:p=1
5	456	-0.93	-4 5	imp:n=1 imp:p=1
6	204	-0.001225	-5	imp:n=1 imp:p=1
7	434	-0.93	-6	imp:n=1 imp:p=1
8	434	-0.93	-7	imp:n=1 imp:p=1
9	434	-0.93	-8	imp:n=1 imp:p=1
10	434	-0.93	-9	imp:n=1 imp:p=1
11	332	-3.35	-10	imp:n=1 imp:p=1

Figure 6.3 Cell cards of our simulation setup.

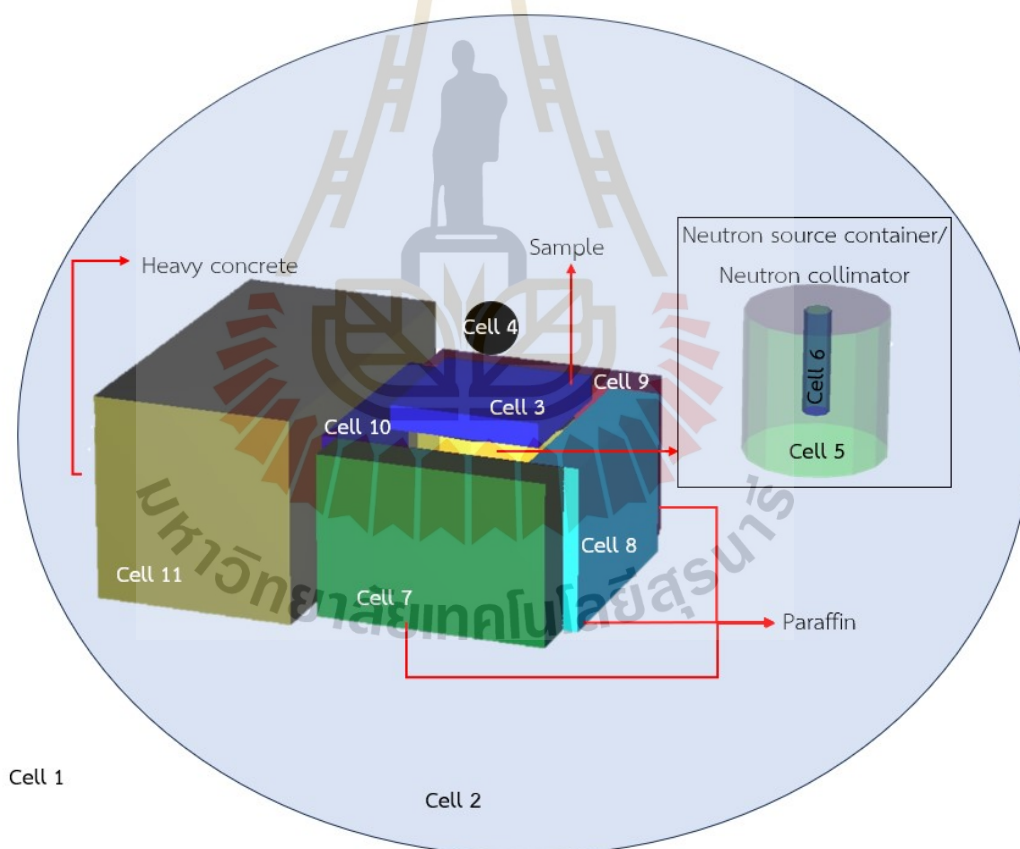


Figure 6.4 Cell position of our simulation setup.

6.4 Material Specification

Material specification in MCNP refers to defining the properties and composition of materials used in the simulation. MCNP allows users to specify various material

properties, such as density, elemental composition, isotopic composition, and thermal properties. Accurate material specification is crucial for accurately simulating particle interactions and tracking within the simulation model. Table 3.2 shows the proportion of chemicals used in each formula. Then, the fraction of each element can be calculated as shown in Table 6.1.

The element fraction data from Table 6.1 will be inserted into the material card as shown in the sample material fraction of F1 in Figure 6.5. where M444 is the material number used to identify the F1 sample material. $Zaid_i$ is either a full ZZZAAA.abX or partial ZZZAAA element or nuclide identifier for each constituent, where

- ZZZ represents the atomic number;
- AAA, if $AAA > 0$, represents the atomic mass number, and if $AAA = 000$ indicates a naturally occurring element (valid for $1 \leq ZZZ \leq 92$);
- ab is the alphanumeric library identifier; and
- X is the class of data. Element fraction is the fraction of the constituent in the material, where if fraction > 0 , then the value is interpreted as an atomic fraction and if fraction < 0 , then the value is interpreted as the weight fraction.

For the material specification of other material and formula samples, see Appendix B.

Material number	$Zaid_i$	Element fraction
m444	1001.70c	-0.087379898
	1002.70c	-0.000020102
	6000.70c	-0.864
	7014.70c	-0.000996102
	7015.70c	-0.000003898
	8016.70c	-0.007297051
	8017.70c	-2.9492E-06
	16032.70c	-0.016291032
	16033.70c	-0.000132646
	16034.70c	-0.000774378
	16036.70c	-1.9436E-06
	30000.70c	-0.0231

Figure 6.5 Materials card of sample F1.

Table 6.1 Element fraction of each formula.

Element	Z	Isotope	ZA	Element fraction of each formula									
				F1	F2	F3	F4	F5	F6	F7	F8	F9	F10
H	1	H-1	1001.70c	0.08738	0.076401	0.06787	0.061052	0.043693	0.060925	0.064397	0.058132	0.06785	0.069972
		H-2	1002.70c	2.01E-05	1.76E-05	1.56E-05	1.40E-05	1.01E-05	1.40E-05	1.48E-05	1.34E-05	1.56E-05	1.61E-05
B	5	B-10	5010.70c	0	0.018132	0.032215	0.043468	0.072121	0.032215	0.032215	0.027593	0.032125	0.03297
		B-11	5011.70c	0	0.080247	0.142572	0.192376	0.319184	0.142572	0.142572	0.122117	0.142176	0.145913
C	6	C-12	6000.70c	0.864	0.782732	0.719601	0.669153	0.540704	0.667868	0.693734	0.75983	0.719242	0.747748
N	7	N-14	7014.70c	0.000996	0.000837	0.000743	0.000669	0.000479	0.000743	0.000743	0.000637	0.001035	0
		N-15	7015.70c	3.9E-06	3.27E-06	2.91E-06	2.62E-06	1.87E-06	2.91E-06	2.91E-06	2.49E-06	4.05E-06	0
O	8	O-16	8016.70c	0.007297	0.006354	0.005645	0.005078	0.003634	0.064301	0.034973	0.004835	0.005629	0.00338
		O-17	8017.70c	2.95E-06	2.57E-06	2.28E-06	2.05E-06	1.47E-06	2.60E-05	1.41E-05	1.95E-06	2.28E-06	1.37E-06
S	16	S-32	16032.70c	0.016291	0.014277	0.012683	0.011409	0.008165	0.012683	0.012683	0.010863	0.013287	0
		S-33	16033.70c	0.000133	0.000116	0.000103	9.29E-05	6.65E-05	0.000103	0.000103	8.85E-05	0.000108	0
		S-34	16034.70c	0.000774	0.000679	0.000603	0.000542	0.000388	0.000603	0.000603	0.000516	0.000632	0
		S-36	16036.70c	1.94E-06	1.70E-06	1.51E-06	1.36E-06	9.74E-07	1.51E-06	1.51E-06	1.30E-06	1.59E-06	0
Zn	30	Zn-64	30000.70c	0.0231	0.020199	0.017943	0.016141	0.011551	0.017943	0.017943	0.015369	0.017893	0
		Total		1	1	1	1	1	1	1	1	1	1

6.5 Source Definition

In MCNP, source definition refers to the description of particle sources inside the simulation model. Users of MCNP can define a variety of particle source types, such as isotropic point sources, directed sources, volumetric sources, and surface sources. For the simulation to accurately simulate particle motion and interactions, a proper source definition is important. In this study, a general source (sdef card) in a point source with Americium-241/Beryllium was chosen for the neutron source. The format for the sdef card is shown in Figure 6.6.

```
sdef POS=-4 0 0 AXS=1 0 0 EXT=0 PAR=n
      erg=d1 VEC=1 0 0
sp1 -2 1.330
```

Figure 6.6 Source definition of our model.

For sdef source, "PAR=n" indicates that source particles are created as neutrons. The neutron radiation source was identified within the collimator hole 4 cm below the sample material (POS=-4 0 0). "AXS=1 0 0" indicates neutrons moving in the x axis through the center. For a volume source, the distance from POS along AXS is 0, indicated by "EXT=0". The sdef card sets up an initial beam of particles traveling along the x-axis (VEC=1 0 0). The energy of the neutron ("erg") is represented by "d1". The "sp1" card described source probability functions in the Maxwell fission spectrum with function No. and input parameters form of "-2 a", when "a" is a parameter for the built-in function to indicate type of source, in case of 241-Am, "a" = 1.330.

6.6 Tallies and Miscellaneous Data Cards

Tally cards are utilized to designate the quantities of interest that users wish to tally or score throughout the simulation. The type of tally, scoring regions, scoring options, and other pertinent parameters are specified on tally cards. The collection of data on particle interactions, fluxes, dose rates, reaction rates, and other quantities for analysis relies heavily on tally cards. In this study, tally F1 was used to find neutron and photon current integrated over the surface of the detector. Figure 6.7 shows that "f11" is the F1 tally to give a quantity of neutrons in units of particles with energy ranging

from 1×10^{-10} MeV to 20 MeV. “f21” is the F1 tally to give a quantity of photons in units of particles with energy ranging from 0 to 10 MeV.

```
f11:n  3
e11    1e-10 299ilog 20
c
f21:p  3
e21    0 299i 10
```

Figure 6.7 Tallies cards of our model.

```
fmesh74:n ORIGIN=-100 -100 -100 GEOM=REC
imesh= 100
iints= 270
jmesh= 100
jints= 270
kmesh= 100
kints= 270
fmesh84:p ORIGIN=-100 -100 -100 GEOM=REC
imesh= 100
iints= 270
jmesh= 100
jints= 270
kmesh= 100
kints= 270
```

Figure 6.8 Fmesh tally card to plot energy in the geometry of our model.

```
mode  n p
nps  5000000
```

Figure 6.9 Miscellaneous cards of our model.

Additionally, the “fmesh” tally is a type of tally card used to score quantities on a mesh-based grid. The fmesh tally allows users to collect and analyze particle fluence or flux data over a three-dimensional mesh grid. It provides a means to obtain spatially resolved information about particle interactions, energy deposition, or reaction

rates within the simulation geometry. Figure 6.8 shows the fmesh tallies that were used in this study to plot energy in the geometry. “fmesh74” and “fmesh84” are the fmesh tallies that find an energy plot for neutrons and photons, respectively. “GEOM=REC” is the control mesh geometry type, which is cartesian. “imesh” is the location of the coarse meshes in the x-direction for rectangular geometry. “iints” is the number of fine meshes within corresponding coarse meshes in the x-direction for rectangular geometry. “jmesh” is the location of the coarse meshes in the y-direction for rectangular geometry. “jints” is the number of fine meshes within corresponding coarse meshes in the y-direction for rectangular geometry. “kmesh” is the location of the coarse meshes in the z-direction for rectangular geometry. “kints” is number of fine meshes within corresponding coarse meshes in the z-direction for rectangular geometry.

In addition to the tally and multiplier cards, a few additional critical data cards are required for MCNP to be able to solve this problem. Figure 6.9 depicts the additional cards required for this input deck. The “mode” card indicates which particle categories are to be tracked and tallied by MCNP. Even though MCNP can only start with one type of source particle, the program can track secondary particles for tally purposes. The “imp” card in Figure 6.3 provides the importance values for each of the problem geometry’s defined cells. In this situation, we wish to track particles that may move within the sample materials or the surrounding medium, but we can save computational time by eliminating particles that exit the cell’s boundary. Since particles that enter this outer volume are destroyed, the user must configure their geometry so that particles in the exterior regions have no or minimal effect on the totals. The “nps” card specifies the number of particle histories to run. The complete input file of our model is given in Appendix B.

6.7 MCNP Execution

To run the problem, we should use the following command line as Figure 6.10

```
<PROMPT> mcnp5 i=<input file name> o=< input file name > <options>
```

Figure 6.10 command line.

For the “i=” statement, we may write “inp=” or “I=”, and the same with “o=”. Figure 6.11 describes the type of option for MCNP execution.

i	Process input file
p	Plot geometry
x	Process cross section
r	Particle transport
z	Plot tally results

Figure 6.11 Options for MCNP execution.

6.8 Results and Discussion

This study has focused on the number of neutron particles that can pass through the neutron shielding material. The particles that passed through the shielding material and the probe, were designated as Tally1, are shown in Table 6.2. Then, we can follow Figure 6.12 to find the neutron transmission of the sample, as shown in Table 6.3. Finally, the microscopic cross section of each sample from the MCNP simulation can be obtained in Table 6.4.

The results of the MCNP simulation demonstrate the effect on the macroscopic cross-section of the sample material of the amount of boron carbide, type of natural rubber, amount of carbon black, vulcanizing accelerator, and type of vulcanizing agent. F1 is a formulation that contains no boron carbide at all, so it is possible that the energy of the neutron may only be reduced, but the number of neutron particles can still partially pass through the material. On the other hand, when boron carbide was added to the material, it could be seen that the number of particles passing through the sample material decreased, meaning that the macroscopic cross section value of the material increased. The macroscopic cross section of F2 was 0.264, which was the highest of all the samples. Conversely, the increase in boron carbide in samples F3, F4, and F5 resulted in a reduction in the macroscopic cross section, or an increase in the number of neutrons that are able to move through the sample material. When the proportion of boron carbide is increased, the ratio of rubber is going to decrease. This indicates that the ability to reduce energy has diminished, resulting in a number of

Table 6.2 The number of neutron particles crossing a detector surface.

Formula	Thickness (cm)						
	0	0.2	0.5	1	1.5	2	2.4
F1	1.50E-01	0.145328	0.138993	0.129571	0.121118	0.113514	0.107398
F2	1.50E-01	1.26E-01	1.12E-01	9.88E-02	8.91E-02	8.07E-02	7.47E-02
F3	1.50E-01	1.21E-01	1.09E-01	9.76E-02	8.82E-02	8.02E-02	7.44E-02
F4	1.50E-01	1.19E-01	1.09E-01	9.73E-02	8.82E-02	8.03E-02	7.46E-02
F5	1.50E-01	1.17E-01	1.08E-01	9.73E-02	8.87E-02	8.13E-02	7.61E-02
F6	1.50E-01	1.21E-01	1.10E-01	9.86E-02	8.95E-02	8.16E-02	7.61E-02
F7	1.50E-01	1.21E-01	1.10E-01	9.82E-02	8.89E-02	8.09E-02	7.52E-02
F8	1.50E-01	1.23E-01	1.11E-01	9.94E-02	9.04E-02	8.25E-02	7.69E-02
F9	1.50E-01	1.21E-01	1.09E-01	9.77E-02	8.83E-02	8.02E-02	7.44E-02
F10	1.50E-01	1.21E-01	1.09E-01	9.72E-02	8.76E-02	7.94E-02	7.37E-02

Table 6.3 Neutron transmission of the sample with different thickness.

Formula	Thickness (cm)						
	0	0.2	0.5	1	1.5	2	2.4
F1	1.00E+00	9.70E-01	9.28E-01	8.65E-01	8.08E-01	7.58E-01	7.17E-01
F2	1.00E+00	8.39E-01	7.45E-01	6.60E-01	5.95E-01	5.39E-01	4.99E-01
F3	1.00E+00	8.09E-01	7.30E-01	6.52E-01	5.89E-01	5.35E-01	4.97E-01
F4	1.00E+00	7.96E-01	7.25E-01	6.50E-01	5.88E-01	5.36E-01	4.98E-01
F5	1.00E+00	7.80E-01	7.20E-01	6.50E-01	5.92E-01	5.43E-01	5.08E-01
F6	1.00E+00	8.10E-01	7.33E-01	6.58E-01	5.97E-01	5.44E-01	5.08E-01
F7	1.00E+00	8.09E-01	7.32E-01	6.55E-01	5.93E-01	5.40E-01	5.02E-01
F8	1.00E+00	8.19E-01	7.39E-01	6.63E-01	6.03E-01	5.51E-01	5.13E-01
F9	1.00E+00	8.09E-01	7.30E-01	6.52E-01	5.89E-01	5.35E-01	4.97E-01
F10	1.00E+00	8.07E-01	7.28E-01	6.49E-01	5.85E-01	5.30E-01	4.92E-01

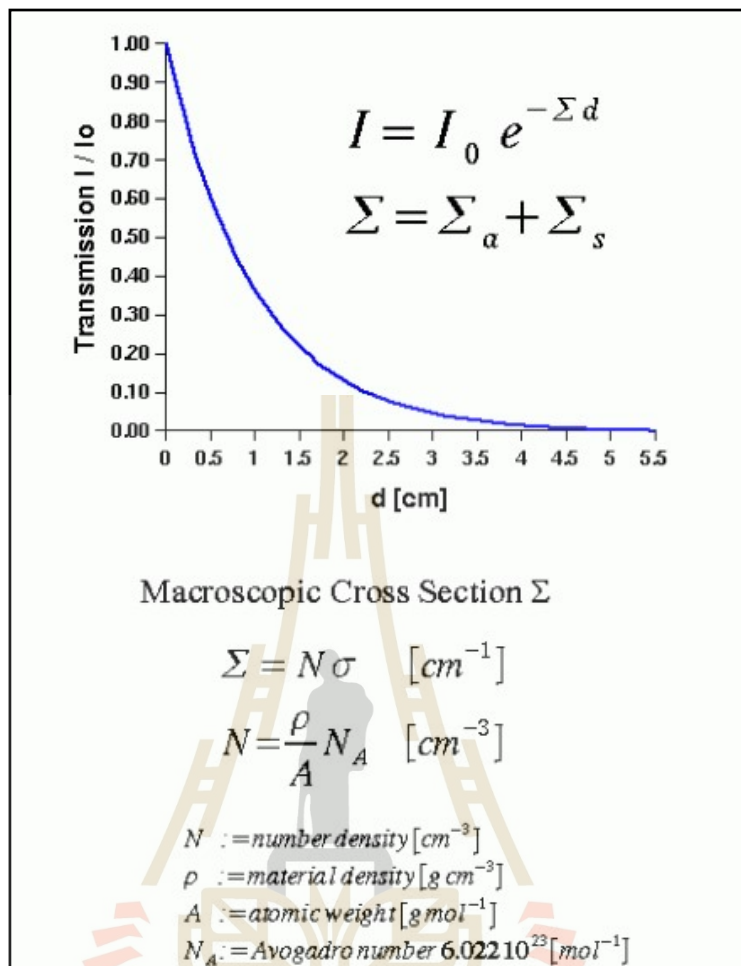


Figure 6.12 Exponential attenuation of neutrons in matter: Beer-Lambert law.

Table 6.4 The microscopic crosssection of each sample from MCNP simulation.

Formula	Macroscopic crosssection
F1	0.138
F2	0.264
F3	0.258
F4	0.253
F5	0.241
F6	0.249
F7	0.253
F8	0.246
F9	0.258
F10	0.262

fast neutrons still existing. As a consequence, the neutron's macroscopic cross section decreases, as one can see in the case of F5, which has the smallest macroscopic cross section of 0.241.

Comparing the effect of rubber type on the macroscopic cross section between NR and ENR, it was discovered that NR shields neutrons better than ENR. This is probably attributed to the presence of hydrogen in ENR (F6), which is less than F7 and F3, respectively. In addition, the increase in carbon black (F8) causes more neutrons to pass through the sample material, which is thought to be due to the decrease in the amount of NR. The increase in the accelerator does not affect the material's neutron shielding ability, since the accelerator has a very small increase in the proportion of the material as a whole. The last formula was to change the vulcanizing agent. It was found that the DCP vulcanizing agent formulations had higher macroscopic cross section values than that of the sulfur vulcanizing agent formulations due to the amount of hydrogen ratio in the sample material. Figure 6.13 and Figure 6.14 show the energy plot of neutrons in 2D geometry.

However, when comparing the macroscopic cross section values between the actual test and the simulation, there is a slight difference, which may be due to many factors, both in the detector's fast neutron detection performance and sensitivity. In addition to controlling neutron travel in geometry, there are many devices and equipment within the lab, including the walls of the room, that may cause the detector to measure neutrons reflected from them. In addition, the thermal neutron filtering efficiency by the cadmium sheet, of which we do not know how many percent can be filtered, since we cannot measure the thermal neutron spectrum exactly due to the limitation of our equipment.

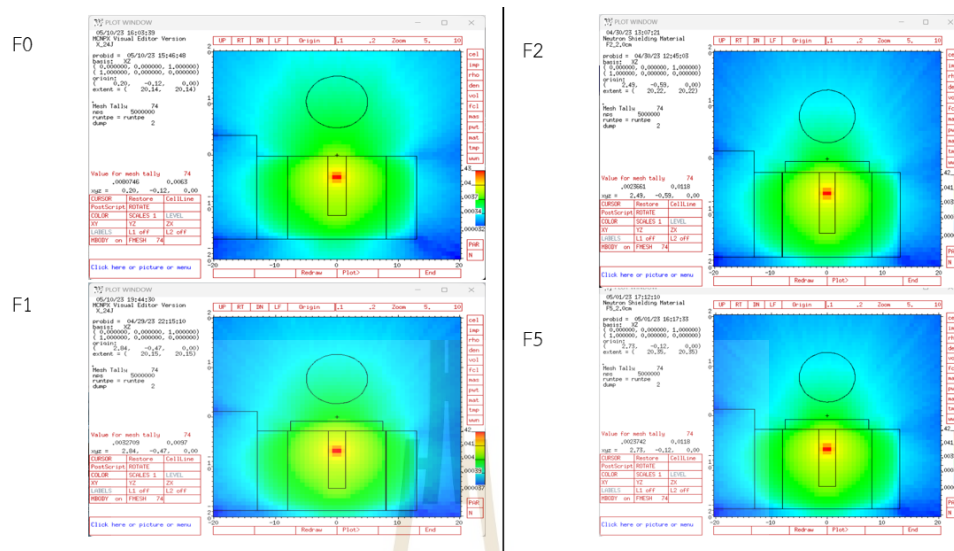


Figure 6.13 Fmesh tally plot results of F0 (no sample), F1, F2, and F5 with 2 cm. thick, neutron, nps = 5000000 partics, XY plane.

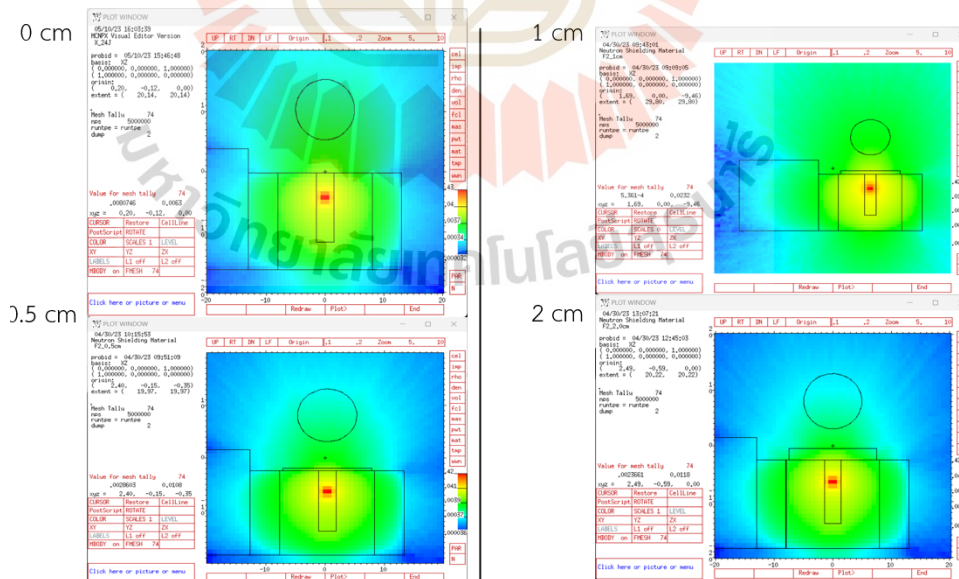


Figure 6.14 Fmesh tally plot results of F2 sample with different of thickness, nps = 5000000 partics, XY plane.

CHAPTER VII

CONCLUSION

The study and fabrication of neutron shielding materials based on natural rubber and boron carbide by comparing the differences in concentration of boron carbide, type of natural rubber, carbon black concentration, accelerator concentration, and type of vulcanizing agent can be summarized as follows:

1. *Effects on the vulcanizing properties* The increase in boron carbide resulted in an increase in mooney viscosity. However, excess amounts at 60 phr resulted in a decrease in the mooney viscosity, indicating the peptizing behavior of boron carbide. In addition, using ENR as the main material resulted in a lower viscosity than using natural rubber. The mooney viscosity increased when carbon black was added, but it decreased when the accelerator was increased. Furthermore, using DCP as a stabilizer resulted in higher mooney viscosity than that of sulphur.

Moreover, the results indicate that increasing the amount of B_4C reduces the vulcanization safety period and accelerates the curing process.

The minimum torque, which reflects the hardness or softness of uncured rubber, increases with the addition of B_4C . Excess B_4C has a peptizing effect, as demonstrated by the lowest minimum torque value in one of the samples. The maximum torque, representing the bond content after vulcanization, is highest in a sample using sulphur as a vulcanizing agent compared to the one using DCP (dichlorophenyl).

Various additives such as ENR (epoxidized natural rubber), carbon black, accelerator, or DCP can reduce scorch time, but using DCP increases the cure time. The sample with the most B_4C has the highest cure rate index, while the sample with the least B_4C has the lowest cure rate index.

The activation energy decreases with B_4C concentrations of 20 and 40 phr (parts per hundred parts of rubber), but increases with concentrations of 60 and 139.6 phr. This suggests that an appropriate amount of B_4C aids in vulcanization, while excessive amounts hinder the process. Additionally, carbon black promotes the formation of sulfur cross-links, enhancing the efficiency of the vulcanization process.

2. *Effects on the mechanical properties* The results of a hardness test conducted on rubber compositions containing B_4C , carbon black, and ENR. The hardness values increased when B_4C and carbon black were added to the sample. However, the rubber composition with ENR was softer compared to the NR sample. Increasing the amount of accelerator and changing the type of vulcanizing agent did not have a significant effect on the strength of the material.

When B_4C (boron carbide) was added to the rubber compound, both the tensile modulus and tensile strength decreased. This indicates a reduction in hardness and resistance to deformation in the sample. Sample F5 exhibited the lowest tensile modulus among all the samples, indicating reduced elasticity and a decreased ability to fully recover from deformation. Consequently, the F5 sample became more rigid and less flexible, leading to a decrease in the break elongation of the rubber.

Comparing NR (F3) with ENR (F6), the NR sample had a lower tensile modulus and strength. This can be attributed to enhanced cross-linking during the epoxidation process, resulting in a more elastic material. Furthermore, the higher break elongation observed in increasing ENR (F6) suggests that the rubber is more flexible and less prone to cracking.

The addition of carbon black (F8) resulted in increased tensile strength and modulus. The strong polarity and substantial surface area of carbon black particles allowed for direct physical connections with the rubber matrix. As a result of these physical linkages, the rubber gained rigidity and lost some of its flexibility. However, it should be noted that carbon black also shortened the length of the break elongation, indicating a decrease in the rubber's ability to stretch before breaking.

As the amount of CBS increased, the tensile modulus, tensile strength, and break elongation decreased. This indicates that the rubber became less rigid, weaker, and less capable of stretching before breaking when CBS was added.

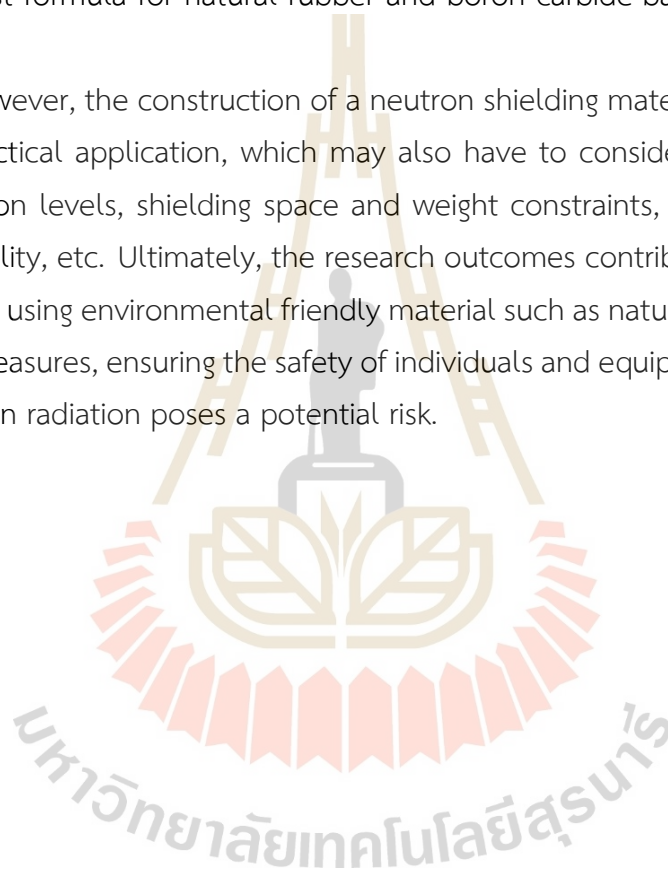
In contrast, using DCP in sample F10 led to a higher tensile strength compared to using sulfur in another sample. This is because DCP increased the cross-link density within the rubber compound and created stronger inter-molecular forces between the rubber chains. As a result, the rubber exhibited greater tensile strength, indicating increased resistance to deformation and breaking.

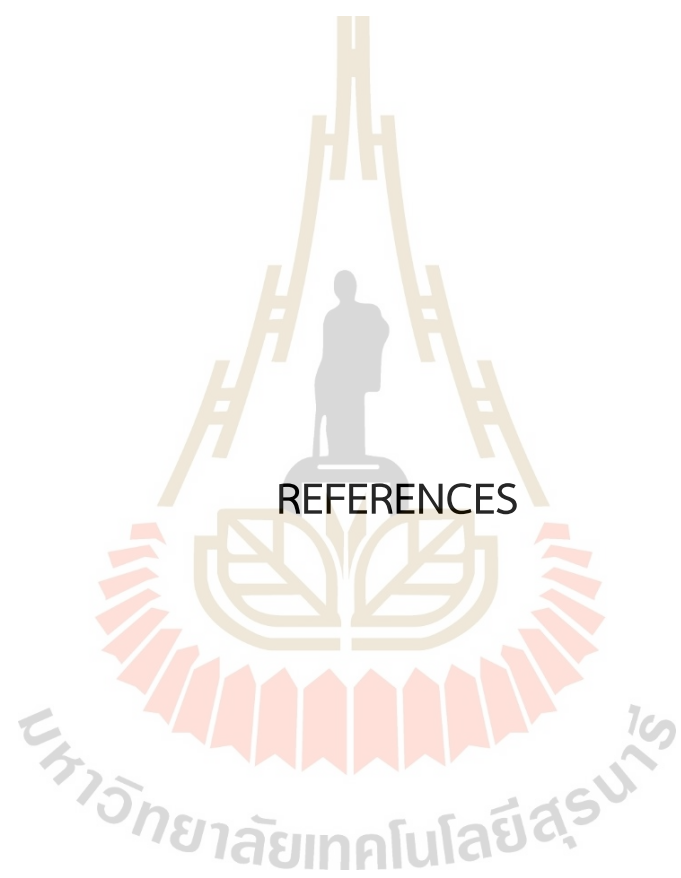
3. *Thermal neutron shielding properties* This study confirms that B_4C can improve the thermal neutron shielding of NR compound samples. B_4C at a content of 139.6 phr had the best thermal neutron shielding properties. Adding ENR, DCP, carbon,

or CBS has no effect on the properties of shielding thermal neutrons.

4. *Fast neutron shielding properties* The experiment results revealed that the attenuation of fast neutrons increased as the boron carbide concentration increased. Furthermore, fast neutron attenuation values in samples containing 50 weight percent boron carbide (F5) were equivalent to those in the commercial product that was obtained from a Japanese company under the non-disclosure agreement. Given that F2's macroscopic cross-section value is comparable to that of F1, F3, F4, and F5, we suggest F2 as the best formula for natural rubber and boron carbide-based neutron shielding materials.

However, the construction of a neutron shielding material must take into account its practical application, which may also have to consider the neutron energy range, radiation levels, shielding space and weight constraints, temperature and mechanical stability, etc. Ultimately, the research outcomes contribute to the overall improvement in using environmental friendly material such as natural rubber for radiation protection measures, ensuring the safety of individuals and equipment in environments where neutron radiation poses a potential risk.





REFERENCES

REFERENCES

- Abdel-Haleem, A., Sroor, A., El-Bahi, S., and Zohny, E. (2001). Heavy metals and rare earth elements in phosphate fertilizer components using instrumental neutron activation analysis. *Applied Radiation and Isotopes*, 55(4), 569–573.
- Afkham, Y., Mesbahi, A., Alemi, A., Zolfagharpour, F., and Jabbari, N. (2020). Design and fabrication of a nano-based neutron shield for fast neutrons from medical linear accelerators in radiation therapy. *Radiation Oncology*, 15, 105.
- Aim-O, P., Wongsawaeng, D., Phruksarojanakun, P., and Tancharakorn, S. (2017). Monte carlo simulation of innovative neutron and photon shielding material composing of high density concrete, waste rubber, lead and boron carbide. 860, 012043.
- Alhussain, A. and Abuhoza, A. (2009). Comparison study of reflected and transmitted thermal neutron flux in water and other moderators.
- Altieri, S. and Protti, N. (2018). A brief review on reactor-based neutron sources for boron neutron capture therapy. *Therapeutic Radiology and Oncology*, 2(0).
- Brüning, K. (2015). *Natural Rubber*, pages 1377–1382. Springer Berlin Heidelberg, Berlin, Heidelberg.
- Chimicaemateriali (2019). Natural rubber: cis-1,4-polyisoprene. Retrieved from https://chimicaemateriali.altervista.org/en/gommanaturale/?doing_wp_cron=1643865910.4574849605560302734375.
- Coran, A. (2013). Chapter 7 - vulcanization. In Mark, J. E., Erman, B., and Roland, C. M., editors, *The Science and Technology of Rubber (Fourth Edition)*, pages 337–381. Academic Press, Boston, fourth edition edition.
- El-Khatib, A. M., Doma, A. S., Badawi, M. S., Abu-Rayan, A. E., Aly, N. S., Alzahrani, J. S., and Abbas, M. I. (2020). Conductive natural and waste rubbers composites-loaded with lead powder as environmental flexible gamma radiation shielding material. *Materials Research Express*, 7(10), 105309.
- Encyclopædia Britannica (2012). Moderated, controlled fission of uranium-235. Retrieved from <https://www.britannica.com/technology/moderator/images-videos/media/1/387128/177366>.

- Güngör, A., Akbay, I., and Özdemir, T. (2019). Epdm rubber with hexagonal boron nitride: A thermal neutron shielding composite. *Radiation Physics and Chemistry*, 165, 108391.
- Jumpee, C., Rattanaplome, T., and Kumwang, N. (2020). A wide energy range neutron shielding material based on natural rubber and boron. 773, 012036.
- Jumpee, C. and Wongsawaeng, D. (2015). Innovative neutron shielding materials composed of natural rubber-styrene butadiene rubber blends, boron oxide and iron(iii) oxide. *Journal of Physics: Conference Series*, 611(1), 012019.
- Kharita, M., Yousef, S., and AlNassar, M. (2011). Review on the addition of boron compounds to radiation shielding concrete. *Progress in Nuclear Energy*, 53(2), 207–211.
- Kuhne, W., Gersey, B., Wilkins, R., Wu, H., Wender, S., George, V., and Dynan, W. (2009). Biological effects of high-energy neutrons measured in vivo using a vertebrate model. *Radiation research*, 172, 473–80.
- Larpkasemsek, A., Raksaksri, L., Chuayjuljit, S., Chaiwutthinan, P., and Boonmahitthisud, A. (2019). Effects of sulfur vulcanization system on cure characteristics, physical properties and thermal aging of epoxidized natural rubber. *Journal of metals, materials and minerals*, 29.
- Mahmoud, R. M. M. (2018). Design of a portable shield for neutron sources using mcnp computer code. *Arab Journal of Nuclear Sciences and Applications*, 51(4), 1–8.
- Martin, T., Mathur, S., and Morgan, I. (1964). The application of nuclear techniques in coal analysis. *The International Journal of Applied Radiation and Isotopes*, 15(6), 331–338.
- Mat Zali, N., Yazid, H., Megat Ahmad, M. H. A. R., Abdul Rahman, I., and Abdullah, Y. (2017). Effect of boron carbide content on properties of thermoplastic natural rubber composite as thermal neutron shielding. In *Current Material Research Using X-Rays and Related Techniques II*, volume 888 of *Materials Science Forum*, pages 179–183. Trans Tech Publications Ltd.
- Miller, D. (2018). Natural rubber: Structure and function. Retrieved from <https://www.halcyonagri.com/en/natural-rubber-structureand-function/::text=When%20considering%20the%20macrostructure%20of,end%2C%20than%20most%20synthetic%20rubbers.>

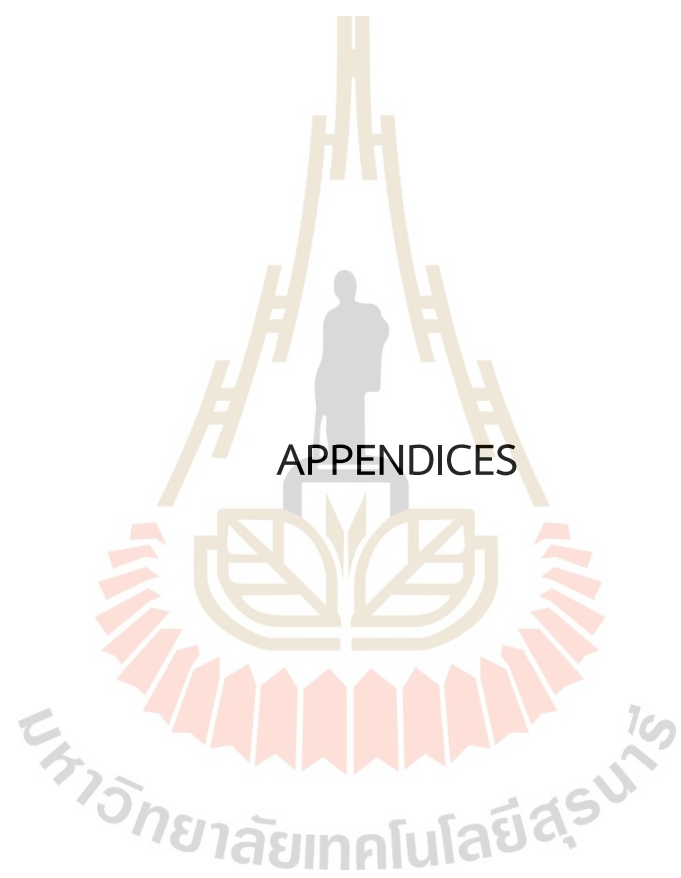
- Ministry of the Environment (2016). Electromagnetic radiation. Retrieved from <https://www.env.go.jp/en/chemi/rhm/basic-info/1st/01-03-03.html>.
- Onjuna, O., Laothonga, N., Pichab, R., Ratanathongchaib, W., and Onjun, T. (2014). Natural rubber blocks as thermal neutron shields. *Progress in Nuclear Science and Technology*, 4, 631–634.
- Saenpoowa, J., Ruksakulpiwat, C., Yenchai, C., and Kobdaj, C. (2023). Fabrication and development of neutron shielding materials based on natural rubber and boron carbide. *Journal of Physics: Conference Series*, 2431(1), 012079.
- Sang, Q., Zhang, S., Li, Y., Dong, M., and Bryant, S. (2018). Determination of organic and inorganic hydrocarbon saturations and effective porosities in shale using vacuum-imbibition method. *International Journal of Coal Geology*, 200, 123–134.
- Sears, V. F. (1992). Neutron scattering lengths and cross sections. *Neutron News*, 3(3), 26–37.
- Surya, I., Maulina, S., and Ismail, H. (2018). Effects of alkanolamide and epoxidation in natural rubber and epoxidized natural rubbers compounds. *IOP Conference Series: Materials Science and Engineering*, 299, 012061.
- Suzuki, M. (2020). Boron neutron capture therapy (bnct): a unique role in radiotherapy with a view to entering the accelerator-based bnct era. *International Journal of Clinical Oncology*, 25, 43–50.
- Szczepankowski, A., Przysowa, R., Perczyński, J., and Kułaszka, A. (2022). Health and durability of protective and thermal barrier coatings monitored in service by visual inspection. *Coatings*, 12(5).
- Tanrattanakul, V., Wattanathai, B., Tiangjunya, A., and Muhamud, P. (2003). In situ epoxidized natural rubber: Improved oil resistance of natural rubber. *Journal of Applied Polymer Science*, 90, 261–269.
- Tiwari, G. (2022). Radioactive decay of an atom. Retrieved from <https://www.toppr.com/guides/physics/nuclei/radioactivity-law-of-radioactive-decay/>.
- Vaysse, L., Bonfils, F., Sainte-Beuve, J., and Cartault, M. (2012). 10.17 - natural rubber. In Matyjaszewski, K. and Möller, M., editors, *Polymer Science: A Comprehensive Reference*, pages 281–293. Elsevier, Amsterdam.

Wikiversity (2021). Types of ionizing radiation. Retrieved from [https://en.wikiversity.org/wiki/Electromagnetic radiation](https://en.wikiversity.org/wiki/Electromagnetic_radiation).

Zaman, M., Shahid, S. A., and Heng, L. (2018). *The Role of Nuclear Techniques in Biosaline Agriculture*, pages 133–164. Springer International Publishing, Cham.

Zhang, P., Wittmann, F. H., Jun Zhao, T., Lehmann, E. H., and Vontobel, P. (2011). Neutron radiography, a powerful method to determine time-dependent moisture distributions in concrete. *Nuclear Engineering and Design*, 241(12), 4758–4766. The 18th International Conference on Nuclear Engineering (ICONE-18).





APPENDIX A

SAMPLE OF INPUT FILE FOR MCNP SIMULATION

Since the content of the input file is quite large, in this section we will only show one sample material, F1 with a thickness of 2 cm.

MCNPX Visual Editor Version X_24J

c Created on: Monday, September 05, 2022 at 03:23

```
1 0 1 imp:n=0 imp:p=0
2 204 -0.001225 -1 2 3 4 5 6 7 8 9 10 imp:n=1 imp:p=1
3 444 -1.50938458 -2 imp:n=1 imp:p=1
4 0 -3 imp:n=1 imp:p=1
5 456 -0.93 -4 5 imp:n=1 imp:p=1
6 204 -0.001225 -5 imp:n=1 imp:p=1
7 434 -0.93 -6 imp:n=1 imp:p=1
8 434 -0.93 -7 imp:n=1 imp:p=1
9 434 -0.93 -8 imp:n=1 imp:p=1
10 434 -0.93 -9 imp:n=1 imp:p=1
11 332 -3.35 -10 imp:n=1 imp:p=1
```

```
1 so 100
2 box 0 -7.5 -7.5 2 0 0 0 15 0 0 0 15
3 s 10.5 0 0 5
4 RCC -16 0 0 16 0 0 8
5 RCC -11.5 0 0 11.5 0 0 1.5
6 box -16 -11.5 8 16 0 0 0 23 0 0 0 5
7 box -16 -16.5 -11.5 16 0 0 0 5 0 0 0 23
8 box -16 11.5 -11.5 16 0 0 0 5 0 0 0 23
```

9 box -16 -11.5 -13 16 0 0 0 23 0 0 0 5
 10 box -16 -18.5 -33 20 0 0 0 38 0 0 0 20

mode n p

m204 7014.70c -0.755636 \$air (US S. Atm at sea level)

8016.70c -0.231475 18036.70c -3.9e-005

18038.70c -8e-006

18040.70c -0.012842

m434 1001.70c -0.148605

6000.70c -0.851395

m444 1001.70c -0.087379898

1002.70c -0.000020102

6000.70c -0.864

7014.70c -0.000996102

7015.70c -0.000003898

8016.70c -0.007297051

8017.70c -2.9492E-06

16032.70c -0.016291032

16033.70c -0.000132646

16034.70c -0.000774378

16036.70c -1.9436E-06

30000.70c -0.0231

m456 1001.70c -0.143716

6000.70c -0.856284

m332 1001.70c -0.003585

8016.70c -0.311622

12024.70c -0.000932

12025.70c -0.000123

12026.70c -0.000141

13027.70c -0.004183

14028.70c -0.009607

14029.70c -0.000504
14030.70c -0.000346
16032.70c -0.102191
16033.70c -0.000832
16034.70c -0.004811
16036.70c -2.4e-005
20040.70c -0.048529
20042.70c -0.00034
20046.70c -2e-006
20043.70c -7.3e-005
20044.70c -0.001138
20048.70c -0.000112
26054.70c -0.002707
26056.70c -0.043643
26057.70c -0.001017
26058.70c -0.000138
56130.70c -0.000465
56132.70c -0.00045
56134.70c -0.010935
56135.70c -0.030014
56136.70c -0.036001
56137.70c -0.05188
56138.70c -0.333655

sdef POS=-4 0 0 AXS=1 0 0 EXT=0 PAR=n

erg=d1 VEC=1 0 0

sp1 -2 1.330 \$241Am

nps 5000000

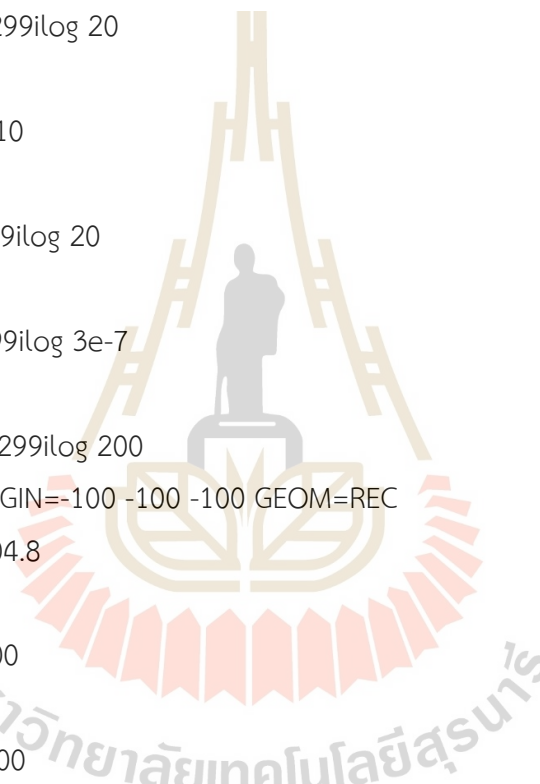
f11:n 3

e11 1e-10 299ilog 20

f21:p 3

e21 0 299i 10

```
f31:n 3
e31 0.01 299ilog 20
f41:n 3
e41 1e-8 299ilog 3e-7
f51:n 3
e51 1e-20 299ilog 200
f14:n 4
e14 1e-10 299ilog 20
f24:p 4
e24 0 299i 10
f34:n 4
e34 0.01 299ilog 20
f44:n 4
e44 1e-8 299ilog 3e-7
f54:n 4
e54 1e-20 299ilog 200
fmesh74:n ORIGIN=-100 -100 -100 GEOM=REC
imesh= 104.8
iints= 270
jmesh= 100
jints= 270
kmesh= 100
kints= 270
fmesh84:p ORIGIN=-100 -100 -100 GEOM=REC
imesh= 104.8
iints= 270
jmesh= 100
jints= 270
kmesh= 100
kints= 270
```



APPENDIX B

FMESH TALLY PLOT FOR SAMPLE

This section shows a sample Fmesh of each sampled object (F1–F10), showing the plot of the neutron and photon energy levels at different points on the ZX-plane of geometry.

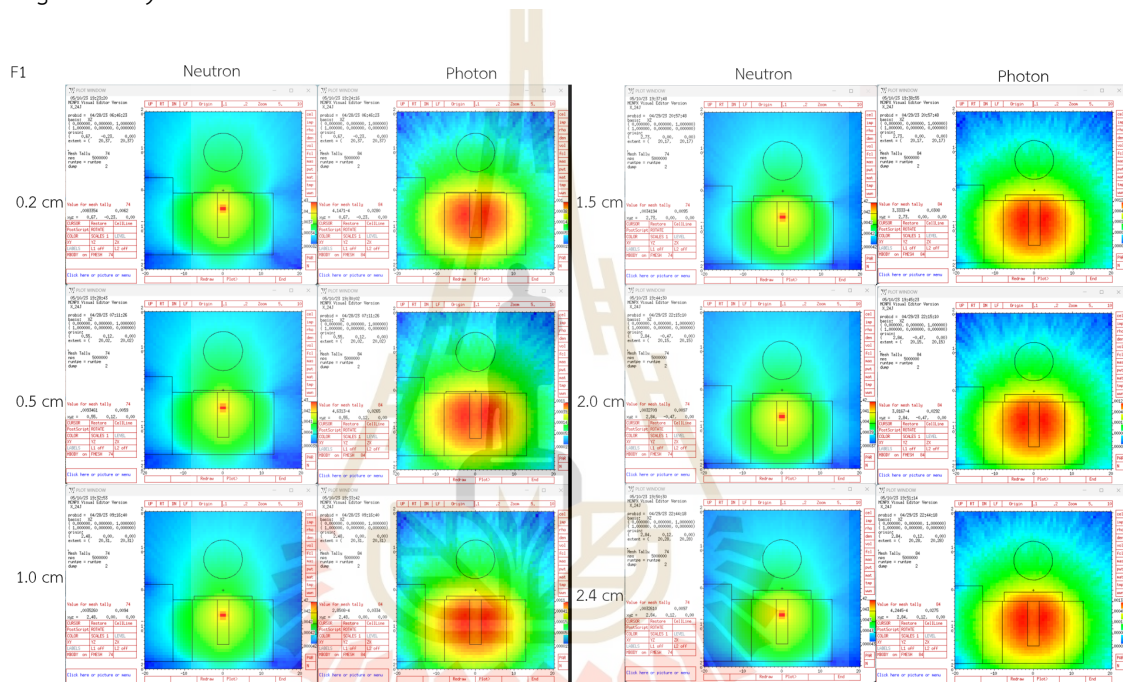


Figure B.1 Fmesh tally plot results of F1 sample with different of thickness, nps = 5000000 partcils, XY plane.

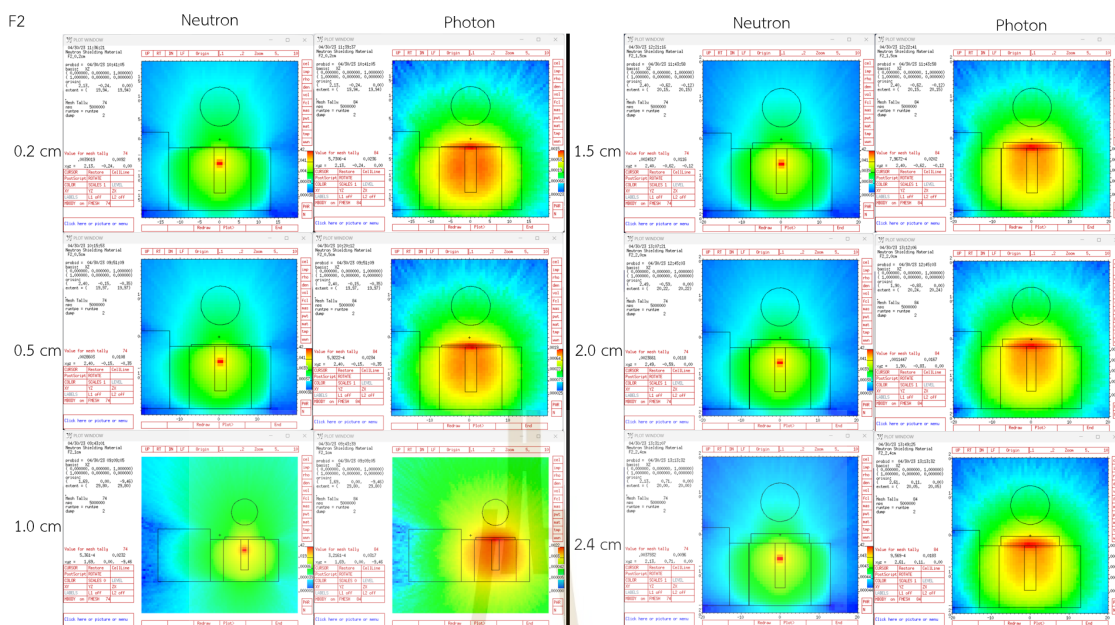


Figure B.2 Fmesh tally plot results of F2 sample with different of thickness, nps = 5000000 particks, XY plane.

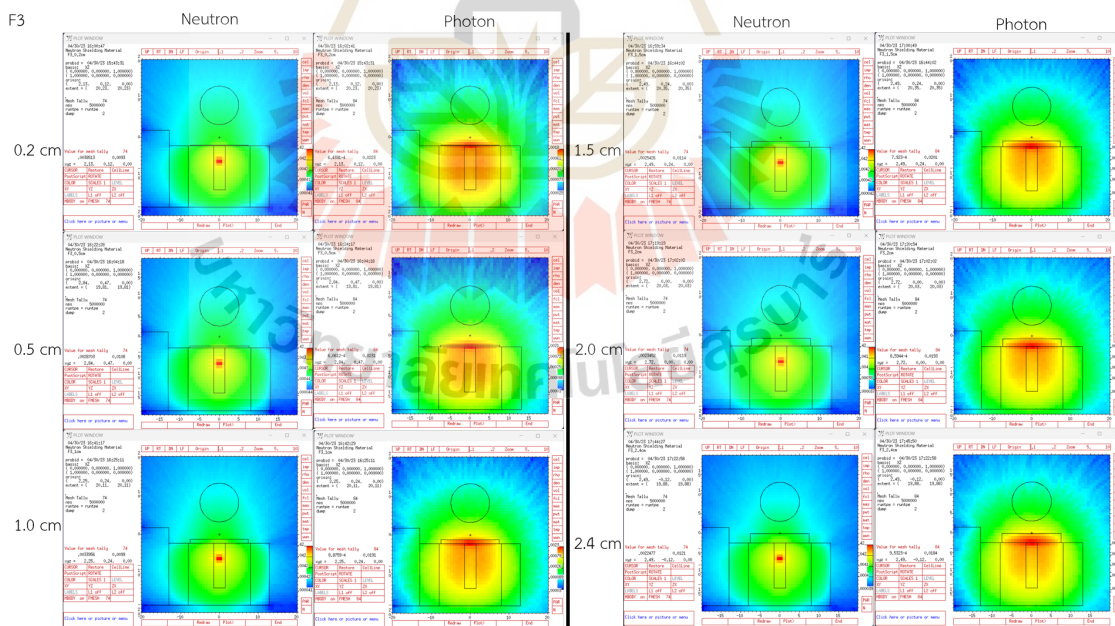


Figure B.3 Fmesh tally plot results of F3 sample with different of thickness, nps = 5000000 particks, XY plane.

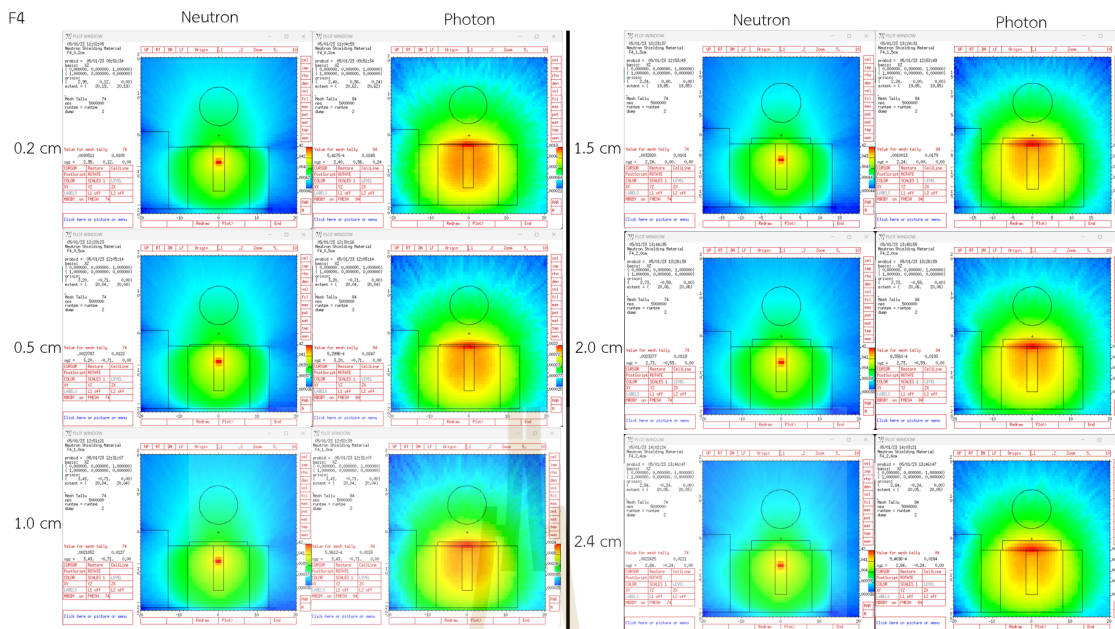


Figure B.4 Fmesh tally plot results of F4 sample with different of thickness, nps = 5000000 particks, XY plane.

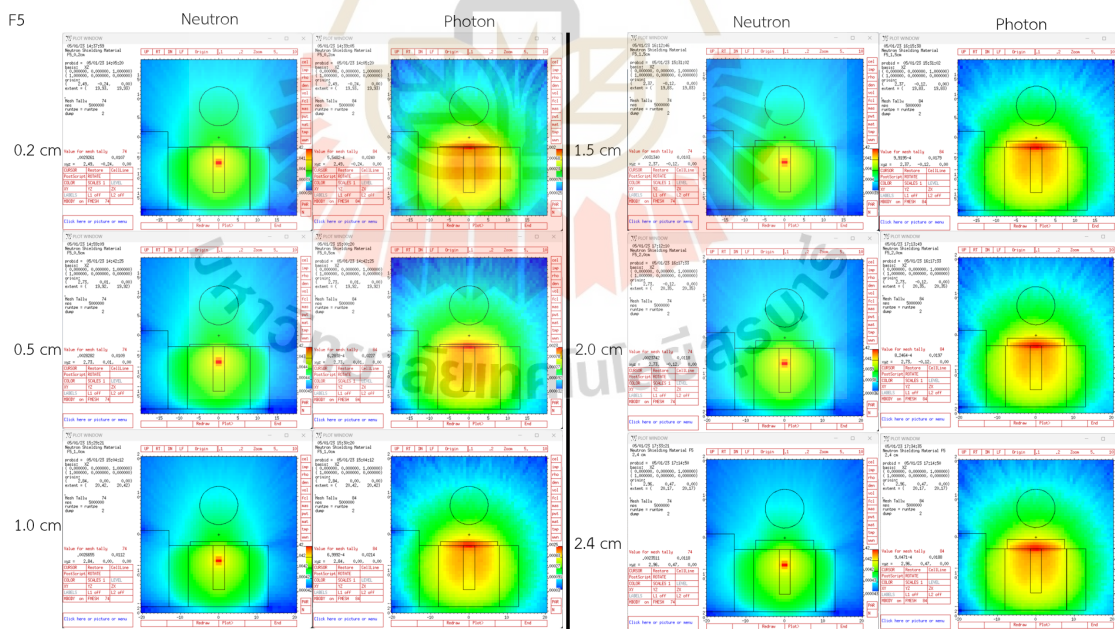


Figure B.5 Fmesh tally plot results of F5 sample with different of thickness, nps = 5000000 particks, XY plane.

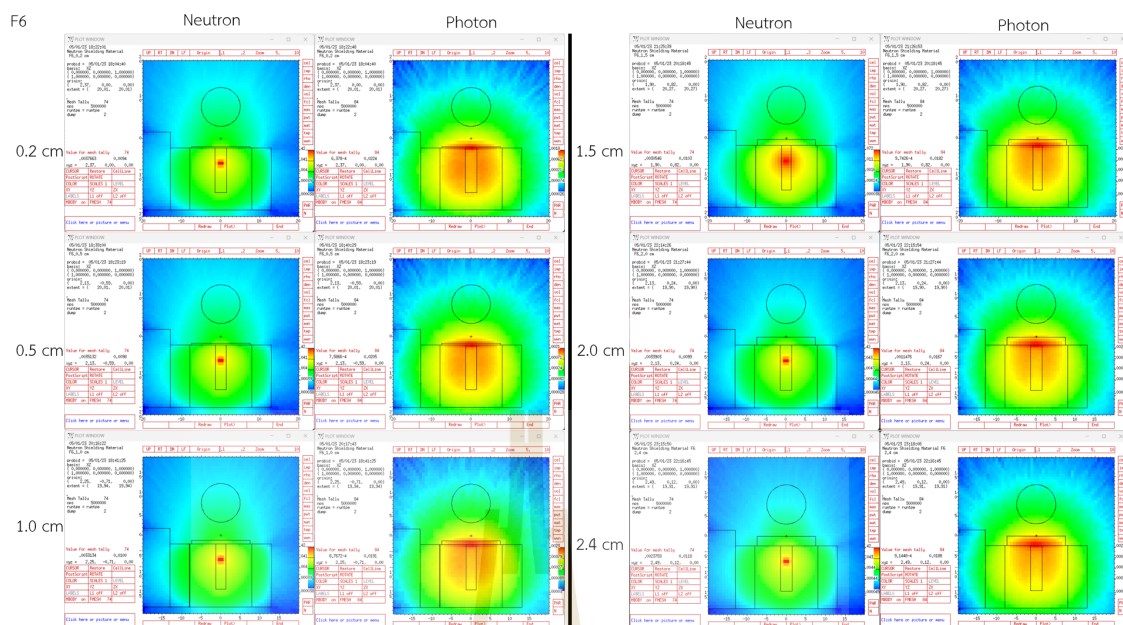


Figure B.6 Fmesh tally plot results of F6 sample with different of thickness, nps = 5000000 particks, XY plane.

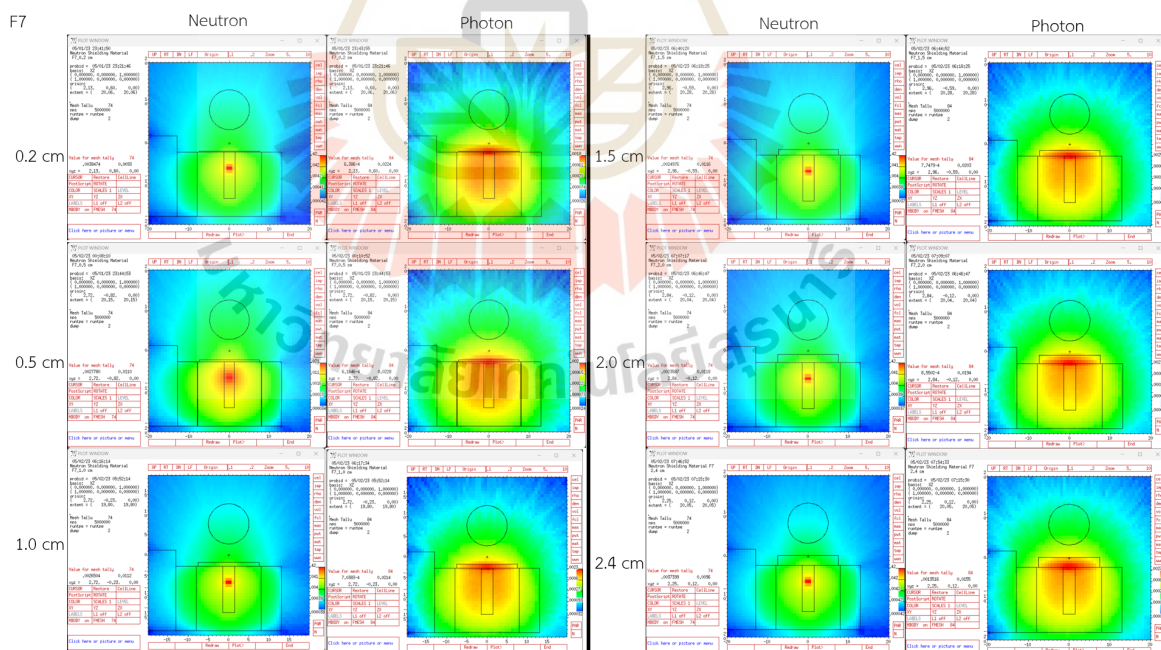


Figure B.7 Fmesh tally plot results of F7 sample with different of thickness, nps = 5000000 particks, XY plane.

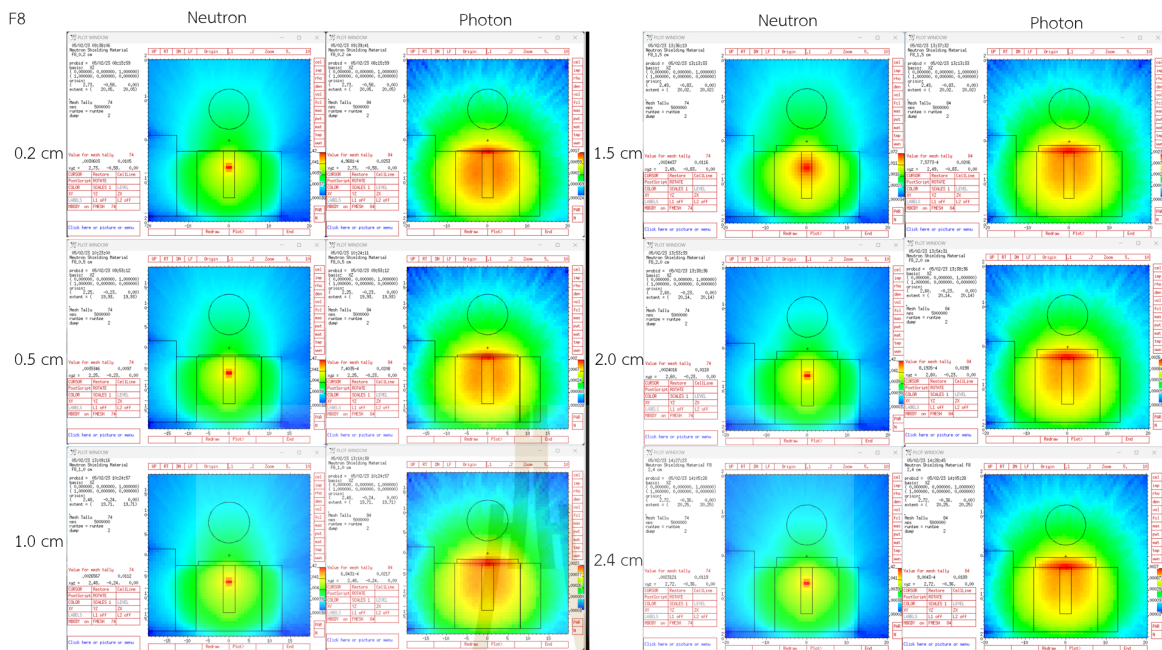


Figure B.8 Fmesh tally plot results of F8 sample with different of thickness, nps = 5000000 particls, XY plane.

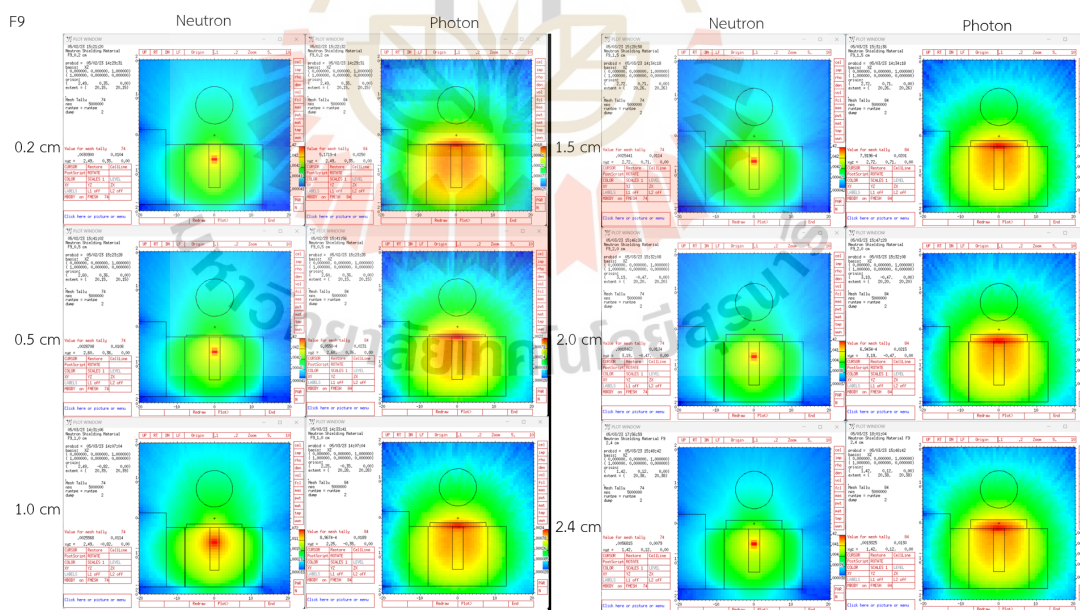


Figure B.9 Fmesh tally plot results of F9 sample with different of thickness, nps = 5000000 particls, XY plane.

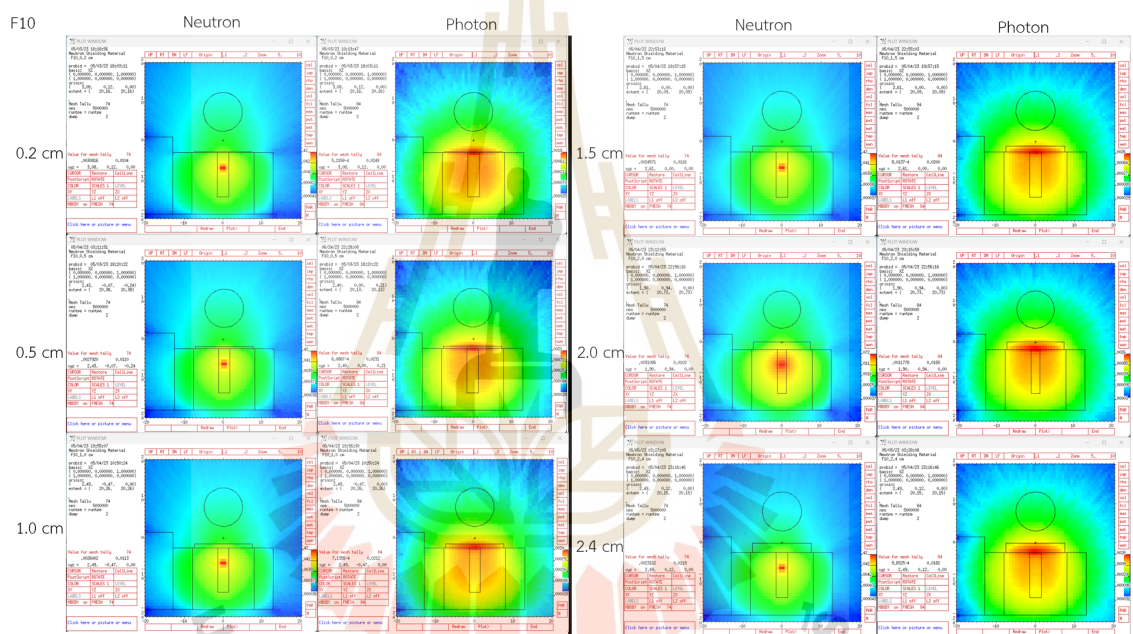


Figure B.10 Fmesh tally plot results of F10 sample with different of thickness, nps = 5000000 partcils, XY plane.

CURRICULUM VITAE

Name : Mr. Jittinun Saenpoowa

Date of Birth : December 21, 1996

Place of Birth : Sakon Nakhon, Thailand

Education :

2012 - 2016 Bachelor of Engineering, School of Chemical Engineering, Institute of Engineering, Suranaree University of Technology, Thailand

2016 - 2023 Master of Science (Applied Physics), School of Physics, institute of Science, Suranaree University of Technology, Thailand

Publications :

1. Jittinun Saenpoowa, Chaiwat Ruksakulpiwat, Chadet Yenchai and Chinorat Kobdaj (2023). Fabrication and development of neutron shielding materials based on natural rubber and boron carbide. *Journal of Physics: Conference Series* (IOP Publishing), 243(1), 012079
2. Jittinun Saenpoowa, Atirat Pitaktrakul, Supharat Inphonlek, Chaiwat Ruksakulpiwat, Chinorat Kobdaj (2023). Design and fabrication of thermal neutron shielding materials based on natural rubber and boron carbide. *MRS Communications*, <https://doi.org/10.1557/s43579-023-00487-3>